Universidade do Minho
Escola de Ciências

Ricardo Manuel Sousa Barbosa

Excitonic Effects in Optical Response of Semiconductors via Real Space Time-Resolved Methods

october 2023

Excitonic Effects in Optical Response of Semiconductors via Real Space Time-Resolved Methods

Ricardo Barbosa

UMinho | 2023

Universidade do Minho
Escola de Ciências

Ricardo Manuel Sousa Barbosa

Excitonic Effects in Optical Response of Semiconductors via Real Space Time-Resolved Methods

Master Dissertation
Master in Physics

Work developed under the supervision of:
Dr. Bruno Amorim (University of Minho/CF-UM-UP)
Dr. Rui Silva (ICMM-CSIC)

october 2023

Copyright and Terms of Use for Third Party Work

License granted to users of this work:

Acknowledgements

First and foremost, I would like to express my gratitude to the University of Minho and the Department of Physics, especially to the professors and the entire institutional body. I know it may sound a bit cliché when we say that teachers can influence and even shape their students, which is indeed true. I had fantastic professors throughout my academic journey who guided me with their knowledge and advice. They were the ones who helped me and convinced me to lead a life of constantly asking, "Why?", and, if possible, try to find an answer.

I would like to express my gratitude to my advisors, Bruno Amorim and Rui Silva, for their support, patience, enjoyable moments, and boundless knowledge. Both have had a significant impact on my education. Professor Bruno possesses a teaching and guiding style that impacted me during this journey. Rui had a strong impact on me as I began to appreciate not only the research area addressed in this work but also the field of simulation and numerical methods. I would like to express my gratitude to Professor Nuno Peres, who has been the professor who has closely accompanied me throughout my academic journey and has had a greater impact on my education than anyone else. Finally, a word of thanks to Professor Ricardo Ribeiro for helping me configuring the access to the Center's workstations. Without his support, half of the results presented here would not be possible.

Finally, I would like to express my gratitude to my partner Joana, my family, friends, and course colleagues. In particular, to Joana, for her patience and unwavering support throughout this journey, and for her effort to understand and tolerate my work. I would also like to thank my mother and sister for their constant help and support. A special word of appreciation goes to my friend, Rui, for his companionship along the way and our engaging conversations, even though I didn't always understand the experimental field of particles and gravitational waves. Well, perhaps it was these differences in our fields that made things even more interesting.

This work was supported by Fundação para a Ciência e a Tecnologia, I.P., (FCT-Portugal) thought project EXPL/FIS-MAC/0953/2021.

Fundação
para a Ciência
e a Tecnologia

Statement of Integrity

I hereby declare having conducted this academic work with integrity.

I confirm that I have not used plagiarism or any form of undue use of information or falsification of results along the process leading to its elaboration.

I further declare that I have fully acknowledged the Code of Ethical Conduct of the University of Minho.

University of Minho, Braga,

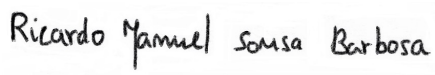

Abstract

In this work, we study time-resolved optical response of noninteracting and interacting electronic systems, including excitonic effects, in the presence of a driving optical field. This study is carried out on an ultrafast timescale by propagating in time the one-particle reduced density matrix, and we have employed a real-space representation using the tight-binding states basis. For this purpose, we consider condensed matter systems with periodic boundary conditions (PBC) based on a tight-binding (TB) description within a time-dependent mean-field Hartree-Fock approximation applied to the reduced density matrix. The coupling of the electrons to the electromagnetic field is described via a Peierls substituion on the TB Hamiltonian. We demonstrate that the linear response can be formulated as a generalized eigenvalue problem associated with the effective two-particle Hamiltonian governing electron-hole interactions. We then apply this formalism to a semiconductor/insulator crystalline system, where we formulate the electron-electron interaction and the excitonic eigenvalue problem in Bloch states. This procedure enable us to establish the Wannier equation, whose solutions provide us with information regarding the excitonic energies and modes. At last, we apply this theory to calculate the average current of one-dimensional (1D) systems, both gapped and gapless, and its optoelectronic dynamics and response of both free carriers and excitons, in both linear and nonlinear regimes. In particular, we study the formation of excitons and Bloch Oscillations (BO's).

Keywords reduced density matrix, time-dependent mean-field Hartree-Fock approximation, Peierls substitution, excitonic response, tight-binding model

Resumo

Neste trabalho, estudámos a resposta ótica resolvida no tempo de sistemas eletrónicos não interatuantes e interatuantes, incluindo efeitos excitónicos, na presença de um campo ótico. Este estudo é realizado em uma escala de tempo ultra-rápida, propagando a matriz de densidade reduzida de uma só partícula no tempo, e empregámos uma representação no espaço real usando a base de estados de tight-binding. Para esse fim, considerámos sistemas de matéria condensada com condições de fronteira periódicas com base numa descrição de tight-binding dentro de uma aproximação de Hartree-Fock dependente do tempo aplicada à matriz de densidade reduzida. O acoplamento dos electrões ao campo eletromagnético é descrito através de uma substituição de Peierls no Hamiltoniano TB. Demonstrámos que a resposta linear pode ser formulada como um problema aos valores próprios generalizado associado ao Hamiltoniano efetivo de duas partículas que governa as interações eletrão-lacuna. Em seguida, aplicámos esse formalismo a um sistema cristalino semicondutor/insulador, onde formulámos a interação eletrão-eletrão e o problema aos valores próprios excitónico nos estados de Bloch. Esse procedimento permite-nos estabelecer a equação de Wannier, cujas soluções nos fornecem informações sobre as energias e modos excitónicos. Por fim, aplicámos essa teoria para calcular a corrente média e estudar sistemas unidimensionais, tanto com gap como sem gap, bem como sua dinâmica optoeletrónica e resposta de portadores livres e de excitões, em regimes lineares e não lineares. Em particular, estudámos a formação de excitões e as Oscilações Bloch.

Palavras-chave matriz densidade reduzida, aproximação Hartree-Fock em campo médio, substituição de Peierls, resposta excitónica, modelo de tight-binding

Contents

List of Figures

1 Introduction

Ever since the groundbreaking discovery of graphene in 2004 [1], two-dimensional (2D) materials have emerged as a fertile ground for pushing the boundaries of device miniaturization across various applications [2, 3, 4, 5]. 2D materials (e.g. graphene [6, 7] and hexagonal boron nitride (hBN) [7, 8, 9, 10], transition metal dichalcogenides (TMDs) [11, 12, 13, 14, 15, 16, 17], and van der Waals (vdW) heterostructures [18, 19, 20, 21]) have emerged prominently due to their promise in investigating quantum many-body phenomena and their vast potential in optics and optoelectronic applications. In particular, TMD's provide exceptionally strong light–matter interaction at room temperature [17, 22]. In TMD's, the reduced dielectric screening that is caused by the reduced dimensionality results in an optical response that is dominated by strongly bound excitons with large (hundreds of meV) binding energies [17, 23, 24]. An exciton consists of a bound state formed by an electron-hole pair through a electrostatic interaction. These quasiparticles arise in materials with bandgaps, such as semiconductors and insulators. From a simplified perspective, considering the simplest gapped crystalline system with a two-band model, excitons form when an electron from the valence band is promoted to the conduction band, leaving behind an unoccupied electronic state or a "hole", which bears the opposite charge of the electron. This electron-hole pair is subbject to an attrative interaction, which results in the formation of a bound state, which is an electrically neutral quasiparticle. Excitons share some similarities with the hydrogen atom (and electron-proton bound state) [25, 26], such as quantized energy levels.

Gaining insights into the fundamental mechanisms governing the functionality of two-dimensional materials is a critical step towards their effective utilization in practical devices. In this scenario, ultrafast spectroscopy [27, 28, 29] offers an additional way to change and potentially control the properties of free carriers [30] and bound states such as excitons [31, 32, 33, 34] on a short time scales. Its unmatched ability to examine physical phenomena with exceptional accuracy highlights its importance [35, 36, 37]. The introduction of ultrashort laser pulses has enabled us to push systems beyond their equilibrium states, opening the door to the investigation of novel quantum phases distinguished by properties that go beyond those observed under equilibrium conditions [38], unlocking a realm of promising applications. These applications encompass the manipulation of topological phases [39, 40, 41, 42, 43], achieving precise control over valley pseudo-spin via optical resonance [44, 45, 46], generating coherent light-induced currents [47, 48, 49], and the intriguing potential to induce transitions from insulating to conducting states using light pulses [50, 51, 52]. Recent years have witnessed significant progress in enabling time-resolved experiments for the observation and understanding of transient state dynamics within nonequilibrium systems. Notably, it is now possible to track electron dynamics on its inherent timescale, operating at the attosecond level (10^{-18}), well before the lattice reacts to external stimuli [53]. In particular, time-resolved spectroscopy has allowed to observe large renormalization of the optical transition energies upon photoexcitation [54, 55] and to track the dynamical exciton response [31, 56, 57]. Attosecond laser pulses also allowed the observation of High-Harmonic generation [58, 59, 60, 61] in atomically-thin materials, a nonlinear phenomena, in which a system responds at frequencies that are very large multiples of the driving frequency. This phenomena has gained significant attention

in recent years and recently associated with the Nobel Prize in Physics 2023.

In this context, a compelling need emerges: the simulation of transient state dynamics in condensed-matter systems under strong laser excitation. This imperative stems from the essential objective to understand the fundamental mechanisms that govern out-of-equilibrium properties and to establish the links between microscopic electron dynamics and macroscopic observables such as the current and the absorption. To precisely capture the intricacies of light-matter interactions, electron dynamics simulations must incorporate the formation of excitons [62, 63]. In this endeavor, we present a real space time-resolved method by propagating the reduced density matrix in time designed to simulate electron dynamics within realistic condensed matter systems operating under nonequilibrium conditions. Conventional tools for dealing with condensed matter systems have limitations. Density Functional Theory (DFT) is a foundational tool for computational material modeling under equilibrium conditions, but it is inadequate for addressing out-of-equilibrium dynamics. To overcome this limitation, three primary alternative approaches have been explored. The first approach involves Time-Dependent Density Functional Theory (TDDFT) [64, 65, 66], which is well-suited for real-time and -space [67] simulations of condensed matter systems interacting with laser pulses. However, it can be computationally costly when incorporating excitonic interactions due to the necessity of implementing a long-range nonlocal exchange functional [68]. The second alternative is Many-Body Perturbation Theory (MBPT). Starting from the Kohn-Sham DFT electronic structure, this approach consists in solving the Bethe–Salpeter equation (BSE) to obtain the energy and wave functions of excitons, expressed as superpositions of single-particle excitations [69, 70, 71]. BSE is an ideal approach for spectroscopy calculations but not suitable for real-time nonequilibrium dynamics [72]. Efforts have also been made to extend BSE into the time domain [73, 74, 75] by solving the Kadanoff–Baym equations rooted in nonequilibrium Green's function theory [76, 77]. Cistaro et al. [63] suggest an approach based on this theoretical framework. They show how the equations of motion (EoM) for the density matrix of the system in reciprocal space can be efficiently implemented and evolved in real time in order to describe realistic ultrafast spectroscopy experiments.

In this work, we propose a method in real-time and -space that enables the study of optoelectronic response in semicondutors in the presence of a driving field by propagating in time the one-particle reduced density matrix [78, 79, 80, 81]. In particular, we show how the equations of motion (EoM) for the reduced density matrix can be efficiently implemented and how propagating it in time opens up the opportunity to observe and manipulate the electronic motion of free carriers as well as bound states such as excitons in an ultrafast timescale.

1.1 Dissertation Structure

In this work, we develop a general nonequilibrium quantum theory to study linear and nonlinear response regime induced by ultrafast attosecond laser pulses applied to condensed matter systems. This theory is based on a tight-binding (TB) description within a time-dependent Hartree-Fock approximation applied to the one-particle reduced density matrix. Futhermore, we couple this formulation to the electromagnetic field via a Peierls substitution [82,

83, 84]. We employ a real space representation, meaning that this study relies on localized orbitals or Wannier basis sets [85], which allow us to investigate effects of disorder in the response as well as provides us with localization information. The role of excitonic effects in the linear current response of the system is accessed by analyzing the Fourier transform of the time-dependent current.

This work is structured as follows. In Chapter II, we introduce the 1D tight-binding toy models that will be studied throughout this work. Then, we propose a way to describe the light-matter coupling in tight-binding systems with Born-von Karman periodic boundary conditions via Peierls substitution.

In Chapter III, we introduce and describe the general properties of the one-particle reduced density matrix. We study its "nearsightedness" properties, in particular, how its properties of locality in real-space depends of the system's characteristics, specifically its temperature and bandgap value.

In Chapter IV, we introduce the theoretical framework that will be used throughout this work, the time-dependent mean-field Hartree-Fock approximation applied to the one-particle reduced density matrix.

In Chapter V, we begin by studying the linear response theory of an interacting fermionic system in the presence of an external time-dependent perturbation term, within the time-dependent Hartree-Fock approximation. Next, we determine the effective two-particle (electron-hole) Hamiltonian by simplifying the previous problem by choosing to work in a basis that diagonalizes the free-particle Hamiltonian and in a zero temperature regime. This approach to the problem enable us to formulate a linear response eigenvalue problem, which corresponds to the linear response within this time-dependent Hartree-Fock scheme. Moreover, we derive the explicit form of the two-particle electron-hole Hamiltonian for crystalline systems in a Bloch states basis and its corresponding excitonic eigenvalue problem. Lastly, we apply the previous general theory to the case of excitons in a cristaline insulator/semiconductor. In particular, we will see how the linear response eigenvalue problem, which describes excitons, can be approximated by an hidrogenoid problem, usually referred to as the Wannier equation.

In Chapter VI, we present the theoretical approach and the numerical implementation involved in this work, namely how we implement and solve the rDM equation of motion for both noninteracting and interacting systems, as well as the expectation value of the current operator, and its Fourier transform, within the Peierls substitution.

In Chapter VII, we present the results for a gapped 1D system being driven out-of-equilibrium via a short-pulse in a linear response regime. We show the results in the time- and in the frequency-domain, both for noninteracting and interacting electrons. We compare the position of the ressonances observed in the Fourier transformed current with the excitonic energies, computed with the Wannier equation.

In Chapter VIII, we simulate the generation Bloch oscillations in a gapless 1D system. We compare the semi-classical approach with the quantum-mechanical, based on the theoretical framework discussed in this work, both analytical and numerically.

Part I

Theoretical Framework

2 Tight-Binding Hamiltonians and the Peierls substitution

In this chapter, we begin by introducing the tight-binding 1D models that will be used throughout this work. Following that, we present a way to perform a light-matter coupling in tight-binding systems with Born-von Karman periodic boundary conditions via Peierls substitution. In this context, we discuss the implications of using PBC in the position's operator definition and how the Peierls substitution solves that issue. As we will see, this approach leads to a breaking of gauge invariance of the system.

2.1 1D Tight-Binding Hamiltonians

Let us start with a toy model of an one-dimensional crystal (see Figure 1) with a periodic alternation of N discrete sites of two types of atoms, A and B. This structure is characterized by its atoms being arranged in an ordered way, such that their equilibrium positions are at the sites of a periodic lattice. In this type of systems, each atom has one orbital and, effectively, one can adopt A and B as two orbitals on an artificial atom, with some particular coupling between these orbitals. There are two atoms and orbitals per unit cell and, since the unit cell corresponds to the repeating unit of a lattice, let us define the distance between consecutive unit cells with value $2a_0$. In the so-called tight-binding approximation, an electron possesses an amplitude for tunneling to a different orbital localized around a nearby atom. The scheme in Figure 1 corresponds to a general formulation of a diatomic linear chain, which corresponds to a gapped system. We can easily construct an equivalent system but without a gap, by changing the types of atoms under consideration. If one takes a tight-binding system constituted by only one type of atom, we would get one orbital per unit cell, and this would correspond to a monoatomic linear chain, a gapless system.

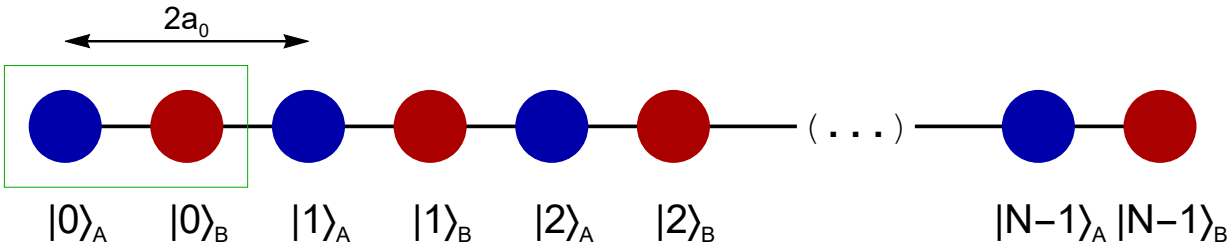

Figure 1: Scheme of an ideal diatomic chain with N discrete sites with Born-von Karman periodic boundary conditions (PBC) constituted by two types of atoms, A and B. The atom's position is catalogued by $|n\rangle_{A/B}$ and the spacing between consecutive atoms of same type has a value of $2a_0$. The green box represents the system's unit cell (or Wigner-Seitz cell) which, in this case, it contains two atoms and two orbitals, and it can be designated as sublattices A and B. The position of these atoms are $s_A = 0$ and $s_B = a_0$ within the unit cell.

2.1.1 Diatomic Linear Chain: A Gapped system

In general, looking at a noninteracting system, the Hamiltonian will be given by the two contributions: the energy on-site term and the hopping term of electrons between consecutives sites, where we take the assumption that the

overlapping of different atomic orbitals decays so rapidly that only the nearest neighbours hopping is relevant. On these conditions, the Hamiltonian in real space is expressed in terms of a tight-binding basis (or in an atomic basis) under periodic boundary conditions

$$\mathcal{H}_{PBC}^{T.B.} = \sum_n \epsilon_A \left(c_n^A\right)^\dagger c_n^A + \sum_m \epsilon_B \left(c_m^B\right)^\dagger c_m^B - h \sum_{\langle n,m\rangle_{A,B}} \left(\left(c_n^A\right)^\dagger c_m^B + h.c.\right) \tag{2.1}$$

where the quantities $\epsilon_A\,(\epsilon_B)$ and h are the on-site energy of type $A\,(B)$ atoms and the hopping integral. The subscript $\langle n,m\rangle_{A,B}$ is labeling the first order of nearest neighbours and we will set $m \to n+\delta$, with δ identifying the first neighbours; the n indexes the unit cell and the position of each site as $|A,n\rangle \to 2a_0 n$ and $|B,n\rangle \to 2a_0 n + s_B$, with $s_B = a_0$. The operators $(c_n^\alpha)^\dagger$ and c_n^α are the creation and annihilation operators that creates and annihilates an electron in the orbital localized at the sublattice $\alpha = \{A,B\}$. The term "$h.c.$" stands for hermitian conjugate. We also assume the atomic orbitals are orthogonal to each other, meaning that it forms a complete discrete orthonormal basis such that the following relation $\langle n|\ m\rangle = \delta_{nm}$ is verified.

Due to the translational symmetry, the Hamiltonian is easily diagonalizable by using Bloch states[1], by doing the following ansatz:

$$c_n^\alpha = \sum_{\mathbf{k}} \langle n,\alpha|\ \psi_{\mathbf{k}}\rangle\, c_{\mathbf{k}}^\alpha \tag{2.2}$$

which leads to

$$c_n^\alpha = \sum_k \frac{e^{ikr_n}}{\sqrt{N}} c_k^\alpha \tag{2.3}$$

$$(c_n^\alpha)^\dagger = \sum_k \frac{e^{-ikr_n}}{\sqrt{N}} (c_k^\alpha)^\dagger \tag{2.4}$$

$$\text{with } k = \frac{2\pi n}{2a_0 N},\ \text{for } n = 0,1,\ldots,N-1 \tag{2.5}$$

with $r_n = 2na_0$. In this new basis, the Hamiltonian (2.1) reads

$$\mathcal{H}_{PBC}^{T.B.} = \epsilon_A \sum_k \left(c_k^A\right)^\dagger c_k^A + \epsilon_B \sum_k \left(c_k^B\right)^\dagger c_k^B - h \sum_k \left[\left(1+e^{i2ka_0}\right)\left(c_k^A\right)^\dagger c_k^B + \left(1+e^{-i2ka_0}\right)\left(c_k^B\right)^\dagger c_k^A\right] \tag{2.6}$$

where we used the fact that Bloch states form a set of discrete basis of orthonormal states, meaning

$$\frac{1}{N}\sum_n e^{-i(k-k')na_0} = \delta_{kk'}$$

The previous result can be thought of a matrix

$$\mathcal{H}_{PBC}^{T.B.} = \sum_k \begin{bmatrix} \left(c_k^A\right)^\dagger & \left(c_k^B\right)^\dagger \end{bmatrix} \mathcal{H}^B \begin{bmatrix} c_k^A \\ c_k^B \end{bmatrix} \tag{2.7}$$

[1] The tight-binding Hamiltonian is written in a localized orbital basis, whose states are not eigenstates. So, the need arises to diagonalize the problem by make a change of basis to a different Hilbert space

where we define the Bloch Hamiltonian of a diatomic 1D linear chain as

$$\mathcal{H}^B = \begin{bmatrix} \epsilon_A & -h\left(1+e^{i2ka_0}\right) \\ -h\left(1+e^{-i2ka_0}\right) & \epsilon_B \end{bmatrix} \tag{2.8}$$

This result allows us to determine the eigenvalues and eigenvectors through the time independent Schrödinger equation, leading to the following eigenvalue problem:

$$\mathcal{H}^B \Psi_k = E_k \Psi_k$$

This eigenvalue problem has an analytic solution, where we determine two bands with eigenvalues $E_k = [\epsilon_{Ak}, \epsilon_{Bk}]^T$

$$\epsilon_k = \frac{\epsilon_A + \epsilon_B}{2} \pm \sqrt{\left(\frac{\Delta}{2}\right)^2 + 2|h|^2\left(1+\cos\left(2ka_0\right)\right)} \tag{2.9}$$

Note that the difference between the two bands are minimal at $ka_0 = \pi/2$, which corresponds to the bandgap Δ. Besides the electronic band, one can also determine the density of states (DoS). This quantity describes the number of energy states per unit energy interval at a given energy E_i per unit cell. Mathematically, if you have a discrete set of energy levels, the normalized DoS can be expressed as:

$$DoS\left(E\right) = \frac{1}{N}\sum_{E_i}\delta\left(E - E_i\right) \tag{2.10}$$

In Figure 2 it is represented the diatomic linear chain's band structure and the corresponding density of states. the system displays time inversion symmetry, meaning that the dispersion relation is symmetric within the 1st Brillouin zone $(\epsilon_k = \epsilon_{-k})$. At $T = 0$K and a chemical potential $\mu = 0\,eV$, the Fermi's level is located in the middle of the bandgap and the valence band is fully occupied, unlike the conduction band, which is completely vacant. Therefore, we are dealing with an semiconductor/insulator system.

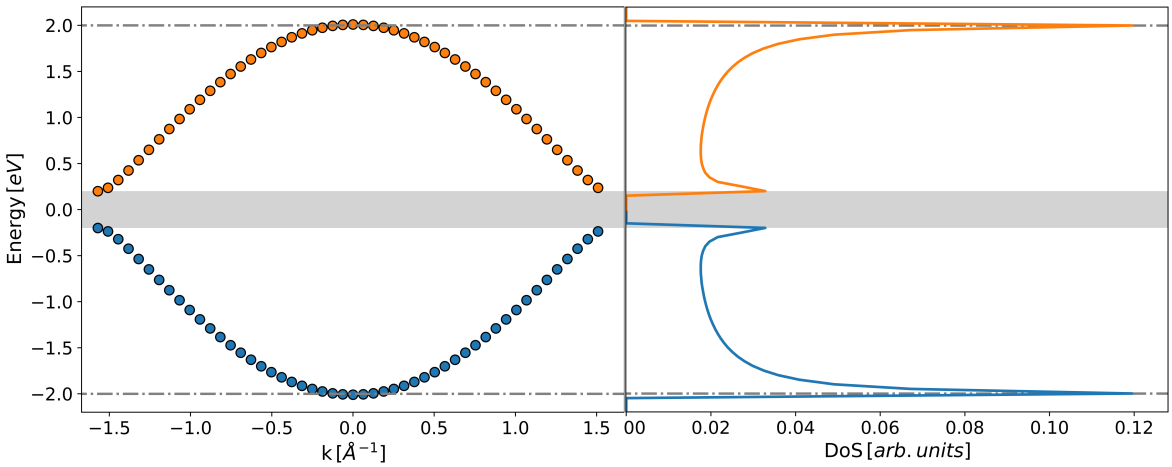

Figure 2: Graphical representation of the band structure within the 1st Brillouin zone and the density of states (DoS) of a diatomic linear chain with a bandgap $\Delta = 0.4\,eV$ (grey region), a hopping energy $h = 1\,eV$ and a lattice parameter $a_0 = 1$Å.

2.1.2 Monoatomic Linear Chain: A Gapless System

The dispersion relation of a monoatomic linear chain is quickly determined considering the previous procedure. With the Scheme 1 in mind, if one considers the A/B chain and set $\epsilon_A = \epsilon_B$, the gap closes, where the system is now constituted by a single atom and a single orbital per unit cell. Then, you can unfold the Brillouin zone, as your periocidity goes from $2a_0$ to a_0. We write the Hamiltonian in a tight-binding basis as

$$\mathcal{H}^{T.B.}_{PBC} = \sum_n \epsilon c_n^\dagger c_n - h \sum_{\langle n,m \rangle} \left(c_n^\dagger c_m + h.c. \right), \tag{2.11}$$

where the operators operators $c_n^\dagger \, (c_n)$ are the creation(annihilation) operators that creates(annihilates) an electron in the orbital localized around the site $n = 0, 1, ..., N-1$. The quantities ϵ and h are the on-site energy and the transfer integral. The term "$h.c.$" stands for hermitian conjugate and the subscript $\langle n, m \rangle$ is labeling the first order of nearest neighbours. We also assume the atomic orbitals are orthogonal to each other, meaning that it forms a complete discrete orthornomal basis such that the following relation $\langle n |\ m \rangle = \delta_{nm}$ is verified.

Like the previous tight-binding system, this one also possesses translational symmetry, enabling it to be diagonalizable by considering Bloch states. For that, we consider the following projection:

$$c_n = \sum_{\mathbf{k}} \langle n |\ \psi_{\mathbf{k}} \rangle \, c_{\mathbf{k}} \tag{2.12}$$

which leads to

$$c_n = \sum_k \frac{e^{ikr_n}}{\sqrt{N}} c_k \tag{2.13}$$

$$c_n^\dagger = \sum_k \frac{e^{-ikr_n}}{\sqrt{N}} c_k^\dagger \tag{2.14}$$

$$\text{with } k = \frac{2\pi n}{a_0 N}, \text{ for } n = 0, 1, \ldots, N-1 \tag{2.15}$$

where quantity $r_n = n a_0$ is the position of site n in the lattice, a_0 is the lattice parameter and N the number of discrete sites. The Hamiltonian (2.11), in this new basis, reads

$$\mathcal{H}^{T.B.}_{PBC} = \sum_k \mathcal{H}^B c_k^\dagger c_k \tag{2.16}$$

with the Bloch Hamiltonian of a monoatomic linear chain being defined as

$$\mathcal{H}^B = \epsilon - 2h \cos\left(k a_0\right) \tag{2.17}$$

in which we used the fact that Bloch states form a set of discrete basis of orthonormal states

$$\frac{1}{N} \sum_n e^{-i(k-k')na_0} = \delta_{kk'}$$

In order to determine the eigenstates and eigenvalues of the problem, all we have to do is to solve the eigenvalue problem impose by the stationary Schrödinger equation for the Hamiltonian in (2.17). So, with generality, we can write

$$\mathcal{H}^B \Psi_k = \epsilon_k \Psi_k \tag{2.18}$$

where the ϵ_k and Ψ_k are the eigenvalues and the eigenstates, respectively. In Figure 3 it is represented the electron "band" and the corresponding density of states, defined in equation (2.10). Under these conditions, the states delimited by Fermi's wave vector k_F are fully occupied and the remaining states in the 1st B.Z. are free to be occupied. Also, the system displays time inversion symmetry, meaning that the dispersion relation is symmetric within the 1st Brillouin zone $(\epsilon_k = \epsilon_{-k})$.

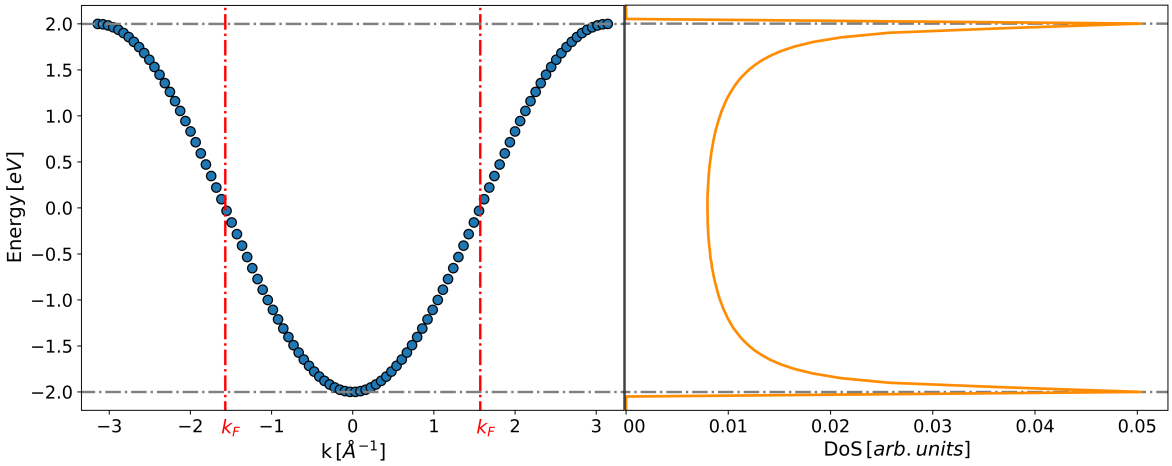

Figure 3: Graphical representation of the "electronic band" within the 1st Brillouin zone and the density of states (DoS) of a monoatomic linear chain with an on-site energy $\epsilon = 0\,eV$, a hopping energy $h = 1\,eV$, and a lattice parameter $a_0 = 1$Å. The Fermi's wave vector, representated by $k_F = |\pi/2a_0|$, delimit the occupied states within the monoband.

2.2 Light-Matter Coupling in a Tight-Binding Model

The topics covered in this section are based on the reference [86].

2.2.1 Peierls substitution for 1D Systems

Let us consider a 1D tight-binding chain subject to an uniform electric field. We will assume that the system is finite with open boundary conditions (OBC). In a length gauge, the Hamiltonian is given by

$$\mathcal{H}_{OBC}(t) = -h \sum_n \left(c_{n+1}^\dagger c_n + c_n^\dagger c_{n+1} \right) + \sum_n e\varepsilon(t)\, a_0 n c_n^\dagger c_n \tag{2.19}$$

where h is the hopping term and the light–matter interaction term is written in the so-called length gauge [63, 87]. We assume that the tight-binding basis is localized, defining the electric potential's matrix elements as

$$\langle n|\phi\left(\mathbf{r}\right)|m\rangle \simeq \phi\left(\mathbf{r}=\mathbf{r}_n\right)\delta_{nm} \tag{2.20}$$

where we consider an uniform electric field being described by an electric potential of the form

$$\phi\left(\mathbf{r}\right) = |e|\boldsymbol{\varepsilon}\left(t\right)\cdot\mathbf{r} \tag{2.21}$$

with $\mathbf{r}$ being the position operator of the electrons in the system. In a 1D system, its definition is given by

$$x = \sum_n n c_n^\dagger c_n \tag{2.22}$$

Note that the choice described in equation (2.21) breaks the spatial translational invariance [82], because the position operator x introduces a position-dependent term that varies from site to site, causing the Hamiltonian to vary spatially.

Let us now consider the evolution of a single electron state written in terms of a localized orbital basis

$$|\psi(t)\rangle = \sum_n \psi_n(t)|n\rangle \tag{2.23}$$

in which its equation of motion of the coefficients $\psi_n\left(t\right)$ is dictated by the time-dependent Schrödinger equation. Manipulating accordingly, we determine

$$i\hbar\frac{\partial\psi_n\left(t\right)}{\partial t} = -h\left[\psi_{n-1}\left(t\right)+\psi_{n+1}\left(t\right)\right] + e\varepsilon\left(t\right)\left(a_0 n\right)\psi_n\left(t\right) \tag{2.24}$$

One can eliminate the electric field term via gauge transformation

$$\psi_n\left(t\right) = e^{\frac{i}{\hbar}eA(t)a_0 n}\tilde{\psi}_n\left(t\right) \tag{2.25}$$

where we can correlate the electric field with the vector potential through the equation $\varepsilon\left(t\right) = -\partial_t A\left(t\right)$ within a Weyl gauge. Equivalently, by applying (2.25) in (2.24), it yields the equation of motion for $\tilde{\psi}_n\left(t\right)$

$$i\hbar\frac{\partial\tilde{\psi}_n\left(t\right)}{\partial t} = -h\left(e^{-\frac{i}{\hbar}eA(t)a_0}\tilde{\psi}_{n-1}\left(t\right)+e^{\frac{i}{\hbar}eA(t)a_0}\tilde{\psi}_{n+1}\left(t\right)\right) \tag{2.26}$$

From the previous equation, we can obtain the *Peierls Hamiltonian*, which reads:

$$\tilde{\mathcal{H}}_{OBC}^{Peierls}\left(t\right) = -h\sum_n\left(e^{-\frac{i}{\hbar}eA(t)a_0}\tilde{c}_{n+1}^\dagger\tilde{c}_n + e^{\frac{i}{\hbar}eA(t)a_0}\tilde{c}_n^\dagger\tilde{c}_{n+1}\right) \tag{2.27}$$

with

$$\tilde{c}_n^\dagger = e^{\frac{i}{\hbar}eA(t)a_0 n}c_n^\dagger$$

Now, let us consider the system with the Born-von Karman periodic boundary conditions (PBC) (see Appendix A.1), where we allow the particle to wrap around the chain and effectively creates a loop, leading to two problems:

(i) the position operator becomes ill-defined (see Appendix A.2) and (ii) an uniform vector potential creates a time-dependent phase which cannot be removed (a vector potential can be seen as due to a magnetic field that is treading the closed ring[2]). As demonstrated in Appendix A.2, the point (ii) can not be resolved and leads to a breaking of gauge invariance of the system. Meanwhile, the implications of the point (i) can circumvented by adopting the Peierls Hamiltonian. So, from equation (2.27), we write the Peierls Hamiltonian with PBC

$$\tilde{\mathcal{H}}_{PBC}^{Peierls}(t) = -h\sum_{n=0}^{N-1}\left(e^{-\frac{i}{\hbar}eA(t)a_0}\tilde{c}^{\dagger}_{\mathsf{mod}(n+1,N)}\tilde{c}_n + e^{\frac{i}{\hbar}eA(t)a_0}\tilde{c}^{\dagger}_n\tilde{c}_{\mathsf{mod}(n+1,N)}\right) \tag{2.28}$$

with

$$\mathsf{mod}\,(n,\,N) = n, n = 0, ...,\, N-1$$
$$\mathsf{mod}\,(n+kN,\,N) = \mathsf{mod}\,(n,\,N)\,,\, k \in \mathbb{Z}$$

[2] Note that the Peierls phase defined in equation (2.28) can be expressed in the form of a time-dependent flux that flows through the ring

$$\phi\,(t) = \int_0^{Na_0} A(t)dx = Na_0A(t)$$

with $\phi_0 = h/e$ being the quanta of magnetic flux. Moreover, note that this phenomenon follows directly from the Third Maxwell equation

$$\int_C \mathbf{E}\cdot dl = -\int_A\left(\frac{\partial \mathbf{B}}{\partial t}\right)\cdot d\mathbf{S}$$

with $d\mathbf{S}$ denoting the differential vector element of surface area **S**, normal to surface C

3 Density Operator and One-Particle Reduced Density Matrix

This chapter is dedicated to the definition and in presenting general properties of the one-particle reduced density matrix or reduced density matrix (rDM), for short. We begin by presenting its equation of motion and expectation value definition. Next, we present its explicit representation in Bloch and Wannier states. Lastly, we study its nearsightedness properties [88]. In particular, how its properties of locality in real-space depends of the system's characteristics, specifically its temperature and bandgap value.

3.1 Density Operator and One-Particle Reduced Density Matrix

When dealing with an ensemble of quantum systems, an effective approach to describe it comprehensively is by employing the density matrix. This mathematical tool provides a complete statistical description of a quantum system, enabling the calculation of observables and make predictions about measurement outcomes. If the system exists in the α-th quantum many-body state with probabilities p_α, the density operator for a mixed quantum state is defined as [89]:

$$\varrho = \sum_\alpha p_\alpha |\alpha\rangle\langle\alpha| \tag{3.29}$$

The principles of Quantum Mechanics can be adapted to describe an ensemble of quantum systems through the use of the density operator. The expectation value of an operator $\mathcal{O}$ is calculated as follows:

$$\langle\mathcal{O}\rangle = \mathrm{Tr}\left(\varrho\mathcal{O}\right) \tag{3.30}$$

It is worth noting that, in the Schrödinger picture, the density operator evolves in time. The equation governing the time evolution of the density matrix is known as the Liouville–von Neumann equation:

$$\frac{d\varrho\left(t\right)}{dt} = \frac{1}{i\hbar}\left[\mathcal{H}\left(t\right), \varrho\left(t\right)\right] \tag{3.31}$$

where the Hamiltonian of the system might be time-dependent quantity.

3.1.1 The Single-Particle Reduced Density Matrix

When we are only interested in expected values of single-particle operators, it becomes advantageous to introduce the single-particle reduced density matrix [89]. By definition, this object corresponds to the following thermal average:

$$\rho_{\beta\beta'} = \left\langle c^\dagger_{\beta'} c_\beta \right\rangle \tag{3.32}$$

where the indices $\{\beta, \beta'\}$ label states in a single-particle basis. Note that its diagonal elements corresponds to the thermal average of the number operator, which represents the number of particles in a determined single-particle state. On the other hand, the non-diagonal elements measure the coherence between two quantum states within the system. They are in general complex numbers and so they can describe interferences.

One can determine the reduced density matrix (rDM)[3] equation of motion by combining both equations (3.31) and (3.32). Its yields

$$\begin{aligned} i\hbar\frac{\partial\rho_{\beta\beta'}}{\partial t} &= i\hbar\frac{\partial}{\partial t}\mathsf{Tr}\left(\varrho\left(t\right)c_{\beta'}^{\dagger}c_{\beta}\right) \\ &= \mathsf{Tr}\left(\left[\mathcal{H}\left(t\right),\varrho\left(t\right)\right]c_{\beta'}^{\dagger}c_{\beta}\right) \\ &= \left\langle\left[c_{\beta'}^{\dagger}c_{\beta},\mathcal{H}\left(t\right)\right]\right\rangle \end{aligned} \tag{3.33}$$

where we used the cyclic properties of the trace. By adopting a noninteracting Hamiltonian with matrix elements

$$\mathcal{H}_{\beta\beta'}\left(t\right) = \left\langle\beta\right|\left(H_0 + V\left(t\right)\right)\left|\beta'\right\rangle$$

where the quantities H_0 and $V\left(t\right)$ are respectively the unperturbed Hamiltonian and the potential energy, respectively. One can evaluate the commutator defined in equation (3.33) as

$$\left\langle\left[c_{\beta'}^{\dagger}c_{\beta},\mathcal{H}_{\beta\beta'}\left(t\right)\right]\right\rangle = \sum_{\alpha}\left(\mathcal{H}_{\beta\alpha}\rho_{\alpha\beta'} - \rho_{\beta\alpha}\mathcal{H}_{\alpha\beta'}\right) \tag{3.34}$$

defining, this way, the reduced density matrix equation of motion [89]:

$$\boxed{i\hbar\frac{\partial\rho_{\beta\beta'}}{\partial t} = \left[\mathcal{H},\rho\right]_{\beta\beta'}} \tag{3.35}$$

In second quantization formalism, we can express the expected value of a single-body operator $\mathcal{O}_1$ [89] as follows:

$$\begin{aligned} \left\langle\mathcal{O}_1\right\rangle &= \sum_{\alpha\alpha'}\mathcal{O}_{\alpha\alpha'}\left\langle c_{\alpha}^{\dagger}c_{\alpha'}\right\rangle \\ &= \sum_{\alpha\alpha'}\mathcal{O}_{\alpha\alpha'}\rho_{\alpha'\alpha} \end{aligned} \tag{3.36}$$

which can be translated into the trace of the matrix elements

$$\boxed{\left\langle\mathcal{O}_1\right\rangle = \mathsf{Tr}\left(\mathcal{O}\rho\right)} \tag{3.37}$$

3.1.2 Explicit Representation of the Reduced Density Matrix in Bloch and Wannier states

We can work out an explicit representation of the one-particle reduced density matrix in both real (in terms of Wannier states) and momentum space (in terms of Bloch states). Let us start by recalling the definition of the reduced density matrix given by the equation (3.32):

$$\rho_{\beta\beta'} = \left\langle c_{\beta'}^{\dagger}c_{\beta}\right\rangle$$

[3] For short, we will start to call it reduced density matrix (rDM)

The idea is to perform a change of basis for the ladder operators. As it is shown in Appendix A.2, we determine the creation and annihilation operators in the new basis

$$c_\beta^\dagger = \sum_\lambda \psi_\lambda^* (\beta)\, c_\lambda^\dagger \tag{3.38}$$

$$c_\beta = \sum_\lambda c_\lambda \psi_\lambda (\beta) \tag{3.39}$$

where we made a change of basis, leading to a different Hilbert space via the projection term $\psi_\lambda (\beta) \equiv \langle \beta | \lambda \rangle$. These results can be applied in the definition of the reduced density matrix, leading to

$$\begin{aligned} \rho_{\beta\beta'} &= \left\langle c_{\beta'}^\dagger c_\beta \right\rangle \\ &= \sum_{\lambda\lambda'} \psi_\lambda^* \left(\beta'\right) \psi_{\lambda'} (\beta) \left\langle c_\lambda^\dagger c_{\lambda'} \right\rangle \\ &= \sum_\lambda f (\epsilon_\lambda)\, \psi_\lambda (\beta)\, \psi_\lambda^* \left(\beta'\right) \end{aligned} \tag{3.40}$$

where λ indexes the eigenstates of the single-particle Hamiltonian and $\{f_{F-D}\}$ are their occupancies dictated by the Fermi-Dirac distribution; the thermal average is evaluated as $\left\langle c_\lambda^\dagger c_{\lambda'} \right\rangle = \delta_{\lambda\lambda'} f (\epsilon_\lambda)$. The equation (3.40) is written at the expense of the basis that diagonalises the Hamiltonian and can be written explicitly as

$$\rho (\mathbf{r}_i, \mathbf{r}_j) = \sum_\lambda f_{F-D} (\epsilon_\lambda)\, \Psi_\lambda (\mathbf{r}_i) \left\{\Psi_\lambda (\mathbf{r}_j)\right\}^* \tag{3.41}$$

One can express this result in terms of Wannier states by writing the eigenfunction in terms of localized orbitals [85]:

$$\Psi_\lambda (\mathbf{r}_i) = \sum_{\mathbf{R},\alpha} \phi_\lambda^\alpha (\mathbf{r}_i)\, w_\alpha (\mathbf{r}_i - \mathbf{R} - \mathbf{s}_\alpha) \tag{3.42}$$

giving

$$\rho (\mathbf{r}_i, \mathbf{r}_j) = \sum_{\mathbf{R},\alpha} \sum_{\mathbf{R}',\beta} w_\alpha (\mathbf{r}_i - \mathbf{R} - s_\alpha)\, \rho_{\alpha\beta} \left(\mathbf{R}, \mathbf{R}'\right) w_\beta^* \left(\mathbf{r}_j - \mathbf{R}' - s_\beta\right) \tag{3.43}$$

where we define $\rho_{\alpha\beta} (\mathbf{R}, \mathbf{R}')$ as

$$\boxed{\rho_{\alpha\beta} \left(\mathbf{R}, \mathbf{R}'\right) = \sum_\lambda f_{F-D} (\epsilon_\lambda)\, \phi_\lambda^\alpha (\mathbf{R}) \left\{\phi_\lambda^\beta \left(\mathbf{R}'\right)\right\}^*} \tag{3.44}$$

By admitting that the system possesses translational symmetry, we can express the equation (3.44) in terms of Bloch states by using the following ansatz:

$$\phi_\lambda^\alpha (\mathbf{R}) \to \phi_{\mathbf{k}n}^\alpha (\mathbf{R}) = \frac{1}{\sqrt{N}} \phi_{\mathbf{k}n}^\alpha e^{i\mathbf{k}\cdot(\mathbf{R}+\mathbf{s}_\alpha)}$$

It reads

$$\boxed{\rho_{\alpha\beta} \left(\mathbf{R}, \mathbf{R}'\right) = \sum_{\mathbf{k}n} f_{F-D} \left(\epsilon_{\mathbf{k}n}\right) e^{i\left(\mathbf{R}+\mathbf{s}_\alpha - \left(\mathbf{R}'+\mathbf{s}_\beta\right)\right)} \phi_{\mathbf{k}n}^\alpha \{\phi_{\mathbf{k}n}^\beta\}^*} \tag{3.45}$$

where the parameters $\mathbf{k}$ and n are the momentum and index of band, respectively.

3.1.3 Decay Properties of the Reduced Density Matrix in Equilibrium applied to Tight-Binding Systems

The reduced density matrix is a diagonal dominant operator, whose off-diagonal elements decay with increasing distance from diagonal. The exact decaying behaviour depends on the material characteristics [78, 79, 80, 81] and its locality properties open up the opportunity to implement linear scaling algorithms [90, 91]. In particular, one can observe an exponential decay for systems with a bandgap and metals at finite temperature. Conversely, the decay is algebraic for metals at $T = 0$K.

With this in mind, in this section we shall study the nearsightedness properties in real-space of the rDM by applying the equation (3.45) to 1D periodic crystalline solids. As an example, we will focus on the monoatomic and diatomic linear chain tight-binding (TB) systems (see Figure 1), corresponding to the situations where we will have a gapless and a gapped system, with Born-von Karman periodic boundary conditions (PBC)[4]. In practice, we will be solving the rDM in equilibrium

$$\rho_{\alpha\beta}\left(\mathbf{R},\mathbf{R}'\right) = \sum_{\mathbf{k}n} f_{F-D}\left(\epsilon_{\mathbf{k}n}\right) e^{i\left(\mathbf{R}+\mathbf{s}_\alpha-\left(\mathbf{R}'+\mathbf{s}_\beta\right)\right)} \phi^{\alpha}_{\mathbf{k}n}\{\phi^{\beta}_{\mathbf{k}n}\}^* \tag{3.46}$$

where the eigenvalues and eigenstates are determined by the stationary Schrödinger equation applied to a Hamiltonian expressed in terms of Bloch states

$$\mathcal{H}^B\Psi_\lambda = \epsilon_\lambda\Psi_\lambda \tag{3.47}$$

where λ indexes the eigenvalues and eigenstates. The Bloch Hamiltonians for both the monoatomic and diatomic linear chains are defined in (2.17) and (2.8), and they are given by

$$\begin{aligned} \mathcal{H}^B_{\text{monoatomic}} &= \epsilon - 2h\cos\left(ka_0\right) \\ \mathcal{H}^B_{\text{diatomic}} &= \begin{bmatrix} \epsilon_A & -h\left(1+e^{i2ka_0}\right) \\ -h\left(1+e^{-i2ka_0}\right) & \epsilon_B \end{bmatrix} \end{aligned} \tag{3.48}$$

3.1.3.1 The Special Case of T = 0K

We want to showcase the properties mentioned above, and, to do so, let us adopt a specific tight-binding system. The simplest system that comes to mind is a monoatomic linear chain, a gapless system, under periodic boundary conditions with N discrete sites and with lattice parameters: on-site energy $\epsilon = 0\,eV$, transfer function (hopping) $h = 1\,eV$ and lattice constant $a_0 = 1\,$Å. In this study, we will be considering a temperature $T = 0$K and a chemical potential $\mu = 0\,eV$.

The reduced density matrix (rDM) possesses special properties at a temperature $T = 0$K, in particular the

[4] For additional information about PBC, see Appendix III

operator has an analytical solution. Starting by its definition, it can be evaluate it by the following matter:

$$\begin{aligned}\rho(\Delta r) &= \frac{1}{N}\sum_k e^{ik\Delta r} f(\epsilon_k) \\ &= \int_{|k|<k_F} \frac{dk}{2\pi} e^{ik\Delta r} \\ &= \frac{1}{2}\,\mathrm{sinc}\,(k_F \Delta r)\end{aligned} \tag{3.49}$$

where we applied the thermodynamic limit, meaning that in the condition $N \to \infty$, we can do

$$\frac{1}{N}\sum_k [\dots] \to \frac{1}{(2\pi)}\int dk\,[\dots] \tag{3.50}$$

Since we set the chemical potential at $\mu = 0\,eV$, it means that we have a half-filled system, setting this way the Fermi's wave vector on the value $|k_F| = \pi/2a_0$. The Figure 4(a) shows the rDM evaluated at $T = 0$K numerically and its correspondence with a fit to a cardinal sin function, dictated by the analytical solution. We also observe an algebraic decay under these conditions. In Figure 4(b) is represented the rDM in its matrix representation in terms of its absolute values. It shows a diagonal dominant matrix, whose off-diagonal elements, associated with local decoherences, decay with increasing distance from the diagonal.

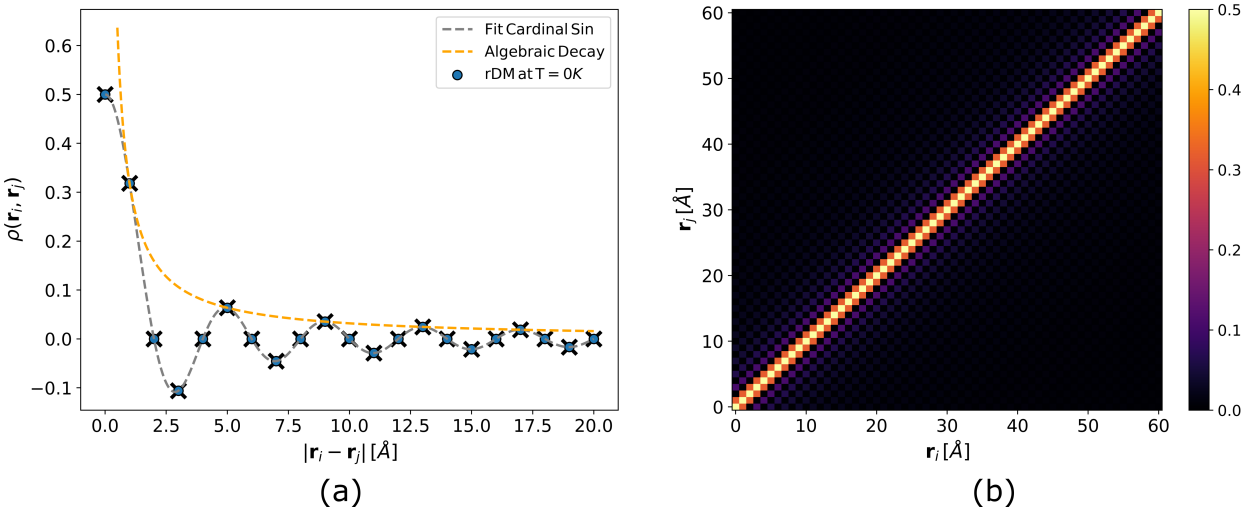

Figure 4: Study of the rDM at $T = 0$K and $\mu = 0\,eV$ **(a)** Graphical representation of the reduced density matrix at $T = 0$K and a fit to a cardinal sin function of a monoatomic linear chain. It is also shown the correspondent algebraic decay. **(b)** Close up of the rDM matrix in terms of its absolute values. Lattice parameters: $\epsilon = 0\,eV$, $h = 1\,eV$, $a_0 = 1$ Å and $N = 400$.

3.1.3.2 Exponential Decay with the Temperature

In this subsection, we want to show that the rDM displays an exponential decaying behaviour with the temperature. So, let us use the following ansatz [81, 90]:

$$\log_{10}\left(\frac{\rho_T(\Delta r)}{\rho_{T=0}(\Delta r)}\right) = -\alpha_0\left(T\right)\Delta r \tag{3.51}$$

where $\Delta r = |\mathbf{r}_i - \mathbf{r}_j|$ and the parameter $\alpha_0\left(T\right) = \alpha T$ is a decay parameter that depends linearly with the temperature.

In Figure 5(a) is a graphical representation of the rDM propagation in real-space in relation to the distance between lattice points for different temperatures. These results show that the introduction of a finite temperature to the system leads to a change of its local decay behaviour. It is also possible to recognize a certain symmetric behaviour with the regard to the rDM midway and at the end as it propagates through the linear chain. This feature is a consequence of adopting the Born-von Karman periodic boundary conditions. Let us study the rDM decay properties by applying the equation (3.51), where in Figure 5(b) are depicted the results. The results show that the decay rate increases with temperature, where the value of the off-diagonal elements of the rDM approaches to numerical zeros. In order to access more information about this dependency with temperature, one can select a region to do a linear fit of the data (see Figure 5(c)) and compute the logarithm of the ratio between rDM at temperature T relative to its absolute zero, $T = 0$K, and perform a linear fit to the numerical data. If we take the slope of each linear fit for a given temperature (the parameter $\alpha_0\left(T\right)$) and plot it in function of the temperatures, as shown in the Figure 5(d), we observe a linear dependency between the rDM's decay rate (α) with the temperature applied to the system. This feature opens up the opportunity to manipulate and control the properties of locality of the rDM in metals.

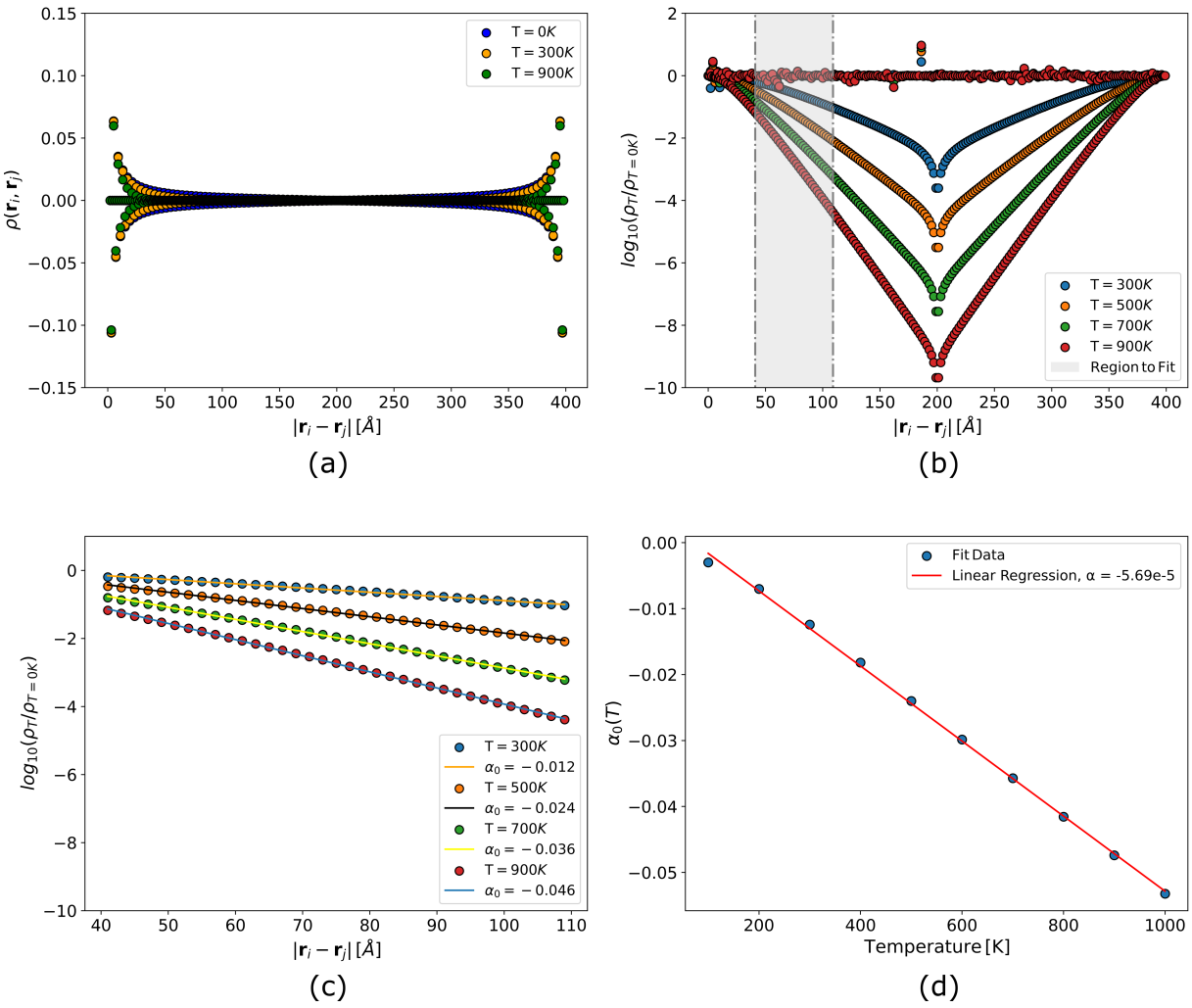

Figure 5: Study of rDM's in real-space decay rate dependency with temperature (T) of the system in a monoatomic linear chain with periodic boundary conditions. **(a)** rDM propagation for three different temperatures **(b)** Here is computed the logarithm of the ratio between the rDM at temperature T relative to absolute zero, $T = 0$K. In grey is delimited the region of data to perform the linear fit. **(c)** Linear fit applied to the numerical data, determining the quantity $\alpha_0\,(T)$. **(d)** Plot of the $\alpha_0\,(T)$ values in function of the temperatures, determining the decay parameter α. Lattice parameters: $\epsilon = 0\,eV$, $h = 1\,eV$, $a_0 = 1\,$Å and $N = 400$. The chemical potential adopted is set at $\mu = 0\,eV$.

3.1.3.3 Exponential Decay with the Gap

In a similar manner to the previous approach, we now aim to access the reduced density matrix dependency with the value of the gap. In this subsection, we will study the rDM propagation in a diatomic linear chain with a bandgap of value Δ and with Born-von Karman periodic boundary conditions. We will consider a temperature $T = 0$K and a chemical potential $\mu = 0\,eV$.

We want to show that the rDM displays an exponential decaying behaviour with the value of the bandgap. So, let us use the following ansatz [81, 90]:

$$\log_{10}\left(\frac{\rho_{\Delta}(\Delta r)}{\rho_{\Delta=0}(\Delta r)}\right) = -\gamma_0\left(\Delta\right)\Delta r \tag{3.52}$$

where $\Delta r = |\mathbf{r}_i - \mathbf{r}_j|$ and the parameter $\gamma_0\left(\Delta\right) = \gamma\Delta$ is a decay parameter that depends linearly with the bandgap value.

In Figures 6(a) and (c) are displayed the results for the logarithm of the ratio between rDM with a bandgap value Δ relative to $\Delta = 0$ for the cases ρ_{11} and ρ_{12}, respectively, which corresponds to the rDM orbital components. One can select a region to perform a linear fit to the numerical data and determine the corresponding slopes (see Figures 6(b) and (d)). If we take the slope of each linear fit (the amplitudes $\gamma_0\left(\Delta\right)$) and plot it in function of the gap value, as shown in Figure 7, we observe a linear dependency between the rDM's decay rate (γ) and the bandgap of the system, opening up the opportunity to manipulate and control the properties of locality of the rDM. Another important observation is that the decay properties of the rDM are more pronounced with respect to the system's bandgap than the temperature. This allows semiconductor/insulator systems to harness the nearsightedness properties of the rDM to their maximum capacity.

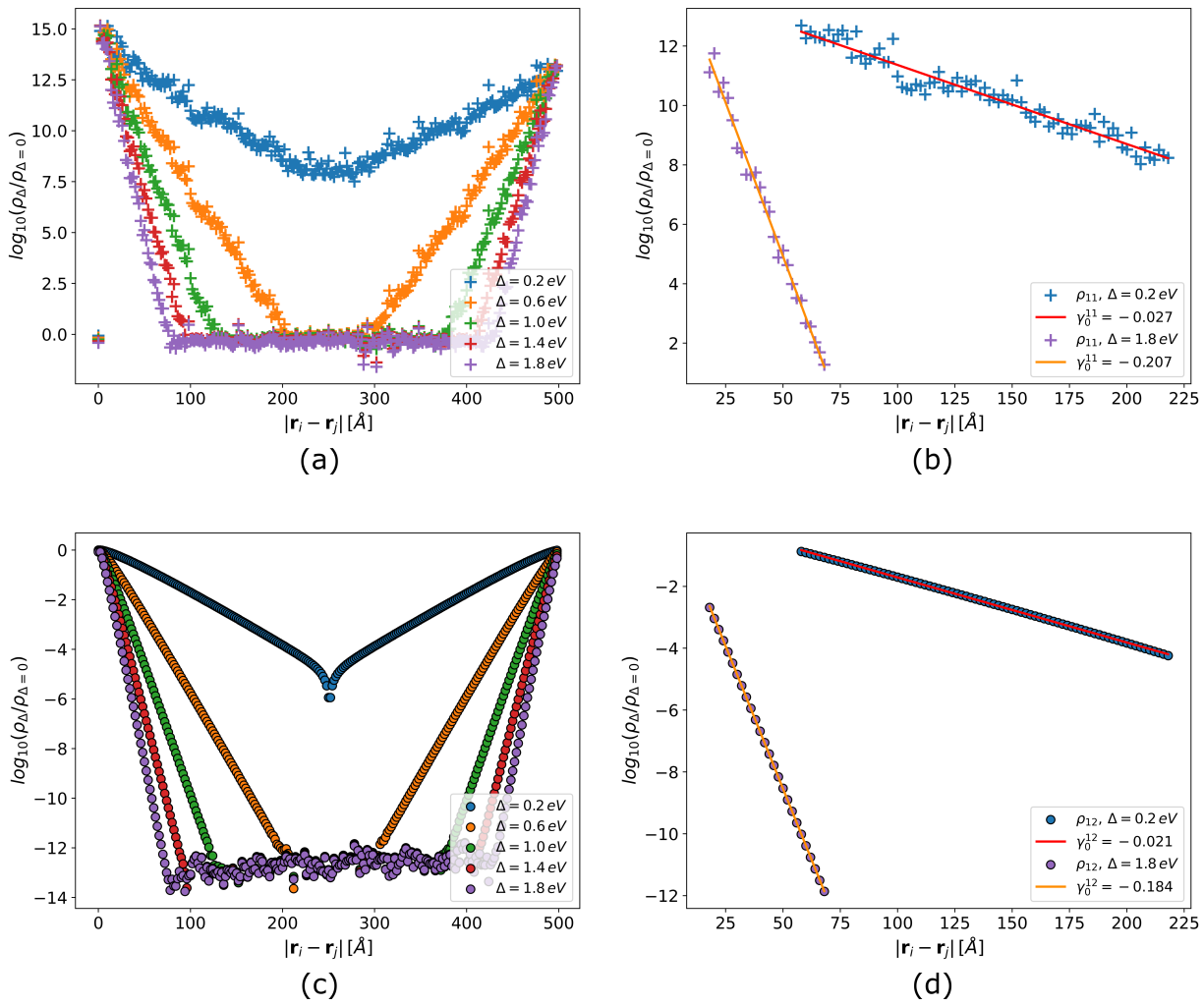

Figure 6: Study of rDM's decay rate dependency with the bandgap (Δ) of the system in a diatomic linear chain with periodic boundary conditions. In **(a)** and **(c)** are computed the logarithm of the ratio between the rDM with bandgap Δ relative to its reference value of $\Delta = 0$ for both orbital components ρ_{11} and ρ_{12}, respectively. In **(b)** and **(d)** are represented the linear fit applied to the numerical data for both rDM orbital components ρ_{11} and ρ_{12}, respectively. This way, we determine the quantities γ_0^{11} and γ_0^{12}. Lattice parameters: $h = 1\,eV$, $a_0 = 1\,$Å and $N = 500$; Fermi parameters: $T = 0$K and $\mu = 0\,eV$.

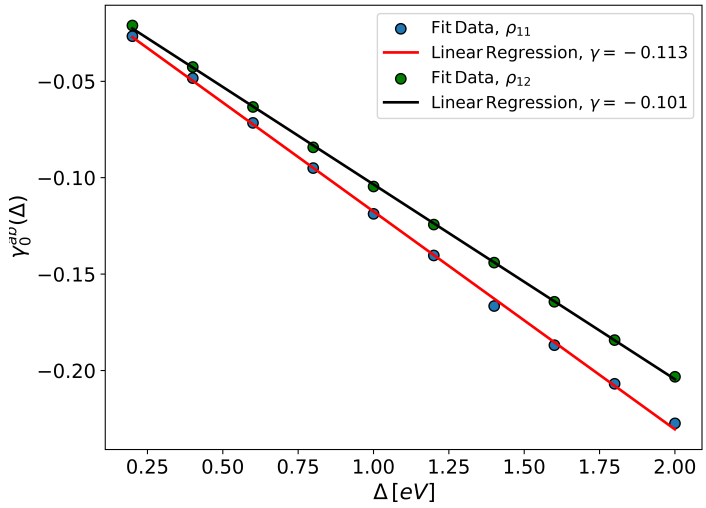

Figure 7: Plot of the respetive values of $\gamma_0^{ab}(\Delta)$ in function of the different values of bandgaps (Δ) for both orbital components ρ_{11} and ρ_{12}, determining the decay parameter γ. The indices $\{ab\}$ correspond to the rDM's orbital components in study. Meaning, that for the case ρ_{11}, the respective amplitude is $\gamma_0^{11}(\Delta)$. Lattice parameters: $h = 1\,eV$, $a_0 = 1\,$Å and $N = 500$; Fermi parameters: $T = 0$K and $\mu = 0\,eV$.

4 Time-dependent Mean-Field Hartree-Fock approximation

In this chapter, we introduce the theoretical framework that will be used throughout this work, based on a time-dependent mean-field Hartree-Fock approximation applied to the single-particle reduced density matrix. The topics covered in this section are based on the reference [92].

4.1 Reduced Density Matrix's Equation of Motion

Take a many-body system of electrons in equilibrium. The system can be described by a Hamiltonian given by two contributions: a single-particle (free of interaction) Hamiltonian and a two-particle Hamiltonian, to contabilize electron-electron interactions. Expanded in an arbitrary electronic basis $\{\phi_a\}$, we can write it in the following compact way[5]:

$$\begin{aligned}\mathcal{H} &= \mathcal{H}_0 + \mathcal{H}_{e-e} \\ &= \sum_{ab} h_{ab} c_a^\dagger c_b + \frac{1}{2}\sum_{abcd} V_{cd}^{ab} c_a^\dagger c_b^\dagger c_c c_d \end{aligned} \tag{4.53}$$

with the Hamiltonians matrix elements being

$$h_{ab} = \int d^3\mathbf{r} \phi_a^* (\mathbf{r}) \left[\frac{p^2}{2m} + U(\mathbf{r})\right] \phi_b (\mathbf{r}) \tag{4.54}$$

$$V_{cd}^{ab} = \int d^3\mathbf{r} d^3\mathbf{r}' \phi_a^* (\mathbf{r}) \phi_b^* (\mathbf{r}') V (\mathbf{r} - \mathbf{r}') \phi_c (\mathbf{r}') \phi_d (\mathbf{r}) \tag{4.55}$$

Here, the operators $c_a^\dagger$ (c_a) create(annihilate) an electron in the state characterized by the wavefunction $\phi_a(\mathbf{r})$, with $\mathbf{r}$ being the electron's position vectors. The indices $\{a, b, c, d\}$ represent general fermionic states within the system, implicitly establishing the system's degrees of freedom[6]. The term h_{ab} describes de free-particle Hamiltonian matrix elements with the kinetic operator and $U(\mathbf{r})$ being a generic static potential[7]. The two-body term V_{cd}^{ab} corresponds to the two-particle interaction matrix elements with a generic electrostatic potential $V(\mathbf{r} - \mathbf{r}')$ between two indistinguishable particles with an interaction range of $|\mathbf{r} - \mathbf{r}'|$. As usual in this type of potentials, the spatial inversion symmetry $V(\mathbf{r} - \mathbf{r}') = V(\mathbf{r}' - \mathbf{r})$ is verified. Consequently, the interaction matrix elements obey the symmetries

$$V_{cd}^{ab} = V_{dc}^{ba} \tag{4.56}$$

$$\left(V_{cd}^{ab}\right)^* = V_{ba}^{dc} \tag{4.57}$$

These results are demonstrated in Appendix A.2.

Consider now that the system, initially in equilibrium, is driven out-of-equilibrium via an external time-dependent stimuli. To the equilibrium Hamiltonian we add a time-dependent perturbation described by a one-particle term,

[5] These results are derived in Appendix A.2

[6] Per example, they could be indices associated momentum $\mathbf{k}$, spin σ, ...

[7] The contribution due to external influences, such as for electrons moving in a periodic potential for a lattice of ions or for atoms in a lattice vibrating about their fixed equilibrium positions

which is switched on for $t \geq t_0$, that couples the external perturbation. In particular, we will consider a perturbation via a time-dependent electric pulse written in a dipole approximation. In second quantization, the Hamiltonian (4.53) now reads

$$\begin{aligned}\mathcal{H}(t) &= \mathcal{H}_0 + \mathcal{H}_{e-e} + \mathcal{H}_I^L(t) \\ &= \sum_{ab} h_{ab}(t)\, c_a^\dagger c_b + \frac{1}{2}\sum_{abcd} V_{cd}^{ab} c_a^\dagger c_b^\dagger c_c c_d\end{aligned} \tag{4.58}$$

where the time-dependent term includes light-matter coupling via Peierls substitution derived in Section 2.2. In this model, other potential effects originating from lattice vibrations, such as phonon interactions, are neglected. This is valid as we intend to investigate extremely brief time intervals within the out-of-equilibrium system, typically in the femtosecond range, where electron motion becomes the relevant contribution [63].

The response of the system to the external "force" can be monitored by measuring different observables. In a linear response regime, we will focus in monitoring the time-evolution of the expectation value of single-particle quantities. By recalling its definition in equation (3.37), a single-particle observable evolves in time as

$$\langle \mathcal{O}_1 \rangle (t) = \sum_{ab} \mathcal{O}_{ab} \rho_{ba}(t) \tag{4.59}$$

where the equal-time rDM is given by

$$\rho_{ba}(t) = \left\langle c_a^\dagger(t)\, c_b(t) \right\rangle \tag{4.60}$$

We will formulate our time-dependent Hartee-Fock approximation with the rDM as the central object and, for that, we need to determine its equation of motion. In a Heisenberg picture, the time evolution of fermionic operators is governed by the Heisenberg equation

$$\frac{d\mathcal{O}_H(t)}{dt} = \frac{i}{\hbar}\left[\mathcal{H}, \mathcal{O}_H(t)\right] \tag{4.61}$$

Accordingly, the rDM equation of motion reads

$$\frac{d\rho_{ab}(t)}{dt} = \frac{i}{\hbar}\left\langle \left[\mathcal{H}, c_b^\dagger(t)\right] c_a(t) \right\rangle + \frac{i}{\hbar}\left\langle c_b^\dagger \left[\mathcal{H}, c_a(t)\right] \right\rangle \tag{4.62}$$

where each of the commutators are computed as

$$\begin{aligned}\left[\mathcal{H}, c_b^\dagger\right] &= h_{\alpha b}(t)\, c_\alpha^\dagger + \frac{1}{2} V_{\gamma b}^{\alpha\beta} c_\alpha^\dagger c_\beta^\dagger c_\gamma - \frac{1}{2} V_{b\delta}^{\alpha\beta} c_\alpha^\dagger c_\beta^\dagger c_\delta \\ \left[\mathcal{H}, c_a\right] &= -h_{a\beta}(t)\, c_\beta + \frac{1}{2} V_{\gamma\delta}^{\alpha a} c_\alpha^\dagger c_\gamma c_\delta - \frac{1}{2} V_{\gamma\delta}^{a\beta} c_\beta^\dagger c_\gamma c_\delta\end{aligned}$$

Here we have used the Einstein's notation such that repeated indices are summed over and omit the time dependency in fermionic operators for brevity. Therefore, by applying the previous results in equation (4.62), the rDM equation of motion is established as

$$\begin{aligned}\frac{d\rho_{ab}(t)}{dt} &= \frac{i}{\hbar} h_{\alpha b}(t)\, \rho_{a\alpha} - \frac{i}{\hbar} h_{a\beta}(t)\, \rho_{\beta b} \\ &+ \frac{i}{2\hbar}\left(V_{\gamma b}^{\alpha\beta} \left\langle c_\alpha^\dagger c_\beta^\dagger c_\gamma c_a \right\rangle - V_{b\delta}^{\alpha\beta} \left\langle c_\alpha^\dagger c_\beta^\dagger c_\delta c_a \right\rangle \right) \\ &+ \frac{i}{2\hbar}\left(V_{\gamma\delta}^{\alpha a} \left\langle c_b^\dagger c_\alpha^\dagger c_\gamma c_\delta \right\rangle - V_{\gamma\delta}^{a\beta} \left\langle c_b^\dagger c_\beta^\dagger c_\gamma c_\delta \right\rangle \right)\end{aligned} \tag{4.63}$$

Note that the interaction term, defined as a two-body term, generated thermal averages with four operators. Handling such terms is quite challenging, since the hierarchy of the equations of motion would never close among themselves. To simplify our model, we introduce a mean-field approximation, where the idea is to decouple the two-body interaction averages into a product of an effective single-particle averages.

4.2 Mean-Field Hartree-Fock Theory

As mentioned above, we want to introduce a mean-field approximation to decouple the quartic term averages into a product of effective single-particle averages [93]. In these conditions, we can then make use of *Wick's theorem* to make all the possible two operator contractions from the four operators in equation (4.63). Let us demonstrate this for the first term

$$\left\langle c_\alpha^\dagger c_\beta^\dagger c_\gamma c_a \right\rangle \simeq \left\langle \overbrace{c_\alpha^\dagger c_\beta^\dagger} c_\gamma c_a \right\rangle + \left\langle \overbrace{c_\alpha^\dagger \, \overbrace{c_\beta^\dagger c_\gamma} \, c_a} \right\rangle + \left\langle \overbrace{c_\alpha^\dagger \, \overbrace{c_\beta^\dagger c_\gamma c_a}} \right\rangle \tag{4.64}$$

with each of the contractions giving

$$\left\langle \overbrace{c_\alpha^\dagger c_\beta^\dagger} c_\gamma c_a \right\rangle = \langle c_\alpha^\dagger c_\beta^\dagger \rangle \langle c_\gamma c_a \rangle \tag{4.65}$$

$$\left\langle \overbrace{c_\alpha^\dagger \, \overbrace{c_\beta^\dagger c_\gamma} \, c_a} \right\rangle = -\langle c_\alpha^\dagger c_\gamma \rangle \langle c_\beta^\dagger c_a \rangle \tag{4.66}$$

$$\left\langle \overbrace{c_\alpha^\dagger \, \overbrace{c_\beta^\dagger c_\gamma c_a}} \right\rangle = \langle c_\alpha^\dagger c_a \rangle \langle c_\beta^\dagger c_\gamma \rangle \tag{4.67}$$

Here, the negative sign in the second contraction arises directly from the anti-commutating nature of the fermionic operators[8]. The term (4.65) is zero, with thermal averages $\langle c^\dagger c^\dagger \rangle = \langle cc \rangle = 0$, as we are in a non-superconducting electronic system[9]. This procedure means that the thermal average described in (4.64) can be written at the expense of the product of single-particle reduced density matrices

$$\left\langle c_\alpha^\dagger c_\beta^\dagger c_\gamma c_a \right\rangle \simeq -\rho_{\gamma\alpha}\rho_{a\beta} + \rho_{a\alpha}\rho_{\gamma\beta} \tag{4.68}$$

Continuing with the same approach, it becomes evident that the remaining terms can be expressed as follows:

$$\langle c_\alpha^\dagger c_\beta^\dagger c_\delta c_a) = -\rho_{\delta\alpha}\rho_{a\beta} + \rho_{a\alpha}\rho_{\delta\beta} \tag{4.69}$$

$$\left\langle c_b^\dagger c_\alpha^\dagger c_\gamma c_\delta \right\rangle = -\rho_{\gamma b}\rho_{\delta\alpha} + \rho_{\delta b}\rho_{\gamma\alpha} \tag{4.70}$$

$$\left\langle c_b^\dagger c_\beta^\dagger c_\gamma c_\delta \right\rangle = -\rho_{\gamma b}\rho_{\delta\beta} + \rho_{\delta b}\rho_{\gamma\beta} \tag{4.71}$$

[8] There is another equivalent way of doing this. One could check for the a minus sign by counting the n times the Wick's contraction line intersects: if n is odd number then there will be a negative sign. Alternatively, we could see it as the number of jumps needed to move an operator from one position to another $\left\langle c_a^\dagger \underbrace{c_b c_c ... c_y}_{n} c_z^\dagger \right\rangle = (-1)^n \left\langle c_a^\dagger c_z^\dagger c_b c_c ... c_y \right\rangle$, where n corresponds to the number of jumps

[9] A superconducting system is an example where this type of operator pairing is nonzero to take into account the Cooper pairs

By going one step further in manipulating these terms by working with the mute indices and exploiting the symmetry properties of the potentials (4.56) and (4.57), the rDM equation of motion given by equation (4.63) reads

$$\begin{aligned} i\hbar\frac{d\rho_{ab}(t)}{dt} &= h_{a\beta}(t)\,\rho_{\beta b}(t) - \rho_{a\alpha}(t)\,h_{\alpha b}(t) \\ &+ \frac{1}{2}\left(\left[V^{a\alpha}_{\delta\gamma} + V^{\alpha a}_{\gamma\delta} - V^{a\alpha}_{\gamma\delta} - V^{\alpha a}_{\delta\gamma}\right]\rho_{\delta\alpha}(t)\right)\rho_{\gamma b}(t) \\ &- \frac{1}{2}\rho_{a\beta}(t)\left(\left[V^{\beta\alpha}_{\delta b} + V^{\alpha\beta}_{b\delta} - V^{\alpha\beta}_{\delta b} - V^{\beta\alpha}_{b\delta}\right]\rho_{\delta\alpha}(t)\right) \end{aligned} \tag{4.72}$$

Now, we define the Hartree and Fock self-energy terms as

$$\Sigma^{H}_{a\gamma}[\rho(t)] = \sum_{\alpha\delta} V^{a\alpha}_{\delta\gamma}\rho_{\delta\alpha}(t) \tag{4.73}$$

$$\Sigma^{F}_{a\gamma}[\rho(t)] = -\sum_{\alpha\delta} V^{a\alpha}_{\gamma\delta}\rho_{\delta\alpha}(t) \tag{4.74}$$

defining the equation (4.72) as

$$\begin{aligned} i\hbar\frac{d\rho_{ab}(t)}{dt} &= h_{a\beta}(t)\,\rho_{\beta b}(t) - \rho_{a\alpha}(t)\,h_{\alpha b}(t) \\ &+ \left(\Sigma^{H}_{a\gamma}[\rho(t)] + \Sigma^{F}_{a\gamma}[\rho(t)]\right)\rho_{\gamma b}(t) - \rho_{a\beta}(t)\left(\Sigma^{H}_{\beta b}[\rho(t)] + \Sigma^{F}_{\beta b}[\rho(t)]\right) \end{aligned} \tag{4.75}$$

Notice that in general the single-particle Hamiltonian h contained in the light-matter coupling Hamiltonian $h_{ab}(t)$ already has its origin in a mean-field calculation. Therefore, in order to avoid a double counting of interaction effects, one should subtract from the self-energies the contribution from equilibrium:

$$\Sigma^{H/F}[\rho(t)] \to \Sigma^{H/F}\left[\rho(t) - \rho^{(0)}\right]$$

By implementating these corrections in the equation (4.75) and by noticing that it can be expressed as a commutator, the expression can be written in a more compact way:

$$\boxed{\begin{aligned} i\hbar\frac{d\rho(t)}{dt} &= \left[\mathcal{H}_{TDHF}(t), \rho(t)\right] \\ \text{with } \mathcal{H}_{TDHF}(t) &= \mathbf{h}(t) + \Sigma^{H}\left[\rho(t) - \rho^{(0)}\right] + \Sigma^{F}\left[\rho(t) - \rho^{(0)}\right] \end{aligned}} \tag{4.76}$$

With this procedure, we define the *time-dependent mean-field Hartree-Fock* Hamiltonian.

A noteworthy commentary is relative to how we identify the Hartree and Fock self-energy terms. Note that we intentionally defined the Fock self-energy term in equation (4.74) as an attractive interaction by introducing the negative sign. This lowers the total energy of the system, promoting the formation of bound electron-hole states. On the other hand, the Hartree self-energy term will govern the renormalization of the exciton binding energy and optical strength (and hence the optical spectrum), as well as spin-splitting effects [94]. It is worth mentioning that while there might not be an apparent distinction between these two terms in this formalism, many-body perturbation theory reveals that the Hartree and Fock interactions are actually screened differently, as we may not apply screening to the Hartree interaction (as one might expect) because doing so would effectively account for screening twice. This

is because the Hartree interaction inherently incorporates a form of self-screening [95, 94, 96, 97], at least within the so-called *S-approximation* [95, 94], which holds true for the type of systems here discussed. For that reason, we will express the potential in equation (4.74) with a symbol "W", representing a screened interaction instead of the bare interaction denoted by "V", which the latter will still be used in the definition of the Hartree term.

5 Excitonic Eigenvalue problem in Crystals

In this chapter, we begin by studying the linear response theory of an interacting fermionic system in the presence of an external time-dependent perturbation term. Next, we determine the electron-hole Hamiltonian, also refer to as the Bethe-Salpeter Hamiltonian, by simplifying the previous problem by choosing to work in a basis that diagonalizes the free-particle Hamiltonian and in a zero temperature regime. This approach to the problem enable us to formulate a linear response eigenvalue problem, which corresponds to the linear response within this time-dependent Hartree-Fock scheme. Moreover, we derive the explicit form of the two-particle electron-hole Hamiltonian for crystalline systems in a Bloch states basis and its corresponding excitonic eigenvalue problem. Lastly, we apply the previous general theory to the case of excitons in a cristaline insulator/semiconductor. In particular, we will see how the linear response eigenvalue problem, which describes excitons, can be approximated by an hidrogenoid problem, usually referred to as the Wannier equation. The topics covered in this section are based on the reference [92].

5.1 Linear Response Theory

One can solve the equations (4.76) in order to obtain the full response of a system (that is otherwise unperturbed and in equilibrium) to a time-varying external perturbation. Nevertheless, quite often, there is an interest in the regime where the "force" is weak, and the system exhibits a linear response to the stimuli. In linear response theory, the idea is to only account for first (linear) order response. Therefore, we start by admiting that rDM can be expanded in a power series of a formal expansion parameter λ

$$\rho\left(t\right)=\sum_{n}\lambda^{n}\rho^{(n)}\left(t\right) \tag{5.77}$$

Substituting this series in the equation of motion defined in (4.76) and by retaining only the terms up to first order, the majority of the terms are null: the term $\left[\mathbf{h}^{(0)},\rho^{(0)}\right]$ is zero, since, in equilibrium, $\rho^{(0)}$ is a function of occupation of the single-particle Hamiltonian $\mathbf{h}^{(0)}$, the terms $\left[\mathbf{h}^{(1)}\left(t\right),\rho^{(1)}\right]$ and $\left[\Sigma^{H}\left[\rho^{(1)}\right]+\Sigma^{F}\left[\rho^{(1)}\right],\rho^{(1)}\right]$ are neglected as they are a second order contributions. Within a *linear approximation*, we obtain

$$i\hbar\frac{d\rho^{(1)}\left(t\right)}{dt}=\left[\mathbf{h}^{(0)},\rho^{(1)}\left(t\right)\right]+\left[\mathbf{h}^{(1)}(t),\rho^{(0)}\right]+\left[\Sigma^{H}\left[\rho^{(1)}\left(t\right)\right]+\Sigma^{F}\left[\rho^{(1)}\left(t\right)\right],\rho^{(0)}\right] \tag{5.78}$$

where we have expanded the interaction term defined via Peierls substitution in a power series of λ with respect to the vector potential $A\left(t\right)$. In zeroth-order approximation, we will have the free-particle term $\mathbf{h}(t)\equiv\mathbf{h}^{(0)}$, with $A\left(t\right)=0$. In a first-order approximation, a linear term $\mathbf{h}^{(1)}$ in $A(t)$. Recalling the definition of the Hartree/Fock self-energies defined in (4.73) and (4.74),

$$\Sigma_{ab}^{H}\left[\rho\right]=\sum_{cd}V_{cb}^{ad}\rho_{cd}$$

$$\Sigma_{ab}^{F}\left[\rho\right]=-\sum_{cd}W_{bc}^{ad}\rho_{cd}$$

we write it more explicitly

$$i\hbar\frac{d\rho_{ab}^{(1)}(t)}{dt}-\left(h_{ac}^{(0)}\rho_{cb}^{(1)}(t)-\rho_{ac}^{(1)}(t)\,h_{cb}^{(0)}\right)=\left(h_{ac}^{(1)}(t)\,\rho_{cb}^{(0)}-\rho_{ac}^{(0)}h_{cb}^{(1)}(t)\right)+\left[\left(V_{ec}^{ad}-W_{ce}^{ad}\right)\rho_{cb}^{(0)}-\rho_{ac}^{(0)}\left(V_{eb}^{cd}-W_{be}^{cd}\right)\right]\rho_{ed}^{(1)}(t) \tag{5.79}$$

Note that here we are omitting the summations involving repeated indices by adopting the Einstein's notation. Expanding both the external perturbation and the correction to the density matrix in a Fourier transform in time,

$$A(t)=\int\frac{d\omega}{2\pi}e^{-i\omega t}A(\omega)$$
$$\rho^{(1)}(t)=\int\frac{d\omega}{2\pi}e^{-i\omega t}\rho^{(1)}(\omega)$$

the equation (5.79) yields

$$i\hbar\omega\rho_{ab}^{(1)}(\omega)-\left(h_{ac}^{(0)}\rho_{cb}^{(1)}(\omega)-\rho_{ac}^{(1)}(\omega)\,h_{cb}^{(0)}\right)=\left(h_{ac}^{(1)}(\omega)\,\rho_{cb}^{(0)}-\rho_{ac}^{(0)}h_{cb}^{(1)}(\omega)\right)+\left[\left(V_{ec}^{ad}-W_{ce}^{ad}\right)\rho_{cb}^{(0)}-\rho_{ac}^{(0)}\left(V_{eb}^{cd}-W_{be}^{cd}\right)\right]\rho_{ed}^{(1)}(\omega) \tag{5.80}$$

We may rewrite the linear response[10] as

$$\left(\hbar\omega\delta_{ab}^{cd}-\mathcal{H}_{ab}^{cd}\right)\rho_{cd}^{(1)}(\omega)=J_{ab}(\omega) \tag{5.81}$$

where $\mathcal{H}_{ab}^{cd}$ represents the effective two-particle Hamiltonian and $J_{ab}(\omega)$ the source term; the compact quantity $\delta_{ab}^{cd}\equiv\delta_{ac}\delta_{bd}$. By comparing equations (5.80) and (5.81), we readily define the source term as

$$J_{ab}(\omega)=\left(h_{ab}^{(1)}(\omega)\,\rho_{bc}^{(0)}-\rho_{ac}^{(0)}h_{cb}^{(1)}(\omega)\right) \tag{5.82}$$

The two-particle Hamiltonian is dictated by two contributions: the noninteracting term and the two interacting terms, given by the Hartree and Fock terms. After some algebraic manipulation by playing with the mute indices while making use of the symmetry properties of the potential, it reads

$$\mathcal{H}_{ab}^{cd}=\left(h_{ac}^{(0)}\delta_{db}-\delta_{ac}h_{db}^{(0)}\right)+\left(V_{ce}^{ad}\rho_{eb}^{(0)}-\rho_{ae}^{(0)}V_{cb}^{ed}\right)-\left(W_{ec}^{ad}\rho_{eb}^{(0)}-\rho_{ae}^{(0)}W_{bc}^{ed}\right) \tag{5.83}$$

where, in the above equation, the first term is the free particle term, the second comes from the Hartree interaction and third from the Fock interaction. The previous expression simplifies significantly if one chooses to work in a basis that diagonalizes the free-particle Hamiltonian, such that

$$h_{ac}^{(0)}=\epsilon_a\delta_{ac}\text{ and }\rho_{ab}^{(0)}=f_a\delta_{ab} \tag{5.84}$$

[10] At linear order, the system response possesses a larger contribution at frequencies ω, which are in resonance with the characteristic frequencies of the system

the source term (5.82) and the two-particle Hamiltonian (5.83) read

$$J_{ab}(\omega) = (f_b - f_a)\, h^{(1)}_{ab}(\omega) \tag{5.85}$$

$$\mathcal{H}^{cd}_{ab} = (\epsilon_a - \epsilon_b)\,\delta_{ac}\delta_{db} + (f_b - f_a)\left(V^{ad}_{cb} - W^{ad}_{bc}\right) \tag{5.86}$$

where ϵ_a is the occupational energy of the state a and $f_a \equiv f_{F-D}(\epsilon_a)$ is the occupation function of the state given by the Fermi-Dirac distribution.

5.1.1 Zero Temperature Regime

Let us consider the case of an insulator at absolute zero. Under this regime, the Fermi-Dirac distribution behaves like a Heaviside function. Now, considering the previous basis that diagonalizes the single-particle Hamiltonian, these conditions restricts the system's degrees of freedom into two possible fermionic states: either is an occupied state $\{o_i\}$ or an empty $\{e_i\}$ state, resulting in $f_o = 1$ or $f_e = 0$. We observe that the Hamiltonian $\mathcal{H}^{cd}_{ab}$ possesses four indices associated with two degrees of freedom, totalling 16 matrix blocks from all different combinations of $a \to o_1/e_1$, $b \to o_2/e_2$, $c \to o_3/e_3$ and $d \to o_4/e_4$. With this, equation (5.80) is explicitly given by

$$\left(\hbar\omega\mathbb{1} - \begin{bmatrix} \mathcal{H}^{e_3e_4}_{e_1e_2} & \mathcal{H}^{e_3o_4}_{e_1e_2} & \mathcal{H}^{o_3e_4}_{e_1e_2} & \mathcal{H}^{o_3o_4}_{e_1e_2} \\ \mathcal{H}^{e_3e_4}_{e_1o_2} & \mathcal{H}^{e_3o_4}_{e_1o_2} & \mathcal{H}^{o_3e_4}_{e_1o_2} & \mathcal{H}^{o_3o_4}_{e_1o_2} \\ \mathcal{H}^{e_3e_4}_{o_1e_2} & \mathcal{H}^{e_3o_4}_{o_1e_2} & \mathcal{H}^{o_3e_4}_{o_1e_2} & \mathcal{H}^{o_3o_4}_{o_1e_2} \\ \mathcal{H}^{e_3e_4}_{o_1o_2} & \mathcal{H}^{e_3o_4}_{o_1o_2} & \mathcal{H}^{o_3e_4}_{o_1o_2} & \mathcal{H}^{o_3o_4}_{o_1o_2} \end{bmatrix}\right) \begin{bmatrix} \rho^{(1)}_{e_3e_4}(\omega) \\ \rho^{(1)}_{e_3o_4}(\omega) \\ \rho^{(1)}_{o_3e_4}(\omega) \\ \rho^{(1)}_{o_3o_4}(\omega) \end{bmatrix} = \begin{bmatrix} J_{e_1e_2}(\omega) \\ J_{e_1o_2}(\omega) \\ J_{o_1e_2}(\omega) \\ J_{o_1o_2}(\omega) \end{bmatrix} \tag{5.87}$$

It is essential to keep in mind that, while we are specifying one degree of freedom, there are additional degrees of freedom concealed within the indices. Consequently, our identity matrix $\mathbb{1}$ is itself constituted by block 4×4 but the dimension of those are not specified. By taking this into account, the occupation function indeed has only two values ($f_o = 1$ or $f_e = 0$), yet the same does not hold true for the occupational energy ϵ. This becomes evident as we look at the quantity $h^{(0)}_{ac} = \epsilon_a\delta_{ac}$, meaning that this quantity also depends on other possible degree of freedom. At zero temperature, several terms in the equations (5.85) and (5.86) are null. The equation (5.87) simplifies into

$$\left(\hbar\omega\mathbb{1} - \begin{bmatrix} \mathcal{H}^{e_3e_4}_{e_1e_2} & 0 & 0 & 0 \\ \mathcal{H}^{e_3e_4}_{e_1o_2} & \mathcal{H}^{e_3o_4}_{e_1o_2} & \mathcal{H}^{o_3e_4}_{e_1o_2} & \mathcal{H}^{o_3o_4}_{e_1o_2} \\ \mathcal{H}^{e_3e_4}_{o_1e_2} & \mathcal{H}^{e_3o_4}_{o_1e_2} & \mathcal{H}^{o_3e_4}_{o_1e_2} & \mathcal{H}^{o_3o_4}_{o_1e_2} \\ 0 & 0 & 0 & \mathcal{H}^{o_3o_4}_{o_1o_2} \end{bmatrix}\right) \begin{bmatrix} \rho^{(1)}_{e_3e_4}(\omega) \\ \rho^{(1)}_{e_3o_4}(\omega) \\ \rho^{(1)}_{o_3e_4}(\omega) \\ \rho^{(1)}_{o_3o_4}(\omega) \end{bmatrix} = \begin{bmatrix} 0 \\ J_{e_1o_2}(\omega) \\ J_{o_1e_2}(\omega) \\ 0 \end{bmatrix} \tag{5.88}$$

Note that the first and last rows of the matrix in (5.88) actually possesses a trivial solution such that

$$\rho^{(1)}_{e_3e_4}(\omega) = 0 \text{ and } \rho^{(1)}_{o_3o_4}(\omega) = 0 \tag{5.89}$$

resulting in

$$\left(\hbar\omega\mathbb{1} - \begin{bmatrix} \mathcal{H}^{e_3o_4}_{e_1o_2} & \mathcal{H}^{o_4e_3}_{e_1o_2} \\ \mathcal{H}^{e_3o_4}_{o_2e_1} & \mathcal{H}^{o_4e_3}_{o_2e_1} \end{bmatrix}\right) \begin{bmatrix} \rho^{(1)}_{e_3o_4}(\omega) \\ \rho^{(1)}_{o_4e_3}(\omega) \end{bmatrix} = \begin{bmatrix} J_{e_1o_2}(\omega) \\ J_{o_2e_1}(\omega) \end{bmatrix} \tag{5.90}$$

where we relable the mute indices $\{e_2, o_1\} \rightleftarrows \{e_1, o_2\}$ and $\{o_3, e_4\} \rightleftarrows \{o_4, e_3\}$ in the states of the second line. In fact, in the above representation, the diagonal and off-diagonal blocks are correlated with each other and this is shown by considering the symmetry properties of the electrostatic potential defined in equations (4.56) and (4.57). In accordance with the derivation in Appendix A.2, we find that

$$\mathcal{H}^{o_4 e_3}_{o_2 e_1} = -\left(\mathcal{H}^{e_3 o_4}_{e_1 o_2}\right)^* \tag{5.91}$$

$$\mathcal{H}^{e_3 o_4}_{o_2 e_1} = -\left(\mathcal{H}^{o_4 e_3}_{e_1 o_2}\right)^\dagger \tag{5.92}$$

and, consequently, the equation (5.90) can be written in a more compact way as

$$\left(\hbar\omega\mathbb{1} - \begin{bmatrix} \boldsymbol{\mathcal{R}} & \boldsymbol{\mathcal{C}} \\ -\boldsymbol{\mathcal{C}}^\dagger & -\boldsymbol{\mathcal{R}}^* \end{bmatrix}\right) \begin{bmatrix} \boldsymbol{\rho}^{(1)}_{eo}(\omega) \\ \boldsymbol{\rho}^{(1)}_{oe}(\omega) \end{bmatrix} = \begin{bmatrix} \boldsymbol{J}_{eo}(\omega) \\ \boldsymbol{J}_{oe}(\omega) \end{bmatrix} \tag{5.93}$$

where we define the effective two-particle Hamiltonian blocks explicitly as

$$\boldsymbol{\mathcal{R}} \equiv \mathcal{H}^{e_3 o_4}_{e_1 o_2} = (\epsilon_{e_1} - \epsilon_{o_2})\,\delta_{e_1 e_3}\delta_{o_2 o_4} + \left(V^{e_1 o_4}_{e_3 o_2} - W^{e_1 o_4}_{o_2 e_3}\right) \tag{5.94}$$

$$\boldsymbol{\mathcal{C}} \equiv \mathcal{H}^{o_3 e_4}_{e_1 o_2} = \left(V^{e_1 e_4}_{o_3 o_2} - W^{e_1 e_4}_{o_2 o_3}\right) \tag{5.95}$$

The sub-matrix $\boldsymbol{\mathcal{R}}$ is Hermitian and is usually refer to as the *resonant* block while $\boldsymbol{\mathcal{C}}$ (the so-called *coupling* block) is a complex symmetric sub-matrix. From equation (5.93), we read the effective two-particle electron-hole Hamiltonian

$$\boldsymbol{\mathcal{H}}_{e-h} = \begin{bmatrix} \boldsymbol{\mathcal{R}} & \boldsymbol{\mathcal{C}} \\ -\boldsymbol{\mathcal{C}}^\dagger & -\boldsymbol{\mathcal{R}}^* \end{bmatrix} \tag{5.96}$$

We this procedure, we introduce the effective two-body electron-hole Hamiltonian, which we will subsequently refer to as the *Bethe-Salpeter Hamiltonian* [69, 71]. Note that, due to the presence of the coupling term, the BS Hamiltonian is non-Hermitian although the operator possesses a real spectrum. Let us focus now on equation (5.93) as we can extract crucial information about the dynamics involved in these type of systems. One can essentialy observe that the resonant block plays a crucial role in describing excitonic effects and represents the fermionic response of the system when its subjected to an external stimuli, here denoted as the source term $\boldsymbol{J}_{eo}(\omega)$. If we consider the simplest gapped crystalline system with a two-model band, looking up to the first row in equation (5.93), one can imagine an interband transition of an electron from the valence band to the conduction band, leavind behind a hole to whom it couples, giving origin to an exciton. Regarding the remaining block, the coupling block treats the coupling (as its name suggests) between excitations and de-excitations within the system, describing the exchange and correlation effects among excitons. Normally, the coupling matrix elements are usually smaller than the resonant ones. In solid state calculations, it is therefore common practice to ignore the $\boldsymbol{\mathcal{C}}$ block (the so-called *Tamm-Dancoff approximation* [69, 71]). Under this assumption the excitonic Hamiltonian is given by a Hermitian operator.

5.2 Excitonic Generalized Eigenvalue problem

5.2.1 Electron-Electron Interaction for Bloch states

We will start by studying the form of the electron-electron interaction in a crystal. By recalling the equation (4.55), we can write this two-body Hamiltonian in terms of field operators as

$$\mathcal{H}_{e-e} = \frac{1}{2}\int d\mathbf{r}\int d\mathbf{r}'\Psi_{\sigma}^{\dagger}\left(\mathbf{r}\right)\Psi_{\sigma'}^{\dagger}\left(\mathbf{r}'\right)V\left(\mathbf{r}-\mathbf{r}'\right)\Psi_{\sigma'}\left(\mathbf{r}'\right)\Psi_{\sigma}\left(\mathbf{r}\right) \tag{5.97}$$

Assuming that the noninteracting Hamiltonian is diagonal in spin and expanding the field operators in terms of Bloch states

$$\Psi_{\sigma}\left(\mathbf{r}\right) = \sum_{\mathbf{k}n}\psi_{\mathbf{k}n}\left(\mathbf{r}\right)c_{\mathbf{k}n\sigma} \tag{5.98}$$

we obtain the Hamiltonian in second quantization

$$\mathcal{H}_{e-e} = \frac{1}{2}\sum_{\{\mathbf{k}_i n_i \sigma_i\}} V_{\mathbf{k}_3 n_3 \sigma_3,\,\mathbf{k}_4 n_4 \sigma_4}^{\mathbf{k}_1 n_1 \sigma_1,\,\mathbf{k}_2 n_2 \sigma_2} c_{\mathbf{k}_1 n_1 \sigma_1}^{\dagger} c_{\mathbf{k}_2 n_2 \sigma_2}^{\dagger} c_{\mathbf{k}_3 n_3 \sigma_3} c_{\mathbf{k}_4 n_4 \sigma_4} \tag{5.99}$$

where the matrix elements are defined as

$$V_{\mathbf{k}_3 n_3 \sigma_3,\,\mathbf{k}_4 n_4 \sigma_4}^{\mathbf{k}_1 n_1 \sigma_1,\,\mathbf{k}_2 n_2 \sigma_2} = \delta_{\sigma_1\sigma_4}\delta_{\sigma_2\sigma_3}V_{\mathbf{k}_3 n_3,\,\mathbf{k}_4 n_4}^{\mathbf{k}_1 n_1,\,\mathbf{k}_2 n_2} \tag{5.100}$$

$$V_{\mathbf{k}_3 n_3,\,\mathbf{k}_4 n_4}^{\mathbf{k}_1 n_1,\,\mathbf{k}_2 n_2} = \int d\mathbf{r}_1\int d\mathbf{r}_2\psi_{\mathbf{k}_1 n_1}^{*}\left(\mathbf{r}_1\right)\psi_{\mathbf{k}_2 n_2}^{*}\left(\mathbf{r}_2\right)V\left(\mathbf{r}_1-\mathbf{r}_2\right)\psi_{\mathbf{k}_3 n_3}\left(\mathbf{r}_2\right)\psi_{\mathbf{k}_4 n_4}\left(\mathbf{r}_1\right) \tag{5.101}$$

Now, let us study the matrix elements $V_{\mathbf{k}_3 n_3,\,\mathbf{k}_4 n_4}^{\mathbf{k}_1 n_1,\,\mathbf{k}_2 n_2}$. We begin by writing the electron-electron interaction potential as a generic Fourier transform

$$V\left(\mathbf{r}\right) = \int_{1stBZ}\frac{d^D\mathbf{q}}{\left(2\pi\right)^D}e^{i\mathbf{q}\cdot\mathbf{r}}V\left(\mathbf{q}\right) \tag{5.102}$$

with D being the system dimensions. Then, substituting the previous equation in (5.101), it reads immediately

$$V_{\mathbf{k}_3 n_3,\mathbf{k}_4 n_4}^{\mathbf{k}_1 n_1,\mathbf{k}_2 n_2} = \int_{\text{1st B.Z.}}\frac{d^D\mathbf{q}}{\left(2\pi\right)^D}V\left(\mathbf{q}\right)\varrho_{\mathbf{k}_1 n_1,\,\mathbf{k}_4 n_4}\left(\mathbf{q}\right)\varrho_{\mathbf{k}_2 n_2,\,\mathbf{k}_3 n_3}\left(-\mathbf{q}\right) \tag{5.103}$$

with the density matrices being defined as

$$\varrho_{\mathbf{k}_1 n_1,\,\mathbf{k}_4 n_4}\left(\mathbf{q}\right) = \int d\mathbf{r}_1\psi_{\mathbf{k}_1 n_1}^{*}\left(\mathbf{r}_1\right)e^{i\mathbf{q}\cdot\mathbf{r}_1}\psi_{\mathbf{k}_4 n_4}\left(\mathbf{r}_1\right) \tag{5.104}$$

$$\varrho_{\mathbf{k}_2 n_2,\,\mathbf{k}_3 n_3}\left(-\mathbf{q}\right) = \int d\mathbf{r}_2\psi_{\mathbf{k}_2 n_2}^{*}\left(\mathbf{r}_2\right)e^{-i\mathbf{q}\cdot\mathbf{r}_2}\psi_{\mathbf{k}_3 n_3}\left(\mathbf{r}_2\right) \tag{5.105}$$

Note that we need to adress the integrals in real space defined within the density matrices. We will write it as sum of integrations over the each unit cell

$$\int d\mathbf{r}_i \to \sum_{\mathbf{R}_i}\int_{UC} d\mathbf{s}_i \tag{5.106}$$

such that $\mathbf{r}_i = \mathbf{R}_i + \mathbf{s}_i$, where $\mathbf{R}_i$ is a Bravais lattice vector and $\mathbf{s}_i$ is the position within the unit cell. By applying this relation in equations (5.104) and (5.105), we determine

$$\varrho_{\mathbf{k}_1 n_1,\,\mathbf{k}_4 n_4}\left(\mathbf{q}\right) = \delta_{\mathbf{k}_1,\{\mathbf{k}_4+\mathbf{q}\}}\varrho_{\mathbf{k}_1 n_1,\,\mathbf{k}_4 n_4}\left(\mathbf{q}\right) \tag{5.107}$$

$$\varrho_{\mathbf{k}_2 n_2,\,\mathbf{k}_3 n_3}\left(-\mathbf{q}\right) = \delta_{\mathbf{k}_3,\{\mathbf{k}_2+\mathbf{q}\}}\varrho_{\mathbf{k}_2 n_2,\,\mathbf{k}_3 n_3}\left(-\mathbf{q}\right) \tag{5.108}$$

where we used the property of the Bloch states $\psi_{\mathbf{k}n}\left(\mathbf{R}+\mathbf{r}\right)=e^{i\mathbf{k}\cdot\mathbf{R}}\psi_{\mathbf{k}n}\left(\mathbf{r}\right)$. The summation over $\mathbf{R}_1$ and $\mathbf{R}_2$ is given by

$$\sum_{\mathbf{R}_1}e^{-i(\mathbf{k}_1-\mathbf{k}_4-\mathbf{q})\cdot\mathbf{R}_1}=N\delta_{\mathbf{k}_1,\{\mathbf{k}_4+\mathbf{q}\}} \tag{5.109}$$

$$\sum_{\mathbf{R}_2}e^{-i(\mathbf{k}_2+\mathbf{q}-\mathbf{k}_3)\cdot\mathbf{R}_2}=N\delta_{\mathbf{k}_3,\{\mathbf{k}_2+\mathbf{q}\}} \tag{5.110}$$

where it was done by taking into account the following relation between both real- and momentum-space:

$$\sum_{\mathbf{R}}e^{i(\mathbf{q}-\mathbf{k}+\mathbf{k}')\cdot\mathbf{R}}=N\sum_{\mathbf{G}}\delta_{\mathbf{q}-\mathbf{k}+\mathbf{k}',\mathbf{G}}$$

In this approach, we introduced the Umklapp scattering notation, which corresponds to the curved brackets denoted as $\{\}$, to denote the process $\mathbf{k}+\mathbf{G}\rightarrow\mathbf{k}$. This notation helps convey that Umklapp scattering involves a change in momentum by adding or subtracting a reciprocal lattice vector $\mathbf{G}=n_1\mathbf{b}_1+n_2\mathbf{b}_2$, with $n_1,n_2\in\mathbb{Z}$, to the original momentum $\mathbf{k}$, with the restriction that $\mathbf{k}$ being a vector that resides within the 1st Brillouin zone. With this procedure, we define the electron-electron interaction potential (5.101) as

$$V^{\mathbf{k}_1n_1,\mathbf{k}_2n_2}_{\mathbf{k}_3n_3,\mathbf{k}_4n_4}=\int_{\text{1st B.Z.}}\frac{d^D\mathbf{q}}{(2\pi)^D}V\left(\mathbf{q}\right)\delta_{\mathbf{k}_1,\{\mathbf{k}_4+\mathbf{q}\}}\delta_{\mathbf{k}_2,\{\mathbf{k}_3-\mathbf{q}\}}\varrho_{\mathbf{k}_1n_1,\,\mathbf{k}_4n_4}\left(\mathbf{q}\right)\varrho_{\mathbf{k}_2n_2,\,\mathbf{k}_3n_3}\left(-\mathbf{q}\right) \tag{5.111}$$

where $\{\mathbf{q}\}$ is the rescriction of a vector $\mathbf{q}$ to the 1st B.Z., i.e., any vector $\mathbf{q}$ can be decomposed as $\mathbf{q}=\{\mathbf{q}\}+\mathbf{G}_{\mathbf{q}}$, where $\mathbf{G}_{\mathbf{q}}$ is a point in the reciprocal lattice. By specifying $\mathbf{k}_4\rightarrow\mathbf{k}$ and $\mathbf{k}_3\rightarrow\mathbf{k}'$, and considering a general momentum vector $\mathbf{q}=\mathbf{p}+\mathbf{G}$, such that $\{\mathbf{p}\}=\{\mathbf{q}+\mathbf{G}\}=\mathbf{q}$, and simplifying the expression, we can write the two-particle in a more compacted way

$$\begin{aligned}\mathcal{H}_{e-e}=\frac{1}{2}\sum_{\mathbf{G}}\int_{\text{1st B.Z.}}\frac{d^D\mathbf{p}}{(2\pi)^D}\sum_{\{n_i\}}\sum_{\mathbf{k}\sigma,\,\mathbf{k}'\sigma'}\delta_{\{\mathbf{k}_1-\mathbf{k}_4\},\{\mathbf{k}_3-\mathbf{k}_2\}}\delta_{\mathbf{p},\{\mathbf{k}_1-\mathbf{k}_4\}}V^{\{\mathbf{k}+\mathbf{p}\}n_1,\{\mathbf{k}'-\mathbf{p}\}n_2}_{\mathbf{k}'n_3,\mathbf{k}n_4}\left(\mathbf{p}+\mathbf{G}\right)\\ \times c^{\dagger}_{\{\mathbf{k}+\mathbf{p}\}n_1\sigma}c^{\dagger}_{\{\mathbf{k}'-\mathbf{p}\}n_2\sigma'}c_{\mathbf{k}'n_3\sigma'}c_{\mathbf{k}n_4\sigma}\end{aligned} \tag{5.112}$$

with

$$V^{\{\mathbf{k}+\mathbf{p}\}n_1,\{\mathbf{k}'-\mathbf{p}\}n_2}_{\mathbf{k}'n_3,\mathbf{k}n_4}\left(\mathbf{p}+\mathbf{G}\right)=\varrho_{\{\mathbf{k}+\mathbf{p}\}n_1,\,\mathbf{k}n_4}\left(\mathbf{p}\right)V\left(\mathbf{p}+\mathbf{G}\right)\varrho_{\{\mathbf{k}'-\mathbf{p}\}n_2,\,\mathbf{k}'n_3}\left(-\left(\mathbf{p}+\mathbf{G}\right)\right) \tag{5.113}$$

The significance of this Hamiltonian, is that it states the Bloch momentum is conserved along the modulo of the reciprocal lattice vectors. In Figure 8 is represented the Feynman diagram for the electron-electron interaction, namely the quantity $V\left(\mathbf{q}\right)$, as this approach gives us valuable information concerning the potential of interaction. The wavy line presents the bosonic nature of the potential of interaction $V\left(\mathbf{p}+\mathbf{G}\right)$ and at the vertices are demonstrated the conservation of quasi-momentum consequence of the Kronecker deltas terms, namely $\delta_{\mathbf{p},\{\mathbf{k}_1-\mathbf{k}_4\}}$ and $\delta_{-\mathbf{p},\{\mathbf{k}_2-\mathbf{k}_3\}}$, connecting the fermionic states from the different propagators.

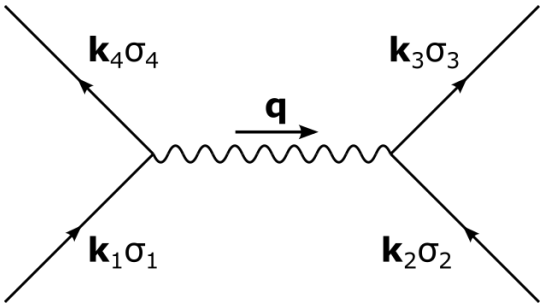

Figure 8: Feynman diagram of the electron-electron interaction defined in equation (5.111). The quantities $\{\mathbf{k}_i, \sigma_i\}$ represent the quasi-momentum and spin of the electron in state i, and $\mathbf{q}$ is the quasi-momentum involved in the electron-electron interaction via an electrostatic potential.

5.2.2 Wannier equation

Let us contemplate a simple two-band system, representative of a semiconductor or an insulator, residing initially in a state of equilibrium. In this equilibrium state, the valence band v is fully occupied, while the conduction band c remains empty. Now, we shall direct our attention to a hypothetical electron characterized by an energy denoted as $\epsilon_{\mathbf{k}v}$, in which $\mathbf{k}$ corresponds to the quasi-momentum. Perturbing the system with an external electric field, electrons from the valence band can be promoted to the conduction band, inducing interband transitions in the system with quasi-momentum $\mathbf{k}+\mathbf{Q}$, where $\mathbf{Q}$ is the center of mass momentum of the exciton, having now associated energy $\epsilon_{\{\mathbf{k}+\mathbf{Q}\}c}$. The information regarding the perturbation is within the source term

$$\boldsymbol{J}_{\{\mathbf{k}+\mathbf{Q}\}c,\,\mathbf{k}v}\left(\omega, \mathbf{Q}+\mathbf{G}\right) \tag{5.114}$$

The linear response defined in (5.93) can be written in way that leads to a hermitian problem by multiplying it by a matrix $\boldsymbol{\mathcal{S}}$, with the identity $\mathbb{1}$ and $-\mathbb{1}$ defined on its diagonal blocks. Taking into consideration the Bloch momentum degrees of freedom, the linear response would be expressed in the followig compact way:

$$\sum_{\mathbf{k}'}\left(\hbar\omega\boldsymbol{\mathcal{S}} - \begin{bmatrix} \boldsymbol{\mathcal{R}}\left(\mathbf{Q}\right) & \boldsymbol{\mathcal{C}}\left(\mathbf{Q}\right) \\ \left[\boldsymbol{\mathcal{C}}\left(\mathbf{Q}\right)\right]^{\dagger} & \left[\boldsymbol{\mathcal{R}}\left(\mathbf{Q}\right)\right]^{*} \end{bmatrix}\right)\begin{bmatrix} \rho^{(1)}_{\{\mathbf{k}'+\mathbf{Q}\}c,\mathbf{k}'v}\left(\omega\right) \\ \rho^{(1)}_{\{\mathbf{k}'+\mathbf{Q}\}v,\mathbf{k}'c}\left(\omega\right) \end{bmatrix} = \boldsymbol{\mathcal{S}}\begin{bmatrix} J_{\{\mathbf{k}+\mathbf{Q}\}c,\mathbf{k}v}\left(\omega, \mathbf{Q}+\mathbf{G}\right) \\ J_{\mathbf{k}v,\{\mathbf{k}+\mathbf{Q}\}c}\left(\omega, \mathbf{Q}+\mathbf{G}\right) \end{bmatrix} \tag{5.115}$$

in which we define the resonant block as

$$\begin{aligned} \boldsymbol{\mathcal{R}}\left(\mathbf{Q}\right) \equiv \mathcal{H}^{\{\mathbf{k}'+\mathbf{Q}\}c,\mathbf{k}'v}_{\{\mathbf{k}+\mathbf{Q}\}c,\mathbf{k}v} &= \left(\epsilon_{\{\mathbf{k}+\mathbf{Q}\}c} - \epsilon_{\mathbf{k}v}\right)\delta_{\{\mathbf{k}+\mathbf{Q}\}c,\{\mathbf{k}'+\mathbf{Q}\}c}\delta_{\mathbf{k}'v,\mathbf{k}v} \\ &+ \left(V^{\{\mathbf{k}+\mathbf{Q}\}c,\mathbf{k}'v}_{\{\mathbf{k}'+\mathbf{Q}\}c,\mathbf{k}v} - W^{\{\mathbf{k}+\mathbf{Q}\}c,\mathbf{k}'v}_{\mathbf{k}v,\{\mathbf{k}'+\mathbf{Q}\}c}\right) \end{aligned} \tag{5.116}$$

and the coupling block as

$$\boldsymbol{\mathcal{C}}\left(\mathbf{Q}\right) \equiv \mathcal{H}^{\{\mathbf{k}'+\mathbf{Q}\}v,\mathbf{k}'c}_{\{\mathbf{k}+\mathbf{Q}\}c,\mathbf{k}v} = \left(V^{\{\mathbf{k}+\mathbf{Q}\}c,\mathbf{k}'c}_{\{\mathbf{k}'+\mathbf{Q}\}v,\mathbf{k}v} - W^{\{\mathbf{k}+\mathbf{Q}\}c,\mathbf{k}'c}_{\mathbf{k}v,\{\mathbf{k}'+\mathbf{Q}\}v}\right) \tag{5.117}$$

where we set the quasi-momenta states $\mathbf{k}_3 \to \{\mathbf{k}' + \mathbf{Q}\}$ and $\mathbf{k}_4 \to \mathbf{k}'$. The matrix $\boldsymbol{\mathcal{S}}$ is given by

$$\boldsymbol{\mathcal{S}} = \begin{bmatrix} \mathbb{1} & 0 \\ 0 & -\mathbb{1} \end{bmatrix} \tag{5.118}$$

Now, let us consider the *Tamm-Dancoff approximation* (TDA, for short) [69, 71], which consists in neglecting the blocks $\boldsymbol{\mathcal{C}}$ in the Bethe-Salpeter Hamiltonian in equation (5.115). This way, the problem is thus reduced to the problem of diagonalizing the $\boldsymbol{\mathcal{R}}$ block, defined in equation (5.116). Notice that the interaction term that has origin in the Fock self-energy gives origin to an attractive interaction between an electron a hole, while the Hartree term contributes with a repulsive term[11]. We will focus on the Fock term, while discarding the Hartree term (which leads to a small correction in the exciton energy levels [92]). Taking into account these considerations, we want to solve the following hermitian generalized eigenvalue problem:

$$\boldsymbol{\mathcal{H}}_{e-h}^{H} \boldsymbol{\Psi}^{\lambda} = E_{\lambda} \boldsymbol{\mathcal{S}} \cdot \boldsymbol{\Psi}^{\lambda} \tag{5.119}$$

with the hermitian Bethe-Salpeter Hamiltonian being defined as $\boldsymbol{\mathcal{H}}^{H} = \boldsymbol{\mathcal{S}} \cdot \boldsymbol{\mathcal{H}}$, where the Bethe-Salpeter Hamiltonian is defined in equation (5.96). By applying here the TDA, the linear response eigenvalue problem (5.119) reduces to

$$\left(\epsilon_{\{\mathbf{k}+\mathbf{Q}\}c} - \epsilon_{\mathbf{k}v}\right) \Psi^{\lambda}_{\mathbf{k},\, cv}\left(\mathbf{Q}\right) - \sum_{\mathbf{R}'} W^{\{\mathbf{k}+\mathbf{Q}\}c,\mathbf{k}'v}_{\mathbf{k}v,\{\mathbf{k}'+\mathbf{Q}\}c} \Psi^{\lambda}_{\mathbf{k}',\, cv}\left(\mathbf{Q}\right) = E_{\lambda} \Psi^{\lambda}_{\mathbf{k},\, cv}\left(\mathbf{Q}\right) \tag{5.120}$$

with the resonant Fock term being defined as

$$\begin{aligned} W^{\{\mathbf{k}+\mathbf{Q}\}c,\mathbf{k}'v}_{\mathbf{k}v,\{\mathbf{k}'+\mathbf{Q}\}c} = \frac{1}{\mathcal{V}} \sum_{\mathbf{G}} \varrho_{\{\mathbf{k}+\mathbf{Q}\}c,\,\{\mathbf{k}'+\mathbf{Q}\}c}\left(\left\{\mathbf{k}-\mathbf{k}'\right\}+\mathbf{G}\right) W\left(\left\{\mathbf{k}-\mathbf{k}'\right\}+\mathbf{G}\right) \\ \times \varrho_{\mathbf{k}'v,\,\mathbf{k}v}\left(-\left(\left\{\mathbf{k}-\mathbf{k}'\right\}+\mathbf{G}\right)\right) \end{aligned} \tag{5.121}$$

where $\mathcal{V}$ is the crystal volume in real space.

We will now assume that our system is a direct bandgap insulator, and approximate the bandstructure close to the band gap as a parabolic band, meaning

$$\epsilon_{\mathbf{k}c} \simeq \frac{\hbar^2 \mathbf{k}^2}{2m_c} + \frac{1}{2} E_{gap} \tag{5.122}$$

$$\epsilon_{\mathbf{k}v} \simeq -\frac{\hbar^2 \mathbf{k}^2}{2m_v} - \frac{1}{2} E_{gap} \tag{5.123}$$

where $m_{c/v}$ is the effective mass of the band. One could assume that small momenta are relevant, resulting in umklapp processes being negligible. Moreover, we may also approximate the density matrices associated with interaction potentials:

$$\varrho_{\{\mathbf{k}+\mathbf{Q}\}c,\,\{\mathbf{k}'+\mathbf{Q}\}c}\left(\left\{\mathbf{k}-\mathbf{k}'\right\}+\mathbf{G}\right) \simeq \varrho_{\mathbf{k}c,\,\mathbf{k}c}\left(0\right) = 1 \tag{5.124}$$

$$\varrho_{\{\mathbf{k}'\}v,\,\{\mathbf{k}\}v}\left(-\left(\left\{\mathbf{k}-\mathbf{k}'\right\}+\mathbf{G}\right)\right) \simeq \varrho_{\mathbf{k}c,\,\mathbf{k}c}\left(0\right) = 1 \tag{5.125}$$

[11] Somewhat confusingly, in the literature on excitons [95], the term involving "W" is referred to as the direct electron-hole interaction term, while "V" is referred to as the exchange electron-hole interaction term

Therefore, we obtain

$$\left(E_{gap}+\frac{\hbar^2\left(\mathbf{k}+\mathbf{Q}\right)^2}{2m_c}+\frac{\hbar^2\mathbf{k^2}}{2m_v}\right)\Psi^{\lambda}_{\mathbf{k},\,cv}\left(\mathbf{Q}\right)-\frac{1}{\mathcal{V}}\sum_{\mathbf{k'}}W\left(\mathbf{k}-\mathbf{k'}\right)\Psi^{\lambda}_{\mathbf{k'},\,cv}\left(\mathbf{Q}\right)=E_{\lambda}\Psi^{\lambda}_{\mathbf{k},\,cv}\left(\mathbf{Q}\right) \tag{5.126}$$

Directing our focus to excitons characterized by zero center-of-mass momentum, denoted as $\mathbf{Q}=0$, and introducing the effective mass of the electron-hole pair defined as

$$\frac{1}{m_{eff}}=\frac{1}{m_c}+\frac{1}{m_v} \tag{5.127}$$

we derive the Wannier equation in momentum space as

$$\left(E_{gap}+\frac{\hbar^2\mathbf{k}^2}{2m_{eff}}\right)\Psi^{\lambda}_{\mathbf{k},\,cv}\left(\mathbf{0}\right)-\int\frac{d\mathbf{k'}}{\left(2\pi\right)^D}W\left(\mathbf{k}-\mathbf{k'}\right)\Psi^{\lambda}_{\mathbf{k'},\,cv}\left(\mathbf{0}\right)=E_{\lambda}\Psi^{\lambda}_{\mathbf{k},\,cv}\left(\mathbf{0}\right) \tag{5.128}$$

Previously, we applied the thermodynamic limit, denoted as $\mathcal{V}\to\infty$. In practical terms, this implies that

$$\frac{1}{\mathcal{V}}\sum_{\mathbf{k'}}\left[\dots\right]\to\frac{1}{\left(2\pi\right)^D}\int d^D\mathbf{k'}\left[\dots\right] \tag{5.129}$$

We can ascertain the corresponding Wannier equation in real space by considering the Fourier transform

$$\Psi^{\lambda}_{\mathbf{k},\,cv}\left(\mathbf{0}\right)=\int d\mathbf{r}e^{-i\mathbf{k}\cdot\mathbf{r}}\Psi^{\lambda}_{cv}\left(\mathbf{r}\right) \tag{5.130}$$

Substituting this in equation (5.128), it gives

$$\left(E_{gap}-\frac{\hbar^2\nabla^2}{2m_{eff}}-W\left(\mathbf{r}\right)\right)\Psi^{\lambda}_{cv}\left(\mathbf{r}\right)=E_{\lambda}\Psi^{\lambda}_{cv}\left(\mathbf{r}\right) \tag{5.131}$$

in which this result is easily determined if one adopts a quasi-momentum translation $\mathbf{k'}\to\mathbf{k}-\mathbf{k''}$ and the momentum operator representation $\mathbf{p}=\hbar\mathbf{k}$ in its differential form, $\mathbf{p}=-i\hbar\nabla$. Note that this equation is nothing more than a Schrödinger equation for a hidrogenoid atom and it constitutes an eigenvalue problem. Which means, that the solutions from it, gives us information about the eigenmodes (excitonic states) and the eigenvalues (excitonic binding energies) of the excitons. In Appendix A.2 is derived the Wannier equation for 1D systems and the necessary guidelines for its numerical implementation.

Part II

Numerical Implementation and Results

6 Optical Response and Numerical Implementation

In this chapter, we begin by presenting the concepts involved in the optical response in a linear response regime, specifying it to the case of a delta-function perturbation. We then discuss the Fourier analysis of the system's optical response and the concepts of relaxation and broadening. After that, we present the theoretical approach and the numerical implementation involved in this work, namely how we implement and solve the rDM equation of motion for both noninteracting and interacting systems. Lastly, we show to calculate the expectation value of the current operator within the Peierls substitution. The Section 6.1 is based on the references [74, 98]. The Sections 6.2 and 6.4 are based on the references [74, 82].

6.1 Linear Response Regime

Let us assume a physical system, initially in equilibrium, is subjected to a driven electric field. The experimental procedure is to submit the system to an external field acting at some point in space $\mathbf{r}'$ and at time t'. In linear response theory, the macroscopic current of a system can be generally written as the convolution of the external electric field $\varepsilon\left(\mathbf{r}', t'\right)$ and the corresponding response function, the linear conductivity $\sigma^{\beta\alpha}\left(\mathbf{r}, t; \mathbf{r}', t'\right)$. This way, the external "force" is defined as

$$j^{\beta}\left(\mathbf{r}, t\right) = \int_{-\infty}^{t} d\mathbf{r}' dt' \sigma^{\beta\alpha}\left(\mathbf{r}, t; \mathbf{r}', t'\right) \varepsilon^{\alpha}\left(\mathbf{r}', t'\right) \tag{6.132}$$

We will assume that $\sigma^{\beta\alpha}$ is a function of both the difference between the two positions, $\mathbf{r}$ and $\mathbf{r}'$, and the times, t and t', meaning that it is invariant under both spatial and time translations, at least in an equilibrium regime. It reads

$$j^{\beta}\left(\mathbf{r}, t\right) = \int_{-\infty}^{+\infty} d\mathbf{r}' dt' \sigma^{\beta\alpha}\left(\mathbf{r} - \mathbf{r}', t - t'\right) \varepsilon^{\alpha}\left(\mathbf{r}', t'\right) \tag{6.133}$$

Note that the domain of integration was extended in dt' by imposing that the the field at a time t' cannot affect the response of the system at an earlier time t, as required by causality,

$$\sigma^{\beta\alpha}\left(\mathbf{r} - \mathbf{r}', t - t'\right) \equiv 0, \text{ for } t' > t \tag{6.134}$$

In this work, we are interested to study light-matter interactions within a length gauge, where we neglect the local spatial dependency on the response. In this scheme of thought, we are only interested in the time response, so we will omit the dependence in the position (per consequence, the momentum contribution). Let us now move to the corresponding frequency domain, ω, by adopting the following Fourier transform

$$\mathcal{A}\left(\omega\right) = \int dt \mathcal{A}\left(t\right) e^{i\omega t} \tag{6.135}$$

and multiply both members of the equation (6.133) by exp $[i\omega t]$ and integrating over the t variables, we determine

$$j^{\beta}\left(\omega\right) = \sigma^{\beta\alpha}\left(\omega\right) \varepsilon^{\alpha}\left(\omega\right) \tag{6.136}$$

We can now derive the reality condition for the conductivity. Firstly, let us consider that the current in the time-domain is necessarily real, which means $j^{\beta}(t) = \left[j^{\beta}(t)\right]^{*}$. By working this out, we observe that

$$j^{\beta}(t) = \left[j^{\beta}(t)\right]^{*} \implies j^{\beta}(\omega) = \left[j^{\beta}(-\omega)\right]^{*} \tag{6.137}$$

a statement that is also true in the case of the electric field

$$\varepsilon^{\beta}(\omega) = \left[\varepsilon^{\beta}(-\omega)\right]^{*} \tag{6.138}$$

where we previously applied the inverse Fourier transform

$$\mathcal{A}(t) = \int \frac{d\omega}{2\pi} \mathcal{A}(\omega)\, e^{-i\omega t} \tag{6.139}$$

The appropriate substitution of the equations (6.137) and (6.138) in the equation (6.136) and the proper algebraic manipulation, leads to a relation between positive- and negative-frequency components of the conductivity

$$\begin{aligned} & j^{\beta}(\omega) = \sigma^{\beta\alpha}(\omega)\, \varepsilon^{\alpha}(\omega) \\ \Leftrightarrow & \left[j^{\beta}(-\omega)\right]^{*} = \left[\sigma^{\beta\alpha}(-\omega)\right]^{*} \left[\varepsilon^{\beta}(-\omega)\right]^{*} \end{aligned}$$

which leads to

$$\sigma^{\beta\alpha}(\omega) = \left[\sigma^{\beta\alpha}(-\omega)\right]^{*} \tag{6.140}$$

We can present this relation in a somewhat different form by decomposing the conductivity into its real and imaginary parts,

$$\mathrm{Re}\left[\sigma^{\beta\alpha}(\omega)\right] = \mathrm{Re}\left[\sigma^{\beta\alpha}(-\omega)\right] \tag{6.141}$$

$$\mathrm{Im}\left[\sigma^{\beta\alpha}(\omega)\right] = -\mathrm{Im}\left[\sigma^{\beta\alpha}(-\omega)\right] \tag{6.142}$$

These results means that the real(imaginary) part of the conductivity must be an even(odd) function of the frequency.

6.1.1 Response to a delta-function perturbation

Adopting a quasi-instantaneous pulse as a perturbing field is especially well suited for extracting the linear response in a single integration of equation (6.133). This becomes obvious if one sets the driven electric field to $\varepsilon(t) = \varepsilon_0 \delta(t)$ and ensures that the field is small in amplitude. In the lowest order, the following holds:

$$j(\omega) \simeq \varepsilon_0 \sigma^{(1)}(\omega) \tag{6.143}$$

which shows, in the frequency domain, the delta function has a magnitude of the unity at all frequencies and a null phase. This property of the Fourier transform is a fundamental result and reflects the fact that the delta function represents an infinitely narrow pulse in the time domain, which contains all possible frequencies in the frequency domain. In practice, since a short pulse excites the system equally at all frequencies, the Fourier transform of $j(t)$ computed as the response to a single instantaneous pulse directly yields the linear conductivity at all frequencies.

6.2 Fourier Analysis of Optical Response

To characterize the response in the frequency domain, we compute the discrete Fourier transform (FT) of the time-domain currents and electric fields. We define the discrete FT of a time-dependent signal $f(t)$ that is sampled at regular intervals τ at a specific frequency ω_k as

$$F_{\omega_k} \equiv \frac{1}{L} \sum_{n=0}^{L-1} f(t_n) e^{i\omega_k t_n} \tag{6.144}$$

where $f(t_n)$ indicates the value of the time-dependent signal at nth sample, the parameter $t_n \equiv n\tau$ is the time associated with each sample, L is the total number of time samples that normalizes the result, ensuring consistent amplitude values and $T \equiv L\tau$ is the total duration of the signal. The variable associated with the frequency is denoted as $\omega_k \equiv 2\pi k/T$ for $k \in \{0, 1, ..., L-1\}$, where k represents the index of the frequency component in the discrete Fourier transform.

The total duration of the simulation or acquisition time (from now on, let us address this quantity as T_{acq}) is intrinsecally connected with the maximum frequency resolution one can achieve and it is by the condition $2\pi/T_{acq}$. So, the time of acquisition, in principle, satisfy $T_{acq} \gtrsim 2\pi/\gamma$, where γ represents the characteristic broadening of the system, so that its Fourier spectrum has at least the resolution imposed by this parameter. This is one of the compromises that ultimately determine the duration of the simulations.

Another trade-off relates to the choice of the time step, δt, for numerically integrating the equation of motion for the rDM. Ideally, δt should be chosen as a fraction of the driving field's fundamental period to prevent the accumulation of numerical errors stemming from the oscillatory behavior of the rDM solution and, consequently, the average current. The time step choice is also subject to a fundamental constraint dictated by the *Nyquist-Shannon theorem* [74] The value of δt used in numerical integration determines the smallest possible sampling interval $(\min \tau = \delta t)$ and, as per the theorem, the maximum frequency captured in a discrete Fourier transform (FT) should be π/τ.

These requirements reflect the computational effort required to accurately simulate the system for the desired frequency resolution. In summary, to balance the numerical accuracy and frequency resolution in simulations, a smaller time step (δt) is needed to capture the oscillatory behavior, and the total duration of the simulation (T_{acq}) needs to be sufficiently long to satisfy the desired frequency resolution.

6.2.1 Relaxation and Broadening

The electronic system described by the rDM equation of motion (4.76) stores all the energy transferred by the external radiation field. The ongoing increase in the system's current can create numerical difficulties when equation (4.76) requires integration over a significant number of time steps. This leads to an increase of amplitude of $j(t)$ linearly in time, which introduces artifacts as $\omega \to 0$ in the numerical Fourier transform. Another issue is correlated with the

fact that the computer has finite memory and computational precision, and it cannot precisely handle Dirac deltas, as one can think of the conductivity $\sigma(\omega)$ as a sum of these. To tackle these issues, we seek a current's function $j(t)$ to perform a Fourier transform with a gradual rather than an abrupt end. This strategy effectively smoothens the sum of Dirac deltas by broadening them.

Using short-pulse excitation, one can incorporate an artificial energy broadening into the Fourier spectrum by modifying equation (6.144) as follows:

$$F_{\omega_k} = \frac{1}{L}\sum_{n=0}^{L-1} f(t_n)\, e^{i(\omega_k + i\gamma)t_n} \tag{6.145}$$

where the parameter γ is a damping artificial parameter and a real quantity. With this approach, broadening is introduced at the post-processing stage, where $\hbar\gamma$ defines the desired energy resolution.

6.3 Theoretical Approach and Numerical Implementation

The core concept of this work lies in the manipulation of the single-particle reduced density matrix and its time evolution. Given our keen interest in excitonic effects, we will tackle this challenge by employing the time-dependent Hartree-Fock approximation. In this analysis, we will discard the Hartree term, which leads to a small corrections in the exciton energy levels [92]. In essence, our goal is to solve the following equation of motion:

$$\boxed{\begin{array}{c} i\hbar\dfrac{d\rho(t)}{dt} = \left[\mathcal{H}_{TDHF}(t), \rho(t)\right] \\ \text{with } \mathcal{H}_{TDHF}(t) = \mathcal{H}_{PBC}^{Peierls}(t) + \Sigma^F\left[\rho(t) - \rho^{(0)}\right] \end{array}} \tag{6.146}$$

where we will employ the Peierls Hamiltonian in PBC (defined in equation (2.28))

$$\mathcal{H}_{PBC}^{Peierls}(t) = -h\sum_n \left(e^{-i2\pi\frac{\phi(t)}{\phi_0 N}} c^\dagger_{\mathsf{mod}(n+1,N)} c_n + e^{i2\pi\frac{\phi(t)}{\phi_0 N}} c^\dagger_n c_{\mathsf{mod}(n+1,N)} \right) \tag{6.147}$$

expressed in a more compact way. The time-dependent phase $\varphi(t)$ is given by

$$\varphi(t) = 2\pi\frac{\phi(t)}{\phi_0 N} \tag{6.148}$$

where the quantity $\phi_0 = h/e$ is the quanta of magnetic flux and $\phi(t)$ is the flux inside the ring that can be related with the vector potential by the relation $\phi(t) = Na_0A(t)$ within a Weyl gauge. In its matrix form, the time-dependent Hartree-Fock Hamiltonian (TDHF), defined at (6.146), reads

$$\mathcal{H}_{TDHF}(t) = \begin{bmatrix} \epsilon_A & -he^{i\varphi(t)} & & & \{-he^{i\varphi(t)}\}^* \\ \{-he^{i\varphi(t)}\}^* & \epsilon_B & -he^{i\varphi(t)} & & \\ & \ddots & \ddots & \ddots & \\ & & \{-he^{i\varphi(t)}\}^* & \epsilon_A & -he^{i\varphi(t)} \\ -he^{i\varphi(t)} & & & \{-he^{i\varphi(t)}\}^* & \epsilon_B \end{bmatrix} + \Sigma^F\left[\rho(t) - \rho^{(0)}\right] \tag{6.149}$$

The one-particle reduced density matrix in equilibrium is defined in (3.44) and it reads

$$\rho_{\alpha\beta}^{(0)}\left(\mathbf{R},\mathbf{R}'\right)=\sum_{\lambda}f_{F-D}\left(\epsilon_{\lambda}\right)\phi_{\lambda}^{\alpha}\left(\mathbf{R}\right)\left\{\phi_{\lambda}^{\beta}\left(\mathbf{R}'\right)\right\}^{*} \tag{6.150}$$

where λ indexes the eigenstates of the single-particle Hamiltonian and $\{f_{F-D}\}$ are their occupancies dictated by the Fermi-Dirac distribution. We are working in real space, so the eigenvalues and eigenvectors applied in the previous equation result from the direct diagonalization of the matrix (6.149) in equilibrium, i.e., at initial time $t=0$.

6.3.1 Electric Pulse definition

In this work, we are interested in perturbing the system via quasi-instantaneous electric field, then arises the need to define it. The idea is to implement a function that behaves like a Dirac $\delta-$function, yet there is no true function that satisfies it. So, we will use a nascent delta function to reproduce its behaviour. We will choose to work with a Lorentzian function, defining an electric field as follow:

$$\varepsilon\left(t,t_0\right)=\varepsilon_0 L_{\eta}\left(t,t_0\right) \tag{6.151}$$

with

$$L_{\eta}\left(t,t_0\right)=\frac{1}{\pi}\frac{\eta}{\eta^2+\left(t-t_0\right)^2} \tag{6.152}$$

where η is the half-width at half-maximum (HWHM).

6.3.2 Fock Interaction definition

Our central objective is to explore the excitonic response in crystalline systems, and to achieve this, there arises the necessity to define a regularized attractive potential in order to define the Fock interaction term. By recalling its definition in equation (4.74), the Fock term is defined as

$$\Sigma_{\alpha\beta}^{Fock}\left(\mathbf{R},\mathbf{R}'\right)=-W\left(\mathbf{R}+\mathbf{s}_{\alpha}-\left(\mathbf{R}'+\mathbf{s}_{\beta}\right)\right)\rho_{\alpha\beta}\left(\mathbf{R},\mathbf{R}'\right) \tag{6.153}$$

where $\{\mathbf{R},\mathbf{R}'\}$ corresponds to the reciprocal translational vectors associated with sublattices $\{\alpha,\beta\}$, respectively; the quantities $\{\mathbf{s}_{\alpha},\mathbf{s}_{\beta}\}$ are the position of each orbital within the unit cell.

For the 1D case, we define the attraction potential as a regularized Coulomb potential

$$W^{1\mathrm{D}}(x)=\frac{V_0}{\sqrt{x_I^2+\lambda_r^2}} \tag{6.154}$$

where V_0 corresponds to the potential amplitude and it possesses a positive value, x_I is the position operator for the interaction term and λ_r is an on-site regularization parameter. Conventionally, we will adopt that the regularization parameter is the order of the lattice constant ($\lambda_r \approx a_0$). Note that the position operator x_I it is not the same as x adopted in the tight-binding formulation, as the latter corresponds to the average distance from the lattice point

$x = 0$. The first stands for the interaction term (hence the label "I") and, working with Born-von Karman periodic boundary conditions, this position operator of interaction has a specific behaviour that is max $(W(x))$ at $x = 0$ and min $(W(x))$ at $x = Na_0/2$, and it is maximum again at $x = (N-1)a_0$. In a 1D ring, it can be viewed as the physical separation in relation to the lattice point $x = 0$. This is issue is adressed in Appendix A.2.

6.4 Calculating Observables: the Current operator

We want to evaluate the response current of the system to an external driven electric field. By definition, the current operator [82] within a Peierls substitution under periodic boundary conditions is defined as

$$\begin{aligned} j_{PBC}^{Peierls}(t) &= -\frac{\delta \mathcal{H}_{TDHF}(t)}{\delta A} \\ &= -i\frac{2\pi a_0 h}{\phi_0}\sum_{n}^{N-1}\left(e^{-i\varphi(t)}c^{\dagger}_{\mathsf{mod}(n+1,\,N)}c_n - e^{i\varphi(t)}c^{\dagger}_n c_{\mathsf{mod}(n+1,\,N)}\right) \end{aligned} \tag{6.155}$$

In its matrix representation, it reads

$$j_{PBC}^{Peierls}(t) = -i\frac{2\pi a_0 h}{\phi_0}\begin{bmatrix} 0 & -e^{i\varphi(t)} & & & \{e^{i\varphi(t)}\}^* \\ \{e^{i\varphi(t)}\}^* & 0 & -e^{i\varphi(t)} & & \\ & \ddots & \ddots & \ddots & \\ & & \{e^{i\varphi(t)}\}^* & 0 & -e^{i\varphi(t)} \\ -e^{i\varphi(t)} & & & \{e^{i\varphi(t)}\}^* & 0 \end{bmatrix} \tag{6.156}$$

By recalling the definition of an observable expected value, one can determine the average current in such a state

$$\langle j_{PBC}^{Peierls}\rangle(t) = \mathsf{Tr}\left(\rho(t)\, j_{PBC}^{Peierls}(t)\right) \tag{6.157}$$

6.4.1 Current in Time with a Damped Parameter

We are interested in studying the current propagation in time that flows within the system. In particular, we will be looking for the response in Fourier. As discussed in Section 6.2.1, due to relaxation and broadening reasons, we want to introduce a dissipative artifact by hand into the equation (6.157) to calculate a post-processing damped current

$$\langle j_{PBC}^{Peierls}\rangle_{\gamma}(t) = e^{-\gamma t}\langle j_{PBC}^{Peierls}\rangle(t) \tag{6.158}$$

where the damping parameter γ is a real quantity. The damping parameter will be fixed at a value $\gamma = 0.003\, fs^{-1}$ for the results presented in Chapter 6.4.2.

6.4.2 Current in Frequency-Domain

The role of the excitons effects in the current response is accessed by analyzing the Fourier transform of the time-dependent current. Numerically, we employ a Fast Fourier Transform (FFT), an algorithm that computes the discrete

Fourier transform (DFT) of a sequence

$$\left\langle j_{PBC}^{Peierls} \right\rangle_{\gamma} (\omega) = \mathrm{FFT} \left\{ \left\langle j_{PBC}^{Peierls} \right\rangle_{\gamma} (t) \right\} \tag{6.159}$$

7 Optoelectronic Dynamics in Linear Response Regime

7.1 Excitonic Effects in 1D Systems: A Toy Model

In this section, we present a 1D toy model with the objective to explore the fundamental properties of excitonic effects in the optical response in 1D crystalline solids, as these systems constitute perfect tools to explore a significant portion of the theoretical knowledge previously written and explored, and its simplicity makes it easy to numerically implement.

Let us consider the following system: a diatomic linear chain (see Figure 1), corresponding to the case where we will have a gap, subject to a short electric pulse along its direction. We will assume a system with Born-von Karman periodic boundary conditions.

7.2 Results and Discussion

In this section, we present the results of the problem depicted in Figure 1, a diatomic linear chain subjected to an external driven field along its direction that will perturb the system out of equilibrium. We are interested in computing the current and the conductance for the noninteracting and interacting system under a linear response regime, following the guidelines provided in the previous chapter.

7.2.1 Optical Driven Field and Average Current in Time

In Figure 9(a) is represented the electric field and the corresponding vector potential, defined by a normalized Lorentzian function and a smooth Heaviside function, direct consequence of the equation (6.151). The pulse simulated parameters are: $\varepsilon_0 = -1^{-5} V/\text{Å}$, $\eta = 0.1\, fs$, $t_0 = 20\, fs$, time step $\delta t = 0.05\, fs$ and time acquisition $T_{acq} = 2000\, fs$. These simulation parameters will remain constant throughout this study. In Figure 9(b) is presented the current's real component in time by applying the equation (6.157), for both noninteracting and interacting systems, where, for the latter, we switch on the Fock term. The Lattice parameters are: bandgap $\Delta = 0.2\, eV$, $h = 1\, eV$, $a_0 = 1\,\text{Å}$, and $N_{UC} = 400$; the interaction term parameters are: $V_0 = 0.1\, eV$ and $\lambda_r = a_0$; the thermodynamic parameters used are $T = 0\text{K}$ and $\mu = 0\, eV$.

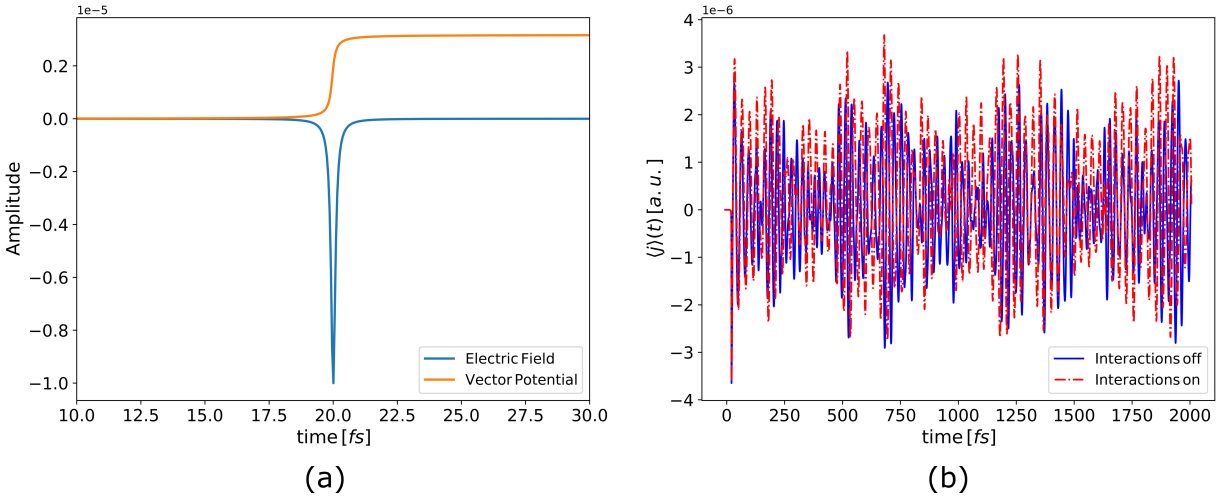

Figure 9: **(a)** Electric field and the corresponding vector potential in the time domain. **(b)** Current propagation in time for system with interactions off and on, where in the latter we switch on the Fock term. Lattice parameters: $\Delta = 0.2\,eV$, $h = 1\,eV$, $a_0 = 1\,$Å and $N_{UC} = 400$; Pulse parameters: $\varepsilon_0 = -1^{-5}\,V/$Å, $t_0 = 20\,fs$, and $\eta = 0.1\,fs$; $V_0 = 0.1\,eV$, and $\lambda_r = a_0$; Simulation parameters: $T_{acq} = 2000\,fs$, and $\delta t = 0.05\,fs$; Thermodynamic parameters: $T = 0$K and $\mu = 0\,eV$. The results are in atomic units.

7.2.2 Response of a Noninteracting System

In this section, we will be considering the noninteracting system, i.e., with the Fock term switched off. In this study, we begin with the study of the current response in the frequencies domain for different sizes for the diatomic chain by doubling the number of unit cells, starting from $N_{UC} = 50$ and to $N_{UC} = 400$. We will also adopt the current response with $N_{UC} = 1000$, given that it is a value that converges well enough and does not require much computational effort, providing results in a timely manner. An important aspect to consider is the fact that the results presented here are determined from the time-dependent current with the post-processing damping term, defined in equation (6.158).

In Figure 10(a)-(b) are displayed these results. We observe a strong response in terms of current around the the value of the conduction band minimum, which makes sense for the noninteracting system. Since we are at a temperature $T = 0$K and a chemical potential with value $\mu = 0\,eV$, we have a semiconductor with the valence band being fully occupied and the conduction band being fully vacant. As a result of our external stimuli via the optical field, electrons are being promoted from the valence band to the conduction band, giving origin to the peaks of ressonance. An interesting curiosity stands out in the results: the fact that we have a current (and conductance) response in the static regime of the system, i.e., a non-zero response at $\omega = 0$. This feature is more pronounced for smaller finite systems (see Figure 10), and moreover, this is not a typical response in semiconductors, but rather in metals due to the Drude weight [99]. This behaviour it is related to the fact that we are using Born-von Karman

periodic boundary conditions. As we discussed before in the Section 2.2, the position operator with PBC is ill-defined, which is solved by working with the Peierls substitution. But does not solve a second point: the fact that a static and uniform vector potential gives origin to a small current, as this can be view as a flux that goes through a ring. Meaning, that this feature is inherent to the system and that it cannot be eliminated. When we perturb the system, we will have a dynamic quasi-momentum dictated by a vector potential $k \to k + eA\left(t\right)/\hbar$. As we have a vector potential described by a positive and smooth Heaviside function, the $k-$states shift to the edge of the 1st Brillouin zone in the positive direction, leading to a negative average velocity, a positive average current and the real part of the conductance with a negative value, as it is shown in Figures 10(a)-(c). As we approach the termodynamic limit, these effects are negligible due to a higher value of the density of states, as it is demonstrated in Figure 11(a). In Figure 10(c)-(d) are computed the real and imaginary parts of the conductance, related to the dispersion and to the absorption, respectively, in a linear response regime. We observe that its behaviour respect the symmetry relations imposed by the equations (6.141) and (6.142), namely the real component must be symmetric and the imaginary component must presents an antisymmetric spectra. For this, we need to confirm that the system is indeed in a linear response regime. One hypothesis would be to linearize the equations (6.146) by expanding them and retaining the linear terms. Another alternative is, as shown in Figure 11(b), for example, to multiply the electric field by a numerical factor, let us say $2\varepsilon_0$, and take the ratio of the Fourier currents between the reference current $\langle j_{\varepsilon_0}\rangle\left(\omega\right)$ and the one multiplied by the numerical factor $\langle j_{2\varepsilon_0}\rangle\left(\omega\right)$. The result should be the ratio of the adopted fields, in this case 0.5, which is confirmed. Another commentary is regarding the oscillations presented in the response for frequency values higher than the gap value. These oscillations correspond to the discretization of energy in momentum space and not, as one might initially deduce, to nonlinear effects. They are intrinsically correlated with the system size, as it is possible to observe in Figure 10(b). As we approach the thermodynamic limit, the results converge, making these oscillations less pronounced.

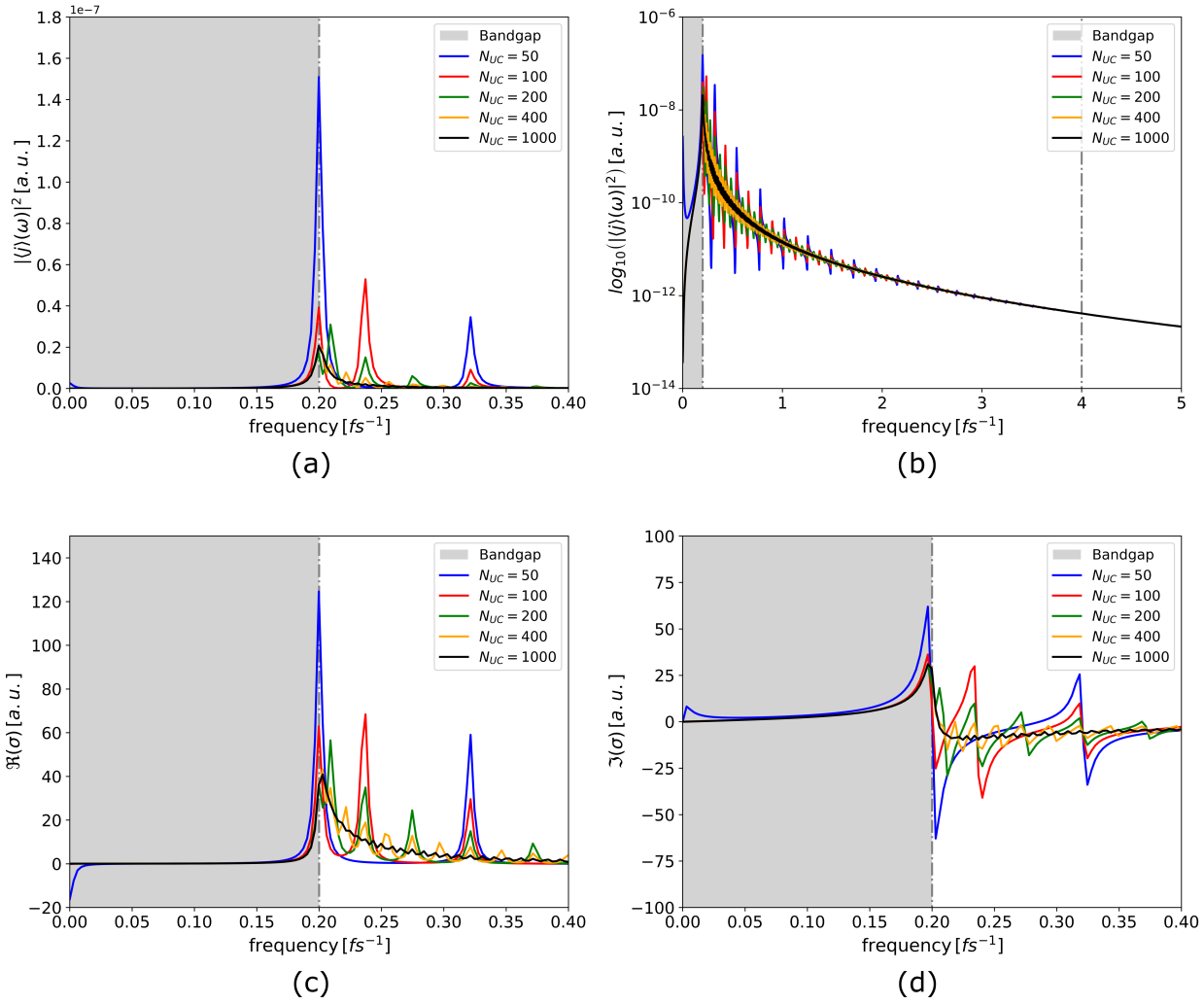

Figure 10: **(a)** Current normalized relative to the number of unit cells (N_{UC}) in the frequencies domain for different number of unit cells and **(b)** the corresponding values in a logarithimic scale. (c) Real and **(d)** Imaginary parts of the conductance normalized relative to the number of unit cells (N_{UC}) with the term of Fock interaction switched off. Lattice parameters: $\Delta = 0.2\,eV$, $h = 1\,eV$, $a_0 = 1$ Å; Pulse parameters: $\varepsilon_0 = -1^{-5}\,V/$Å, $t_0 = 20\,fs$ and $\eta = 0.1\,fs$; Simulation parameters: $T_{acq} = 2000\,fs$ and $\delta t = 0.05\,fs$; Fermi parameters: $T = 0$K and $\mu = 0\,eV$. The results are in atomic units.

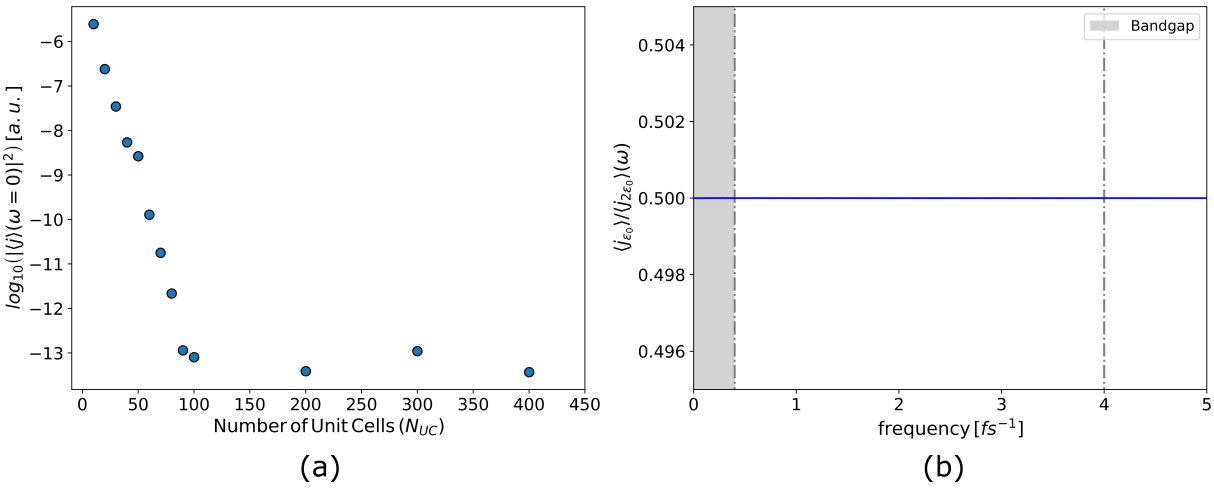

Figure 11: **(a)** Current logarithm in the static regime ($\omega = 0$) for different values of unit cells (N_{UC}). **(b)** Linear response regime testing. Here is computed the quotient between the currents $\langle j_{\varepsilon_0} \rangle$ and $\langle j_{2\varepsilon_0} \rangle$ is computed for $\varepsilon_0 = -1^{-5}\, V/\text{Å}$. Lattice parameters: $\Delta = 0.2\, eV$, $h = 1\, eV$, $a_0 = 1\,\text{Å}$ and $N_{UC} = 400$; Pulse parameters: $t_0 = 20\, fs$, and $\eta = 0.1\, fs$; $V_0 = 0.1\, eV$, and $\lambda_s = a_0$; Simulation parameters: $T_{acq} = 2000\, fs$ and $\delta t = 0.05\, fs$; Thermodynamic parameters: $T = 0$K and $\mu = 0\, eV$. The results are in atomic units.

7.2.3 Response of an Interacting System

In this section, we will be considering the Fock term switched on in order to promote the formation of bound states in the system. In this study, we begin with the study of the current response in the frequency domain for different values of attraction amplitudes, namely the values from $V_0 = 0.1\, eV$ to $V_0 = 0.6\, eV$, with increments of $0.1\, eV$. Regarding the simulation parameters, overall are the same as in the previous section, where we will adopt $N_{UC} = 400$, given that it is a value that converges well enough and does not require much computational effort, providing results in a timely manner. An important aspect to consider is the fact that the results presented here are determined from the time-dependent current with the post-processing damping term, defined in equation (6.158).

In Figure 12, we show the results of the current in the frequency-domain for both noninteracting and interacting systems, the latter with the Fock term switched one. We observe the peak of ressonance for the noninteracting system around the mininum of the conduction band (as expected) and also a set of ressonance peaks inside the bandgap for the case when we consider the Fock interaction term. When an excitonic level resides below the conduction band, it indicates that the exciton's energy is lower than that of a free electron in the conduction band, potentially leading to the formation of bound states. So, we must assess if these signatures correspond effectively to excitonic quantized levels by solving the 1D Wannier equation in real space (the 1D Wannier equation's numerical implementation is demonstrated in Appendix A.2). The parameters used were $E_{gap} = 0.2\, eV$, $N = 800$, $\Delta x = a_0$ and the electron-hole pair's reduced mass is $\mu = m_e * m_h/(m_e + m_h)$, with an effective mass

$m_e^{-1} = \hbar^{-2}\partial^2\epsilon_k/\partial k^2\big|_{k=K}$, with ϵ_k being the diatomic chain's relation of dispersion and K being the point at the edge of the 1st Brillouin zone. Its solutions are depicted in Figure 13(a)-(b), where it is possible to observe a set of eigenvalues both negative and positive, and the corresponding eigenvectors. We are interested in negative energies, since they correspond to binding energies associated with hydrogen-like bound states, the excitons. Each of one is associated with an eigenvector corresponding to the bound states eigenmodes. Per example, note that the case of $V_0 = 0.1\,eV$ only supports one bound state, because only possesses one negative eigenvalue. Which means, that our system only allows the formation of bound states associated with the 1st excitonic mode. On the other hand, for the case of $V_0 = 0.6\,eV$, we have three negative eigenvalues, associated with the 1st, the 2nd and the 3rd excitonic modes (see Figure 13(b)), where the odd modes are symmetric and the even are anti-symmetric. So, the Wannier equation, gives us a way to predict the excitons localization inside the bandgap, which is what is depicted in vertical lines in Figure 12. These results show an excellent agreement between the excitonic resonance peaks and the Wannier solutions. One can also compute the real and imaginary components of the conductance (see Figure 14(a)-(b)), which it shows that they also agree with the 1D Wannier solutions as well as they respect the symmetry relations imposed by the equations (6.141) and (6.142), namely the real component must be symmetric and the imaginary component must present an antisymmetric response profile.

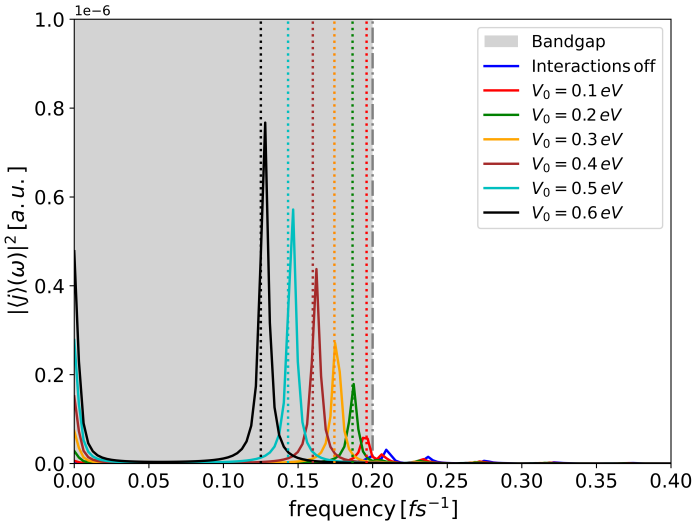

Figure 12: Current normalized relative to the number of unit cells (N_{UC}) with the Fock term switched on. The vertical lines correspond to the the first negative eigenvalues (energies of bound states) determined by the 1D Wannier equation, depicted in Figure 13. Lattice parameters: $\Delta = 0.2\,eV$, $h = 1\,eV$ and $a_0 = 1$ Å; Fock term parameters: $\lambda_r = a_0$; Pulse parameters: $\varepsilon_0 = -1^{-5}\,V/$Å, $t_0 = 20\,fs$ and $\eta = 0.1\,fs$; Simulation parameters: $T_{acq} = 2000\,fs$ and $\delta t = 0.05\,fs$; Fermi parameters: $T = 0$K and $\mu = 0\,eV$. The results are in atomic units.

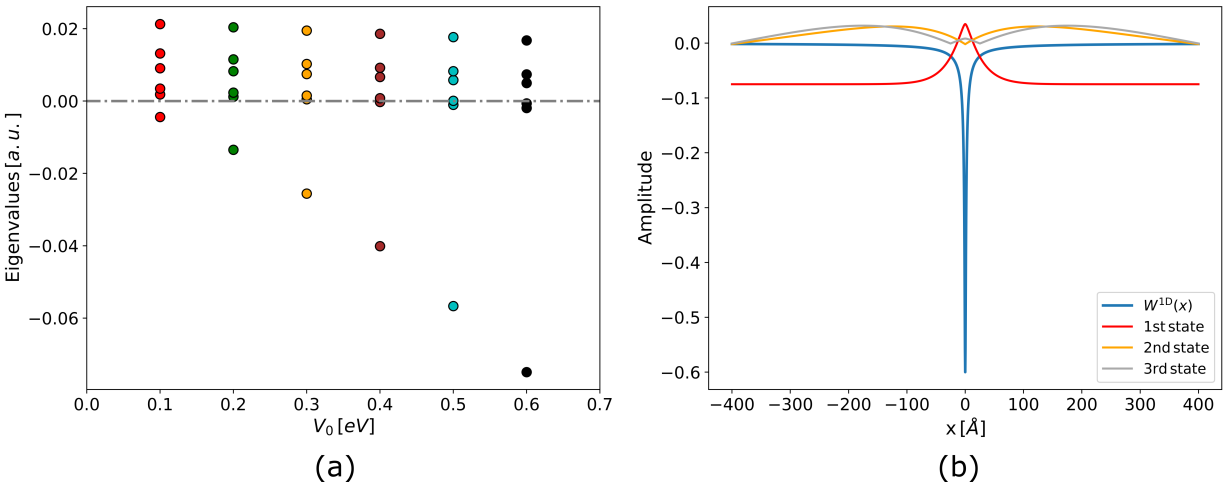

Figure 13: Solutions of the 1D Wannier equation. In **(a)** are presented the eigenvalues for the different values of amplitude of attraction V_0 and in **(b)** the eigenmodes in terms of absolute value for the case $V_0 = 0.6\,eV$. Here is computed the quantity $E + |\Psi|$, where E and Ψ are the negative eigenvalues and the corresponding eigenvectors, respectively. The parameters used were: $E_{gap} = 0.2\,eV$, $N = 800$, $\Delta x = a_0$ and $\lambda_r = a_0$. The results are in atomic units.

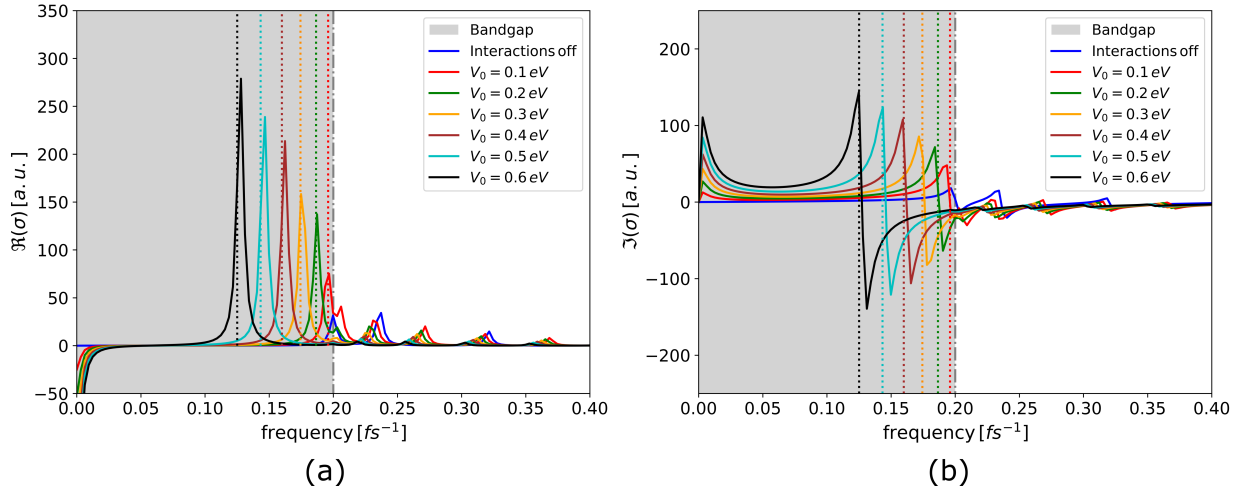

Figure 14: **(a)** Real and **(b)** Imaginary parts of the conductance normalized relative to the number of unit cells (N_{UC}) with the term of Fock interaction switched on. Lattice parameters: $\Delta = 0.2\,eV$, $h = 1\,eV$ and $a_0 = 1$ Å; Fock term parameters: $\lambda_r = a_0$; Pulse parameters: $\varepsilon_0 = -1^{-5}\,V/$Å, $t_0 = 20\,fs$ and $\eta = 0.1\,fs$; Simulation parameters: $T_{acq} = 2000\,fs$ and $\delta t = 0.05\,fs$; Fermi parameters: $T = 0$K and $\mu = 0\,eV$. The results are in atomic units.

8 Optoelectronic Dynamics in Nonlinear Response Regime

8.1 Nonlinear Bloch Oscillations

Bloch Oscillations (BO's), as the name suggests, refer to the coherent oscillation of a particle's average position and velocity when subject to a periodic potential and an uniform electric field (see Section 2.2). This behaviour is described by the Hamiltonian

$$\mathcal{H}(t) = \mathcal{H}_0 + \mathcal{H}_I(t) \tag{8.160}$$

where

$$\mathcal{H}_0 = \frac{\mathbf{p}^2}{2m} + U(\mathbf{r}), \text{ with } U(\mathbf{r}+\mathbf{R}) = U(\mathbf{r}) \tag{8.161}$$

$$\mathcal{H}_I(t) = |e|\boldsymbol{\varepsilon}(t)\cdot\mathbf{r} \tag{8.162}$$

One would classically expect a particle subject to a constant electric field would undergo with an uniform acceleration through space. However, the introduction of a periodic potential disrupts this classical expectation, leading to oscillatory motion of the particle instead. We will see that this behavior is present in both semi-classical limit and a purely quantum scenario, the underlying nature of this phenomenon remains the same: it originates from the fundamental concept that a particle is characterized by wave-like attributes, and the normal modes of a periodic Hamiltonian obeys the Bloch's theorem.

Let us consider a gapless 1D tight-binding system constituted by a monoatomic chain subjected to a classical and monochromatic electric pulse, which is polarized in the direction of the solid (see the Figure 1). We will admit that we will have a single electron confined within an electronic band and we want evaluate its dynamics over time, in the absence of collisions, which will lead, under certain circumstances, to nonlinear Bloch oscillations. This prediction is entirely based on the knowledge of the band structure of the metal/insulator, i.e., the dispersion relation is upon the form of $\epsilon_n(\mathbf{k}(t))$ and upon no other explicit information about the periodic potential of the ions. This way we can relate the band structure to the transport properties, i.e., the response of the electrons to applied external fields.

8.1.1 Bloch Oscillations in a Gapless 1D System

8.1.1.1 Semi-Classical Description

According to Bloch's theorem, the solutions to the Schrödinger equation in a periodic potential can be described as a combination of plane waves modulated by a periodic function

$$\psi_{n\mathbf{k}}(\mathbf{r}) = e^{i\mathbf{k}\cdot\mathbf{r}}u_n(\mathbf{r}) \tag{8.163}$$

where $u_n(\mathbf{r})$ is a periodic function with the same periodicity as the periodic potential and the index n indicates the band[12]. Now, let us consider a generic single particle Hamiltonian diagonalizable by these wavefunctions:

$$\mathcal{H}_0 |\psi_{n\mathbf{k}}\rangle = \epsilon_{n\mathbf{k}} |\psi_{n\mathbf{k}}\rangle \tag{8.164}$$

The mean velocity of a Bloch wave [100] is written as

$$v_n(\mathbf{k}) = \frac{1}{\hbar}\frac{\partial \epsilon_n(\mathbf{k})}{\partial \mathbf{k}} \tag{8.165}$$

This result[13] provides a way to calculate the mean velocity of a particle by knowing the dispersion relation $\epsilon_n(\mathbf{k})$ of a given band n. Moreover, it give us a way of determine the position's time evolution of the same particle by noticing that $\dot{\mathbf{r}}_n(\mathbf{k}) \equiv \mathbf{v}_n(\mathbf{k})$.

When an electric field is introduced, it generates an equation of motion for the quasi-momentum $\mathbf{k}$. Consequently, the Hamiltonian takes the following form [100]:

$$\mathcal{H} = \mathcal{H}_0 + \phi(\mathbf{r}) \tag{8.166}$$

such that $-\nabla\phi = e\boldsymbol{\varepsilon}$, where $\boldsymbol{\varepsilon}$ denotes the electric field and e is the particle's charge. The motivation for obtaining the second semi-classical equation stems from the principle of energy conservation. In other words, we should expect each wave packet to move so that the energy introduced by the potential $\phi(\mathbf{r}(t))$ in the time interval from t to $t+dt$ must be equivalent to the $\epsilon_n(\mathbf{k}(t))$ time variation in the same interval [100]. As $dt \to 0$, we can express this condition as

$$\frac{d\epsilon_n(\mathbf{k}(t))}{dt} - \frac{d\phi(\mathbf{r}(t))}{dt} = 0 \tag{8.167}$$

By manipulating the previous equation, it gives

$$\frac{\partial \epsilon_n(\mathbf{k}(t))}{\partial \mathbf{k}} \cdot \dot{\mathbf{k}} - \nabla\phi(\mathbf{r}(t)) \cdot \dot{\mathbf{r}} = 0 \tag{8.168}$$

Taking into account that $\dot{\mathbf{r}}_n(\mathbf{k}) \equiv \mathbf{v}_n(\mathbf{k})$ and the equation (8.165), we realize that equation (8.168) is satisfied if

$$\hbar\dot{\mathbf{k}} = -e\boldsymbol{\varepsilon} \tag{8.169}$$

We arrive at a close set of differential equations that describe the average motion of a particle subjected to a periodic potential along with an uniform electric field. In the case of one dimension, these equations can be expressed in a concise form as follow:

$$\hbar\frac{dk}{dt} = -e\varepsilon \tag{8.170}$$

$$v_n(k) = \frac{1}{\hbar}\frac{\partial \epsilon_n(k)}{\partial k} \tag{8.171}$$

[12] In this problem, the index n will be a constant of motion since the particle is confined to a monoband

[13] Note that this result can be traced back to the group velocity of a wave-packet, which is given by $\partial\omega/\partial\mathbf{k}$

Note that this formalism is designed in the absence of magnetic field or for systems with weak magnetic response [100].

If one chooses a tight-binding 1D system dictated by a monoatomic chain's dispersion relation

$$\epsilon_{k(t)} = -2h\cos\left(k\left(t\right)a_0\right) \tag{8.172}$$

with h being the hopping integral between first neighbours and a_0 the lattice constant, being perturbed by a monochromatic driven electric field with frequency $\hbar\omega_l$, the equations of motion (8.165) and (8.169) yield

$$k\left(t\right) = k_0 + \frac{eA_0}{\hbar}\sin\left(\omega_l t\right) \tag{8.173}$$

$$\langle v\rangle\left(t\right) = \frac{2ha_0}{\hbar}\sin\left(\left(k_0 + \frac{eA_0}{\hbar}\sin\left(\omega_l t\right)\right)a_0\right) \tag{8.174}$$

where we are defining the electric field as $\varepsilon(t) = \varepsilon_0\cos(\omega_l t)$ and $\varepsilon(t) = -\partial_t A(t)$, within a Weyl gauge choice. From the time integration, arises the quantity $k_0 \equiv k\left(t = t_0\right)$ that corresponds to the single electronic state at $t = t_0$ and we are assuming that $A\left(t = t_0\right) = 0$. Moreover, we will adopt that $t_0 = 0$. Under these considerations, we define the current of one single state in the band as

$$\begin{aligned}\langle j\rangle\left(t\right) &= -e\langle v\rangle\left(t\right)\\ &= \frac{2\pi ea_0}{\phi_0}\left[\cos\left(\frac{ea_0A_0}{\hbar}\sin\left(\omega_l t\right)\right)\epsilon_{k_0-\frac{\pi}{2a_0}} + \sin\left(\frac{ea_0A_0}{\hbar}\sin\left(\omega_l t\right)\right)\epsilon_{k_0}\right]\end{aligned} \tag{8.175}$$

This expression is written in a compact way by considering the trigonometric identity formula $\sin\left(a+b\right) = \sin(a)\cos(b)+\sin(b)\cos(a)$ and the dispersion relation defined in (8.172), where we decoupled the time-dependent term from the constant term.

Besides inspecting the system's response to a time-dependent external perturbation, we also want to study the optical response in the frequency domain through the Fourier analysis. By recalling the definition of a continuous Fourier transform

$$F\left(\omega\right) = \int_{-\infty}^{+\infty} f\left(t\right)e^{i\omega t}dt$$

we may determine the electric field and in the current's average in the Fourier space

$$\varepsilon\left(\omega\right) = \pi\varepsilon_0\left[\delta\left(\omega+\omega_l\right) + \delta\left(\omega-\omega_l\right)\right] \tag{8.176}$$

$$\begin{aligned}\langle j\rangle\left(\omega\right) = {}& \frac{4\pi^2 ea_0}{\phi_0}J_0\left(\frac{ea_0A_0}{\hbar}\right)\delta\left(\omega\right)\epsilon_{k_0-\frac{\pi}{2a_0}}\\ &+ \frac{4\pi^2 ea_0}{\phi_0}\sum_{n=1}^{+\infty}J_{2n}\left(\frac{ea_0A_0}{\hbar}\right)\left[\delta\left(\omega+2n\omega_l\right) + \delta\left(\omega-2n\omega_l\right)\right]\epsilon_{k_0-\frac{\pi}{2a_0}}\\ &- i\frac{4\pi^2 ea_0}{\phi_0}\sum_{n=1}^{+\infty}J_{2n-1}\left(\frac{ea_0A_0}{\hbar}\right)\delta\left(\omega+\left(2n-1\right)\omega_l\right)\epsilon_{k_0}\\ &+ i\frac{4\pi^2 ea_0}{\phi_0}\sum_{n=1}^{+\infty}J_{2n-1}\left(\frac{ea_0A_0}{\hbar}\right)\delta\left(\omega-\left(2n-1\right)\omega_l\right)\epsilon_{k_0}\end{aligned} \tag{8.177}$$

where ω_l is the monochromatic electric pulse's frequency, $J_n(z)$ represents the Bessel function of the first kind of order n, ε_0 and A_0 are the electric field and vector potential amplitudes. The previous results were determined by considering the Jacobi-Anger expansions, which allow us to express the previous harmonic functions in a series representation of complex exponential function in terms of Bessel functions and trigonometric functions

$$\sin\left(C_0 \sin\left(\omega_l t\right)\right) = 2\sum_{n=1}^{+\infty} J_{2n-1}\left(C_0\right) \sin\left(\left(2n-1\right)\omega_l t\right)$$

$$\cos\left(C_0 \sin\left(\omega_l t\right)\right) = J_0\left(C_0\right) + 2\sum_{n=1}^{+\infty} J_{2n}\left(C_0\right) \cos\left(2n\omega_l t\right)$$

It was also employed the well-known integral representation for the Dirac delta function

$$\delta\left(\omega\right) = \frac{1}{2\pi}\int_{-\infty}^{+\infty} e^{i\omega t} dt \tag{8.178}$$

8.1.1.2 Quantum-Mechanical Description

Let us start by explicitly expressing the Hamiltonian for a monoatomic chain written in a tight-binding basis with Born-von Karman periodic boundary conditions (PBC) perturbed by an electric driven field. As we saw at Section 2.2, we can do the light-matter coupling via Peierls substitution:

$$\mathcal{H}\left(t\right) = -h\sum_{n=0}^{N-1}\left(e^{-i2\pi\frac{\phi(t)}{\phi_0 N}} c_{n+1}^{\dagger} c_n + e^{i2\pi\frac{\phi(t)}{\phi_0 N}} c_n^{\dagger} c_{n+1}\right) \tag{8.179}$$

where the quantity $\phi_0 = h/e$ is the quanta of magnetic flux and $\phi\left(t\right)$ the flux inside the ring that can be related with the electric field by the relation

$$\phi\left(t\right) = \int_0^{Na_0} A\left(t\right) dx = Na_0 A\left(t\right) \tag{8.180}$$

where a_0 is the lattice parameter and A is the vector potential is correlated with the electric field via $\varepsilon\left(t\right) = -\partial_t A\left(t\right)$ within a Weyl gauge. Due to the translational symmetry, the Hamiltonian (8.179) is easily diagonalizable by using Bloch states, leading to the following expression:

$$\mathcal{H}\left(t\right) = -2h\sum_k \cos\left(2\pi\frac{\phi\left(t\right)}{\phi_0 N} + ka_0\right) c_k^{\dagger} c_k \tag{8.181}$$

Within a Peierls substitution, we write the current operator as

$$\begin{aligned} j\left(t\right) &= -\frac{\delta\mathcal{H}}{\delta A} \\ &= -\frac{e}{a_0}\sum_k v\left(k\left(t\right)\right) c_k^{\dagger} c_k \end{aligned} \tag{8.182}$$

with the velocity being defined as

$$v\left(k\left(t\right)\right) = \frac{2ha_0}{\hbar} \sin\left(k\left(t\right) a_0\right) \tag{8.183}$$

and the quasi-momentum varies in time with the flux accordingly to

$$k\left(t\right)=k+\frac{2\pi\phi\left(t\right)}{a_{0}N\phi_{0}} \tag{8.184}$$

Note that these results reflect the behaviour described by the semi-classical equations (8.173) and (8.174).

Let us determine how the density matrix evolves in time, starting by writing its equation of motion

$$\begin{aligned}\frac{d\rho_{kk'}\left(t\right)}{dt}&=\frac{i}{\hbar}\left[\mathcal{H}_{kk}\left(t\right)\rho_{kk'}\left(t\right)-\rho_{kk'}\left(t\right)\mathcal{H}_{k'k'}\left(t\right)\right]\\&=\frac{i}{\hbar}\left[\mathcal{H}_{kk}\left(t\right)-\mathcal{H}_{k'k'}\left(t\right)\right]\rho_{kk'}\left(t\right)\\&=-i\frac{2h}{\hbar}\left[\cos\left(ka_{0}+\frac{2\pi\phi\left(t\right)}{a_{0}N\phi_{0}}\right)-\cos\left(k'a_{0}+\frac{2\pi\phi\left(t\right)}{a_{0}N\phi_{0}}\right)\right]\rho_{kk'}\left(t\right)\end{aligned} \tag{8.185}$$

where we used the fact that the Hamiltonian is diagonal in this basis. Let us then start with a thermalized state [101] at $t=0$

$$\begin{aligned}\rho_{kk'}\left(0\right)&=f_{F-D}\left(\epsilon_{k}\right)\delta_{kk'}\\\xrightarrow{\text{time evolution}}\rho_{kk'}\left(t\right)&=\begin{cases}0, & \text{if } k\neq k'\\ \rho_{kk}\left(0\right), & \text{if } k=k'\end{cases}\end{aligned} \tag{8.186}$$

where we establish the density matrix's time evolution. We can determine the average current in such a state already written in terms of the monoatomic 1D linear chain's dispersion relation

$$\begin{aligned}\left\langle j\right\rangle\left(t\right)&=\text{Tr}\left(\rho\left(t\right)j\left(t\right)\right)=-\frac{2he}{\hbar}\sum_{k}f_{F-D}\left(\epsilon_{k}\right)\sin\left(ka_{0}+2\pi\frac{\phi\left(t\right)}{N\phi_{0}}\right)\\&=\frac{e}{\hbar}\left(\cos\left(2\pi\frac{\phi\left(t\right)}{N\phi_{0}}\right)\sum_{k}f_{F-D}\left(\epsilon_{k}\right)\epsilon_{k-\frac{\pi}{2a_{0}}}+\sin\left(2\pi\frac{\phi\left(t\right)}{N\phi_{0}}\right)\sum_{k}f_{F-D}\left(\epsilon_{k}\right)\epsilon_{k}\right)\end{aligned} \tag{8.187}$$

where the charge density here is described by the Fermi-Dirac distribution. The monoatomic linear chain's Peierls Hamiltonian displays time inversion symmetry in the first Brillouin zone, resulting in a symmetric dispersion relation. Meaning, that $\epsilon_{k}=\epsilon_{-k}$, with $k\in$ 1st B.Z.. This has consequences in the occupation function, in particular, $f_{F-D}\left(\epsilon_{k}\right)=f_{F-D}\left(\epsilon_{-k}\right)$. This implies that the first term is zero, since the sine function, defined implicitly in the term $\epsilon_{k-\frac{\pi}{2a_{0}}}$, is anti-symmetric. So, we conclude that average density current evolves in time as

$$\left\langle j\right\rangle\left(t\right)=\frac{e}{\hbar}\sin\left(2\pi\frac{\phi\left(t\right)}{N\phi_{0}}\right)\sum_{k}f_{F-D}\left(\epsilon_{k}\right)\epsilon_{k} \tag{8.188}$$

This result emerges from perturbing the initial thermalized state using a time-varying electric field, giving rise to nonequilibrium oscillatory dynamics in the observed current.

For a given uniform system, the local current operator should displays the same oscillations as in equation (8.188). The local current operator, which describes the current through a single bond $n\rightarrow n+1$ from the Peierls Hamiltonian defined in (8.179), it gives

$$\begin{aligned}j_{n}\left(t\right)&=-\frac{\delta\mathcal{H}}{\delta A}\\&=-i\left(\frac{ea_{0}}{\hbar}\right)\left(e^{-i2\pi\frac{\phi(t)}{\phi_{0}N}}c_{n+1}^{\dagger}c_{n}-e^{i2\pi\frac{\phi(t)}{\phi_{0}N}}c_{n}^{\dagger}c_{n+1}\right)\end{aligned} \tag{8.189}$$

where its average time-evolution gives us

$$\begin{aligned}\langle j_n \rangle (t) &= -i\frac{hea_0}{\hbar}\left(e^{-i2\pi\frac{\phi(t)}{\phi_0 N}}\left\langle c_{n+1}^{\dagger}c_n\right\rangle - e^{i2\pi\frac{\phi(t)}{\phi_0 N}}\left\langle c_n^{\dagger}c_{n+1}\right\rangle\right) \\ &= -\frac{2hea_0}{\hbar}\sum_k f_{F-D}(\epsilon_k)\sin\left(ka_0 + 2\pi\frac{\phi(t)}{\phi_0 N}\right)\end{aligned} \tag{8.190}$$

where here we applied the relation

$$\begin{aligned}\left\langle c_{n+1}^{\dagger}c_n\right\rangle &= \sum_{kk'}\left\langle c_k^{\dagger}c_{k'}\right\rangle e^{-ika_0} = \sum_{kk'}\rho_{k'k}\delta_{kk'}e^{-ika_0} \\ &= \sum_k f_{F-D}(\epsilon_k)\, e^{-ika_0}\end{aligned} \tag{8.191}$$

8.1.1.3 Results and Discussion

Before diving in into the results, I want to point out that the numerical implementation guideline of the quantum approach via Peierls substitution is presented in the Chapter II.

The resulting currents in time are compared in Figure 15(a) and they show a perfect agreement between the semi-classical approach with the quantum-mechanical description of the problem through the Peierls substitution. The current exhibits multiple oscillation periods: on the timescale $2\pi/\omega_l$, which corresponds to the period of the vector potential $A(t)$, the current has a nonsinusoidal time dependence (nonlinear Bloch oscillations). These oscillations occur due to the large amplitude A_0. When we turn on the external stimuli, the $k-$states, initially static, are now time-dependent with the vector potential, meaning $k \to k + eA(t)/\hbar$, in which the electrons will move with $A(t)$, passing through the boundaries of the 1st Brillouin zone, leading to a reversal of the current [82]. From these results, one can examine the response in the frequency-domain by performing a discrete Fourier transform. In Figure 15(b) are presented these results and it shows the presence of several peaks of ressonances which correspond to the generation of nonlinear harmonics. It shows that they coincide with the linear harmonic at $\omega = \omega_l$, which corresponds to the laser frequency, and the remain nonlinear harmonics are defined at odd frequencies, where these agree with the analytical solutions (in dark grey) in equation (8.177) for the initial state $k_0 = 0$ (at the center of the 1st Brillouin zone). We previously discussed in equation (8.188) that these results are actually dictated by the time-inversion symmetry of the problem. In light grey, we have these solutions represented, the even solutions, that would correspond to the case in which the electron had an initial state $k_0 = \pi/2a_0$. We observe that they are not allowed due to the symmetry properties of the problem's Brillouin Zone.

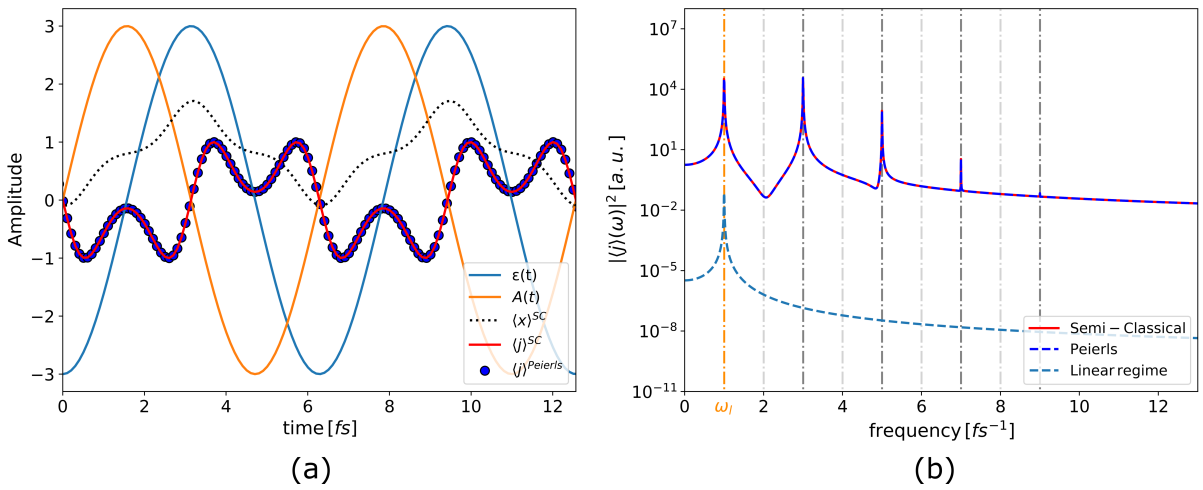

Figure 15: Bloch Oscillations in a 1D gapless system perturbed by a monochromatic electric field for both a semi-classical and a quantum mechanical approaches for a single fermionic state. In **(a)** are results in the time domain, where it is depicted the electric field $(\varepsilon(t))$, the vector potential $(A(t))$, the average position $\langle x \rangle$ (this quantity is determined by integrating in time the equation (8.174)), and the average current via semi-classical (SC) and quantum mechanical (Peierls) approaches. In **(b)** it is represented the average current in the frequencies domain, with the analytic solutions defined in equation (8.177) in vertical lines, for $k_0 = 0$ (in dark grey) and $k_0 = \pi/2a_0$ (in light grey). Pulse parameters: $E_0 = -3\,V/\text{Å}$, pulse frequency $\omega_l = 1\,fs^{-1}$; Lattice parameters: $h = 1/2\,eV$, $a_0 = 1\,\text{Å}$, $N_{UC} = 3$; Simulation parameters: $T_{acq} = 750\,fs$ and $\delta t = 0.1\,fs$; Fermi parameters: $T = 0\text{K}$ and $\mu = 0\,eV$. The results are in atomic units.

9 Final Remarks and Future Work

In this work, we developed a general nonequilibrium quantum theory to study linear and nonlinear response regime induced by ultrafast attosecond laser pulses applied to condensed matter systems. In particular, we propose a method in real-time and -space that enables the study of optoelectronic response in semiconductors in the presence of a driving field by propagating in time the one-particle reduced density matrix. We show that our formalism based on a time-dependent mean-field Hartree-Fock approximation applied to the one-particle reduced density matrix can be efficiently implemented and how its propagation in time opens up the opportunity to observe the electronic motion of free carriers as well as bound states, managing to capture the formation of excitons in an ultrafast timescale.

In this study, we employed 1D tight-binding models as a platform to investigate optoelectronic dynamics in both linear and nonlinear response regimes. In our first case of study, we considered a diatomic linear chain with Born-von Karman periodic boundary conditions being driven out-of-equilibrium via an electric short-pulse in a linear response regime. We studied the dynamics of free carriers and the formation of excitons by switching on the Fock interaction term. The role of the excitonic effects in this regime is accessed by analyzing the Fourier transform of the time-dependent current. We observed that the free carriers case possess a strong optical response around the minimum of the conduction band, as we are promoting electrons from the valence band to the conduction band. When we turn on the Fock interaction term, we observe the formation of ressonance peaks inside the bandgap of the system, which we attribute this to bound states. We then solved the Wannier equation and found that the resonance peaks coincide with the excitonic binding energies, signifying that these signatures constitute a set of excitonic quantized energy levels. We also noticed that the frequency of these peaks and their amplitude of response are directly connected with the strength of attraction adopted in the Fock term. We observed that as we increased the amplitude of attraction, the peaks of ressonance are redshifted, making the excitons become more localized in the lattice. Lastly, we investigate the generation of nonlinear Bloch oscillations in a monoatomic linear chain with Born-von Karman periodic boundary conditions. We considered the system being driven out-of-equilibrium by a monochromatic electric pulse with a very high electric field amplitude, pushing the system into a nonlinear response regime. We demonstrated that this phenomenom is captured in both semi-classical limit, which possesses an analytical solution, and a purely quantum scenario, which is captured by our formalism. We showed that the results from both approaches coincide perfectly.

As future lines of research, it would be interesting to apply the formalism to 2D layered systems, such as TMDs (e.g. hBN) or van der Waals (vdW) heterostructures, to explore optoelectronic phenomena in both linear and nonlinear regimes. A phenomenon of great interest to study would be the High-Harmonic generation (HHG). It constitutes a nonlinear phenomenon in solids that has gained significant attention in recent years and recently associated with the Nobel Prize in Physics 2023, due to its crucial importance in giving information regarding the fundamental optoelectronic dynamics properties, in both free carriers and excitons. Our real-space approach opens up the opportunity to implement atomic defects, which would be interesting to study how they affect the excitonic response. It would also be of great importance to compare results between simulations and time-resolved experiments in the attosecond timescale in order to compare and even predict outcomes. Another interesting aspect

to explore would be to exploit the locality properties of the reduced density matrix in the development of a linear scaling algorithm to calculate observables.

Bibliography

[1] K. S. Novoselov, A. K. Geim, S. V. Morozov, D. Jiang, Y. Zhang, S. V. Dubonos, I. V. Grigorieva, and A. A. Firsov. Electric field effect in atomically thin carbon films. *Science*, 306(5696):666–669, 2004.

[2] et al. Andrea C. Ferrari. Science and technology roadmap for graphene, related two-dimensional crystals, and hybrid systems. *Nanoscale*, 7:4598–4810, 2015.

[3] B. Radisavljevic, A. Radenovic, J. Brivio, V. Giacometti, and A. Kis. Single-layer mos2 transistors. *Nature Nanotechnology*, 6:147–150, 2011.

[4] Guo Jun Ye Qingqin Ge Xuedong Ou Hua Wu Donglai Feng Xian Hui Chen Likai Li, Yijun Yu and Yuanbo Zhang. Black phosphorus field-effect transistors. *Nature Nanotechnology*, 9:372–377, 2014.

[5] Daniele Chiappe Carlo Grazianetti Marco Fanciulli Madan Dubey Alessandro Molle Li Tao, Eugenio Cinquanta and Deji Akinwande. Silicene field-effect transistors operating at room temperature. *Nature Nanotechnology*, 10:227–231, 2015.

[6] R. Jalil B. D. Belle F. Schedin et al. L. Britnell, R. V. Gorbachev. Field-effect tunneling transistor based on vertical graphene heterostructures. *Science*, 335(6071):947–950, 2012.

[7] Wenjie Liang Rongming Wang Jingang Wang, Fengcai Ma and Mengtao Sun. Optical, photonic and optoelectronic properties of graphene, h-bn and their hybrid materials. *Nanophotonics*, 6(5):943–976, 2017.

[8] Jeonghyeon Park Semi Im et al. Seokho Moon, Jiye Kim. Hexagonal boron nitride for next-generation photonics and electronics. *Advanced Materials*, 35(4):2204161, 2023.

[9] Leonardo Viti and Miriam Serena Vitiello. Tailored nano-electronics and photonics with two-dimensional materials at terahertz frequencies. *Journal of Applied Physics*, 130(17):170903, 2021.

[10] Minmin Shi Mingsheng Xu, Tao Liang and Hongzheng Chen. Graphene-like two-dimensional materials. *Chemical Reviews*, 113(5):3766–3798, 2013.

[11] Thomas Muller and Ermin Malic. Exciton physics and device application of two-dimensional transition metal dichalcogenide semiconductors. *npj 2D Materials and Applications*, 2:29, 2018.

[12] Peter Schmidt Mark B. Lundeberg Simone Latini Sten Haastrup et al. Mathieu Massicotte, Fabien Vialla. Dissociation of two-dimensional excitons in monolayer wse2. *Nature Communications*, 92.

[13] Gang Wang, Alexey Chernikov, Mikhail M. Glazov, Tony F. Heinz, Xavier Marie, Thierry Amand, and Bernhard Urbaszek. Colloquium: Excitons in atomically thin transition metal dichalcogenides. *Rev. Mod. Phys.*, 90:021001, Apr 2018.

[14] Hongyi Yu, Xiaodong Cui, Xiaodong Xu, and Wang Yao. Valley excitons in two-dimensional semiconductors. *National Science Review*, 2(1):57–70, 2015.

[15] Jamie M. Fitzgerald Joshua J. P. Thompson Roberto Rosati Samuel Brem Raul Perea-Causin, Daniel Erkensten and Ermin Malic. Exciton optics, dynamics, and transport in atomically thin semiconductors. *APL Materials*, 10(10):100701, 2022.

[16] Fengyuan Xuan and Su Ying Quek. Valley zeeman effect and landau levels in two-dimensional transition metal dichalcogenides. *Phys. Rev. Res.*, 2:033256, Aug 2020.

[17] Diana Y. Qiu, Felipe H. da Jornada, and Steven G. Louie. Optical spectrum of mos_2: Many-body effects and diversity of exciton states. *Phys. Rev. Lett.*, 111:216805, Nov 2013.

[18] Iacopo Torre António T. Costa et al. A. Reserbat-Plantey, Itai Epstein. Quantum nanophotonics in two-dimensional materials. *ACS Photonics*, 8(1):85–101, 2021.

[19] Hongyi Yu, Gui-Bin Liu, and Wang Yao. Brightened spin-triplet interlayer excitons and optical selection rules in van der waals heterobilayers. *2D Materials*.

[20] Xidong Duan Hung-Chieh Cheng Yu Huang Yuan Liu, Nathan O. Weiss and Xiangfeng Duan. Van der waals heterostructures and devices. *PNature Reviews Materials*, 1:16042, 2016.

[21] Xinyi Cui Shi-Jun Liang, Bin Cheng and Feng Miao. Van der waals heterostructures for high-performance device applications: Challenges and opportunities. *Advanced Materials*, 32(27):1903800, 2020.

[22] Jung-Hwan Song Pieter G. Kik Jorik van de Groep, Qitong Li and Mark L. Brongersma. Impact of substrates and quantum effects on exciton line shapes of 2d semiconductors at room temperature. *Nanophotonics*, 12(16):3291–3300, 2023.

[23] Yuan Wang Jun Xiao, Mervin Zhao and Xiang Zhang. Excitons in atomically thin 2d semiconductors and their applications. *Nanophotonics*, 6(6):1309–1328, 2017.

[24] Kaiyuan Yao, Aiming Yan, Salman Kahn, Aslihan Suslu, Yufeng Liang, Edward S. Barnard, Sefaattin Tongay, Alex Zettl, Nicholas J. Borys, and P. James Schuck. Optically discriminating carrier-induced quasiparticle band gap and exciton energy renormalization in monolayer mos_2. *Phys. Rev. Lett.*, 119:087401, Aug 2017.

[25] Alexey Chernikov, Timothy C. Berkelbach, Heather M. Hill, Albert Rigosi, Yilei Li, Burak Aslan, David R. Reichman, Mark S. Hybertsen, and Tony F. Heinz. Exciton binding energy and nonhydrogenic rydberg series in monolayer ws_2. *Phys. Rev. Lett.*, 113:076802, Aug 2014.

[26] R.S. Knox. *in Collective Excitations in Solids*. Springer, 1983.

[27] Lorenzo Gatto Salvatore Stagira Eugenio Cinquanta, Eva Arianna Aurelia Pogna and Caterina Vozzi. Charge carrier dynamics in 2d materials probed by ultrafast thzspectroscopy. *Advances in Physics: X*, 8(1):2120416, 2023.

[28] Martin Schultze, Krupa Ramasesha, C.D. Pemmaraju, S.A. Sato, D. Whitmore, A. Gandman, James S. Prell, L. J. Borja, D. Prendergast, K. Yabana, Daniel M. Neumark, and Stephen R. Leone. Attosecond band-gap dynamics in silicon. *Science*, 346(6215):1348–1352, 2014.

[29] Sheng-Chih Lin Jacob A. Spies Alfred Zong, Bailey R. Nebgen and Michael Zuerch. Emerging ultrafast techniques for studying quantum materials. *Nature Reviews Materials*, 8:224–240, 2023.

[30] Joel D. Cox Tony Zhu Francisco Silva Stephan Teichmann Mathieu Massicotte Frank Koppens Leonid S. Levitov F. Javier García de Abajo Mathias Baudisch, Andrea Marini and Jens Biegert. Ultrafast nonlinear optical response of dirac fermions in graphene. *Nature Communications*, 9:1018, 2018.

[31] Nicholas J. Borys Malte Selig et al. Chiara Trovatello, Florian Katsch. The ultrafast onset of exciton formation in 2d semiconductors. *Nature Communications*, 11:5277, 2020.

[32] Seongkwang Bae, Sanghee Nah, Doeon Lee, Muhammad Sajjad, Nirpendra Singh, Ku Min Kang, Sanghoon Kim, Geun-Ju Kim, Jaekyun Kim, Hionsuck Baik, Kyusang Lee, and Sangwan Sim. Exciton-dominated ultrafast optical response in atomically thin ptse2. *Small*, 17(45):2103400, 2021.

[33] Po-Cheng Tsai et al. Hsu-Sheng Tsai, Yung-Hung Huang. Ultrafast exciton dynamics in scalable monolayer mos2 synthesized by metal sulfurization. *ACS Omega*, 5:10725–10730, 2020.

[34] Tobias Hertel Konrad Birkmeier and Achim Hartschuh. Probing the ultrafast dynamics of excitons in single semiconducting carbon nanotubes. *Nature Communications*, 13:6290, 2022.

[35] Paul Birk Gergana Borisova Christian Ott Maximilian Hartmann, Veit Stooß and Thomas Pfeifer. Attosecond precision in delay measurements using transient absorption spectroscopy. *Opt. Lett.*, 44(19):4749–4752, 2019.

[36] Stephen R. Leone Krupa Ramasesha and Daniel M. Neumark. Real-time probing of electron dynamics using attosecond time-resolved spectroscopy. *Annual Review of Physical Chemistry*, 67(1):41–63, 2016.

[37] Giacinto D. Lucarelli Bruno Moio Giacomo Inzani Rocío Borrego-Varillas et al. Matteo Lucchini, Shunsuke A. Sato. Unravelling the intertwined atomic and bulk nature of localised excitons by attosecond spectroscopy. *Nature Communications*, 12(1):1021, 2021.

[38] R. D. Averitt D. N. Basov and D. Hsieh. Towards properties on demand in quantum materials. *Nature Materials*, 16:1077–1088, 2017.

[39] Takashi Oka and Hideo Aoki. Photovoltaic hall effect in graphene. *Phys. Rev. B*, 79:081406, Feb 2009.

[40] Jun ichi Inoue and Akihiro Tanaka. Photoinduced transition between conventional and topological insulators in two-dimensional electronic systems. *Phys. Rev. Lett.*, 105:017401, Jun 2010.

[41] Yi-Hsien Lee Liang Fu Jing Kong Edbert J. Sie, James W. McIver and Nuh Gedik. Valley-selective optical stark effect in monolayer ws_2. *Nature Materials*, 14:290–294, 2015.

[42] F. U. Stein et al. J. W. McIver, B. Schulte. Light-induced anomalous hall effect in graphene. *Nature Physics*, 16:38–41, 2020.

[43] O. Smirnova Á. Jiménez-Galán, R. E. F. Silva and M. Ivanov. Lightwave control of topological properties in 2d materials for sub-cycle and non-resonant valley manipulation. *Nature Photonics*, 14:728–732, 2020.

[44] Ming-Che Chang Di Xiao and Qian Niu. Berry phase effects on electronic properties. *Rev. Mod. Phys.*, 82:1959–2007, Jul 2010.

[45] Di Xiao Xiaodong Xu, Wang Yao and Tony F. Heinz. Spin and pseudospins in layered transition metal dichalcogenides. *Nature Physics*, 10:343–350, 2014.

[46] S. Schlauderer M. Gmitra et al. F. Langer, C. P. Schmid. Lightwave valleytronics in a monolayer of tungsten diselenide. *Nature*, 557:76–80, 2018.

[47] Heiko B. Weber Christian Heide, Takuya Higuchi and Peter Hommelhoff. Coherent electron trajectory control in graphene. *Phys. Rev. Lett.*, 121:207401, Nov 2018.

[48] C. P. Schmid F. Langer et al. J. Reimann, S. Schlauderer. Subcycle observation of lightwave-driven dirac currents in a topological surface band. *Nature*, 562:396 – 400, 2018.

[49] Konrad Ullmann Heiko B. Weber Peter Hommelhoff Takuya Higuchi, Christian Heide. Light-field-driven currents in graphene. *Nature*, 550:224 – 228, 2017.

[50] Tomohiko Yamaguchi Akira Suda Hiroki Mashiko, Katsuya Oguri and Hideki Gotoh. Petahertz optical drive with wide-bandgap semiconductor. *Nature Physics*, 12:741–745, 2016.

[51] Annkatrin Sommer Simon Holzner Wolfgang Schweinberger et al. Martin Schultze, Elisabeth M. Bothschafter. Controlling dielectrics with the electric field of light. *Nature*, 493:75–78, 2013.

[52] Nicholas Karpowicz Vadym Apalkov et al. Agustin Schiffrin, Tim M. Paasch-Colberg. Optical-field-induced current in dielectrics. *Nature*, 493:70–74, 2013.

[53] Stephen R. Leone and Daniel M. Neumark. Attosecond science in atomic, molecular, and condensed matter physics. *Faraday Discuss*, 194:15–39, 2016.

[54] Domenico De Fazio Cristian Manzoni et al. Eva A. A. Pogna, Margherita Marsili. Photo-induced bandgap renormalization governs the ultrafast response of single-layer mos2. *ACS Nano*, 10:1182–1188, 2016.

[55] Sang-Jun Choi Kenji Watanabe Takashi Taniguchi et al. Tae Young Jeong, Hakseong Kim. Spectroscopic studies of atomic defects and bandgap renormalization in semiconducting monolayer transition metal dichalcogenides. *Nature Communications*, 10:3825, 2019.

[56] Georg A. Reider Gugang Chen Yumeng You et al. Dezheng Sun, Yi Rao. Observation of rapid exciton–exciton annihilation in monolayer molybdenum disulfide. *Nano Letters*, 14:5625–5629, 2014.

[57] Matthew Z. Bellus Frank Ceballos, Qiannan Cui and Hui Zhao. Exciton formation in monolayer transition metal dichalcogenides. *Nanoscale*, 8:11681–11688, 2016.

[58] Ferenc Krausz Stanislav Yu. Kruchinin and Vladislav S. Yakovlev. Colloquium: Strong-field phenomena in periodic systems. *Rev. Mod. Phys.*, 90:021002, Apr 2018.

[59] Shambhu Ghimire and David A. Reis. High-harmonic generation from solids. *Nature Physics*, 15:10–16, 2019.

[60] Michael Heigl Michael Lohmann et al. Sergey Zayko, Ofer Kfir. Ultrafast high-harmonic nanoscopy of magnetization dynamics. *Nature Communications*, 12:6337, 2021.

[61] Alexander Guggenmos Daniel M. Neumark Romain Geneaux, Hugo J. B. Marroux and Stephen R. Leone. Transient absorption spectroscopy using high harmonic generation: a review of ultrafast x-ray dynamics in molecules and solids. *Phys. Rev. Lett.*, 377:20170463, April 2019.

[62] Luiz G. M. Tenório Maurício F. C. Martins Quintela, João C. G. Henriques and Nuno M. R. Peres. Theoretical methods for excitonic physics in 2d materials. *physica status solidi (b)*, 259(7):2200097, 2022.

[63] Juan José Esteve-Paredes Alejandro José Uría-Álvarez Rui E. F. Silva Fernando Martín Juan José Palacios Giovanni Cistaro, Mikhail Malakhov and Antonio Picón. Theoretical approach for electron dynamics and ultrafast spectroscopy (edus). *Journal of Chemical Theory and Computation*, 19(1):333–348, 2023. PMID: 36480770.

[64] Fernando M. S. Nogueira-Eberhard K. U. Gross Miguel A. L. Marques, Neepa T. Maitra and Angel Rubio. *Fundamentals of time-dependent density functional theory*. Lecture Notes in Physics. 2012.

[65] Y. Shinohara T. Otobe K. Yabana, T. Sugiyama and G. F. Bertsch. Time-dependent density functional theory for strong electromagnetic fields in crystalline solids. *Phys. Rev. B*, 85:045134, Jan 2012.

[66] Erich Runge and E. K. U. Gross. Density-functional theory for time-dependent systems. *Phys. Rev. Lett.*, 52:997–1000, Mar 1984.

[67] Yuta Hirokawa Mitsuharu Uemoto Takashi Takeuchi-et al. Masashi Noda, Shunsuke A. Sato. Salmon: Scalable ab-initio light–matter simulator for optics and nanoscience. *Computer Physics Communications*, 235:356–365, 2019.

[68] Sahar Sharifzadeh Jeffrey B. Neaton Sivan Refaely-Abramson, Manish Jain and Leeor Kronik. Solid-state optical absorption from optimally tuned time-dependent range-separated hybrid density functional theory. *Phys. Rev. B*, 92:081204, Aug 2015.

[69] Rodolfo Del Sole Stefan Albrecht, Lucia Reining and Giovanni Onida. Ab initio calculation of excitonic effects in the optical spectra of semiconductors. *Phys. Rev. Lett.*, 80:4510–4513, May 1998.

[70] Michael Rohlfing and Steven G. Louie. Electron-hole excitations in semiconductors and insulators. *Phys. Rev. Lett.*, 81:2312–2315, Sep 1998.

[71] Denis Jacquemin Xavier Blase, Ivan Duchemin and Pierre-François Loos. The bethe–salpeter equation formalism: From physics to chemistry. *Phys. Rev. Lett.*, 11:7371–7382, Sep 2020.

[72] Christian Vorwerk, Benjamin Aurich, Caterina Cocchi, and Claudia Draxl. Bethe–salpeter equation for absorption and scattering spectroscopy: implementation in the exciting code. *Electronic Structure*, 1(3):037001, aug 2019.

[73] M. Grüning C. Attaccalite and A. Marini. Real-time approach to the optical properties of solids and nanostructures: Time-dependent bethe-salpeter equation. *Phys. Rev. B*, 84:245110, Dec 2011.

[74] Paolo E. Trevisanutto Emilia Ridolfi and Vitor M. Pereira. Expeditious computation of nonlinear optical properties of arbitrary order with native electronic interactions in the time domain. *Phys. Rev. B*, 102:245110, Dec 2020.

[75] D. Sangalli. Excitons and carriers in transient absorption and time-resolved arpes spectroscopy: An ab initio approach. *Phys. Rev. Mater.*, 5:083803, Aug 2021.

[76] M. Kira and S.W. Koch. Many-body correlations and excitonic effects in semiconductor spectroscopy. *Progress in Quantum Electronics*, 30(5):155–296, 2006.

[77] H. Haug and S. Koch. *Quantum Theory of Optical and Electronic Properties of Semiconductors*. 4th ed. edition, 2004.

[78] Sohrab Ismail-Beigi and T. A. Arias. Locality of the density matrix in metals, semiconductors, and insulators. *Phys. Rev. Lett.*, 82:2127–2130, Mar 1999.

[79] Antonio Redondo and Jean C. Marshall. Single-particle density matrix method for the solution of the many-electron problem. *The Journal of Chemical Physics*, 91(9):5492–5499, 11 1989.

[80] Antonio Redondo. Density-matrix formulation of ab initio methods of nonrelativistic quantum mechanics. *Phys. Rev. A*, 39:4366–4376, May 1989.

[81] S. Goedecker. Decay properties of the finite-temperature density matrix in metals. *Phys. Rev. B*, 58:3501–3502, Aug 1998.

[82] Giacomo Mazza Andrew J. Millis Antoine Georges Jiajun Li, Denis Golez and Martin Eckstein. Electromagnetic coupling in tight-binding models for strongly correlated light and matter. *Phys. Rev. B*, 101:205140, May 2020.

[83] Olesia Dmytruk and Marco Schiró. Gauge fixing for strongly correlated electrons coupled to quantum light. *Phys. Rev. B*, 103:075131, Feb 2021.

[84] Morten Førre and Aleksander Skjerlie Simonsen. Generalized velocity-gauge form of the light-matter interaction hamiltonian beyond the dipole approximation. *Phys. Rev. A*, 93:013423, Jan 2016.

[85] Jonathan R. Yates Ivo Souza Nicola Marzari, Arash A. Mostofi and David Vanderbilt. Maximally localized wannier functions: Theory and applications. *Rev. Mod. Phys.*, 84:1419–1475, Oct 2012.

[86] Bruno Amorim. Lectures notes on peierls substitution vs length gauge. Private Notes.

[87] Claudio Aversa and J. E. Sipe. Nonlinear optical susceptibilities of semiconductors: Results with a length-gauge analysis. *Phys. Rev. B*, 52:14636–14645, Nov 1995.

[88] E. Prodan and W. Kohn. Nearsightedness of electronic matter. *Proceedings of the National Academy of Sciences*, 102(33):11635–11638, 2005.

[89] Giovanni Consalvo Cistaro. *Attosecond Spectroscopy in the X-ray Regime in Complex Systems*. Phd thesis, Universidad Autónoma de Madrid, UAM. Departamento de Química, 2022. Available at https://repositorio.uam.es/handle/10486/705177.

[90] S. Goedecker. Linear scaling electronic structure methods. *Rev. Mod. Phys.*, 71:1085–1123, Jul 1999.

[91] James C. Womack Alice E. A. Allen et al. Joseph C. A. Prentice, Jolyon Aarons. The onetep linear-scaling density functional theory program. *The Journal of Chemical Physics*, 152(17):174111, 05 2020.

[92] Bruno Amorim. Lectures notes from qmss 2023 - excitations. Private Notes. Also available at https://github.com/BacAmorim/QMSS$_2$023$_E xcitations$.

[93] Michael G. Cottam and Zahra Haghshenasfard. *Many-Body Theory of Condensed Matter Systems: An Introductory Course*. 2020.

[94] Felipe H. da Jornada Diana Y. Qiu and Steven G. Louie. Solving the bethe-salpeter equation on a subspace: Approximations and consequences for low-dimensional materials. *Phys. Rev. B*, 103:045117, Jan 2021.

[95] Lorin X. Benedict. Screening in the exchange term of the electron-hole interaction of the bethe-salpeter equation. *Phys. Rev. B*, 66:193105, Nov 2002.

[96] W. Hanke and L. J. Sham. Many-particle effects in the optical spectrum of a semiconductor. *Phys. Rev. B*, 21:4656–4673, May 1980.

[97] Michael Rohlfing and Steven G. Louie. Electron-hole excitations and optical spectra from first principles. *Phys. Rev. B*, 62:4927–4944, Aug 2000.

[98] Gonçalo Bastos Ventura. *Nonlinear Optical Response of Two-dimensional Crystals*. Phd thesis, University of Porto, UP. Departamento de Física e Astronomia, 2021. Available at https://repositorio-aberto.up.pt/handle/10216/139780.

[99] Raffaele Resta. Drude weight and superconducting weight. *Journal of Physics: Condensed Matter*, 30(41):414001, sep 2018.

[100] N. W. Ashcroft and N. D. Mermin. *Solid State Physics*. Saunders College Publishing, 1st ed. edition, 1976.

[101] João Manuel Alendouro Oliveira Pinho. *From Bloch Oscillations to Stationary Currents in Mesoscopic Systems*. Phd thesis, University of Porto, UP. Departamento de Física e Astronomia, 2022. Available at https://repositorio-aberto.up.pt/handle/10216/147152.

Part III

Appendices

A Notes on Periodic Boundary Conditions

This appendix is dedicated to the Born-von Karman periodic boundary conditions and their implications on the position operator in tight-binding systems. This chapter is based in the reference [100].

A.1 Born-von Karman Periodic Boundary Conditions

Born-von Karman periodic boundary conditions, also known as periodic boundary conditions or, in short, PBCs, consists in restricting the continuous variable quasi-momentum **k** defined by the Bloch theorem into a discrete set. This restriction is usually convenient in terms of numerical purposes to mimic an infinite system by imposing periodicity on the boundaries of a finite simulation box. This eliminates edge effects and allows for the simulation of bulk properties of a material or system. Mathematically, the discretization of this quantum number can be interpreted as the quantization of the wavefunctions in the box defined by a set of discrete translation operations of the type

$$\mathbf{R} = n_1\mathbf{a}_1 + n_2\mathbf{a}_2 + n_3\mathbf{a}_3, \text{ with } n_1, n_2, n_3 \, in \, \mathbb{Z} \tag{A.192}$$

where the primitive translation vectors $\{\mathbf{a}_i\}_{i=1,2,3}$ as the ones that form the grid's structure basis of the Bravais lattice. The volume delimited by the three lattice vectors is known as unit cell and represents the unity of volume repeated throughout the whole space.

If the system consists of $N = N_1 \times N_2 \times N_3$ unit cells distributed along the lattice vectors $\{\mathbf{a}_i\}_{i=1,2,3}$, then the following equation must be satisfied:

$$\psi_{n\mathbf{k}}\left(\mathbf{r} + N_i\mathbf{a}_i\right) = \psi_{n\mathbf{k}}\left(\mathbf{r}\right), \text{ for } i = 1, 2, 3 \tag{A.193}$$

Consequent of the Bloch theorem [100], it is easy to reach a condition that restricts the quasi-momentum values:

$$\mathbf{k} = \sum_i \frac{n_i}{N_i}\mathbf{b}_i$$
$$\text{with } n_i = 0, 1, ..., N_i - 1 \tag{A.194}$$

where the quantity $\mathbf{b}_i$ represent the reciprocal lattice vectors that must satisfy the condition $\mathbf{b}_i \cdot \mathbf{a}_j = 2\pi\delta_{ij}$. The Brillouin zone is reduced to a set of discrete points, equidistant along the crystal directions.

A.2 Position operator

In the context of quantum mechanics, the position operator is a fundamental observable that represents the position of a particle in the space domain. In a 1D linear chain, the position operator should intuitively give us the location of a particle along the chain. However, when we consider a linear chain with Born von-Karman boundary conditions, the position operator becomes ill-defined due to the imposed periodicity of the system. This periodicity of the system allows the particle to wrap around the chain and effectively creates a loop. When we assign positions to the atoms,

we find that once we reach the starting point after traversing the chain, the difference between the positions of the first and final atoms is not their actual distance in the physical space, not reflecting their true physical separation. This means that the particle can appear at multiple positions along the chain, and its "exact" position becomes ambiguous. In practical terms, because we are in a system with periodic boundary conditions, the position operator for a 1D linear system

$$x = \sum_n n c_n^\dagger c_n \tag{A.195}$$

is ill-defined at the borders, since the difference between the last and initial position should be 1 and is, instead, N. In Figure 16 are represented the position operator in a 1D system with PBC and a graphical representation of its behaviour. In blue, we show the modulo distance, where it mirrors the behaviour

$$\text{mod}\,(n,\, N) = n, n = 0, ...,\, N-1$$
$$\text{mod}\,(n + kN,\, N) = \text{mod}\,(n,\, N)\,,\, k \in \mathbb{Z}$$

which corresponds to the average position from the origin ($x = 0$). This will be used in the position operator's definition in the tight-binding system under PBC. In green, it is depicted the physical separation between the origin and the discrete lattice points. This is the distance that counts for the interaction's terms.

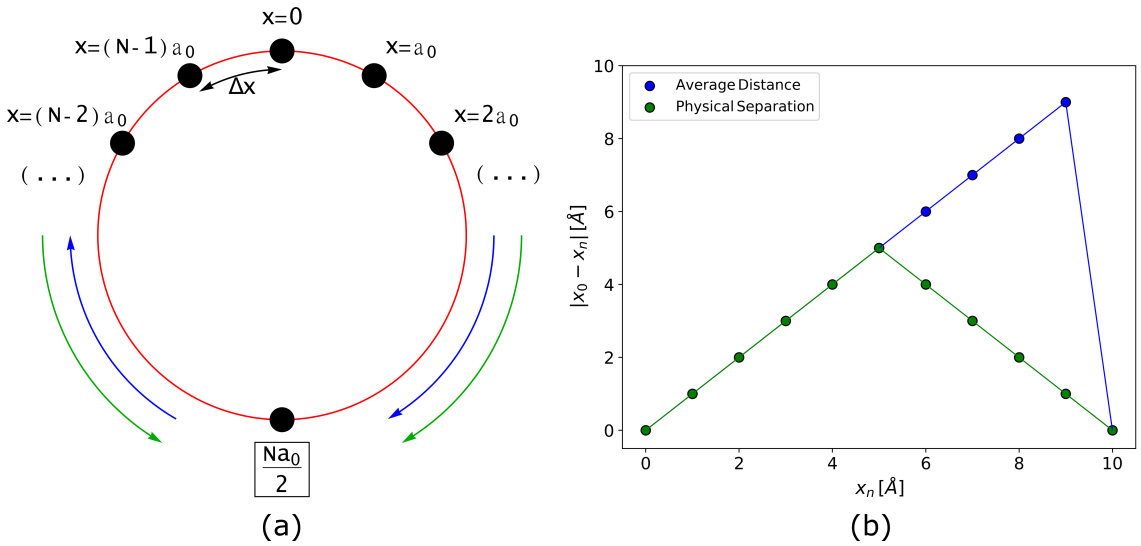

Figure 16: Position operator in a 1D tight-binding system with Born-von Karman periodic boundary conditions (PBC) **(a)** Scheme of a linear chain under periodic boundary conditions that closes itself, creating a ring. In blue is depicted the average position from the origin ($x = 0$) and, in green, the physical separation between the origin and the discrete lattice points **(b)** Graphical representation of the position operator in a 1D periodic system, which shows the discontinuity of the position operator under periodic boundary conditions for both behaviours depicted in (a). Lattice parameters: lattice constant $a_0 = 1$ Å and the number of discrete sites $N = 10$.

B Breakdown of Peierls Hamiltonian's Gauge Invariance under Periodic Boundary Conditions

The chapter is based on the reference [86].

The Peierls Hamiltonian for a 1D system with Born-von Karman periodic boundary conditions is defined in equation (2.28). For this analysis, we will include a constant vector potential

$$\tilde{\mathcal{H}}_{PBC}^{Peierls}(\varphi) = -h\sum_{n=0}^{N-1}\left(e^{-i\varphi}\tilde{c}^{\dagger}_{\mathrm{mod}(n+1,N)}\tilde{c}_n + e^{i\varphi}\tilde{c}^{\dagger}_n\tilde{c}_{\mathrm{mod}(n+1,N)}\right)$$

where the phase factors arise via the Peierls substitution. Furthermore, we define

$$\mathrm{mod}(n,\,N) = n, n = 0, ...,\, N-1$$
$$\mathrm{mod}(n+kN,\,N) = \mathrm{mod}(n,\,N),\; k \in \mathbb{Z}$$

In its matrix form, the Peierls Hamiltonian reads

$$\tilde{h}(\varphi) = \begin{bmatrix} 0 & -he^{i\varphi} & & & \{-he^{i\varphi}\}^* \\ \{-he^{i\varphi}\}^* & 0 & -he^{i\varphi} & & \\ & \ddots & \ddots & \ddots & \\ & & \{-he^{i\varphi}\}^* & 0 & -he^{i\varphi} \\ -he^{i\varphi} & & & \{-he^{i\varphi}\}^* & 0 \end{bmatrix}$$

Let us now consider the time-independent Schrödinger and expand the wave function of a single electron state in a localized orbital basis. By adopting

$$|\psi\rangle = \sum_n \psi_n |n\rangle \tag{B.196}$$

it reads

$$\begin{aligned}
\tilde{\mathcal{H}}_{PBC}^{Peierls}(\varphi)\,|\psi\rangle &= E\,|\psi\rangle \\
\Leftrightarrow -h\sum_{n=0}^{N-1}\left(e^{-i\varphi}\tilde{c}^{\dagger}_{\mathrm{mod}(n+1,N)}\tilde{c}_n + e^{i\varphi}\tilde{c}^{\dagger}_n\tilde{c}_{\mathrm{mod}(n+1,N)}\right)\left(\sum_m \psi_m |m\rangle\right) &= E\left(\sum_m \psi_m |m\rangle\right) \\
\Leftrightarrow -h\sum_n\left(e^{-i\varphi}|n\rangle\langle \mathrm{mod}(n-1,N)| + e^{i\varphi}|n\rangle\langle \mathrm{mod}(n+1,N)|\right)\left(\sum_m \psi_m |m\rangle\right) &= E\left(\sum_m \psi_m |m\rangle\right) \\
\Leftrightarrow -h\sum_{nm}\left(e^{-i\varphi}\delta_{\mathrm{mod}(n-1,N),\,m}\psi_m + e^{i\varphi}\delta_{\mathrm{mod}(n+1,N),\,m}\psi_m\right)|n\rangle &= E\left(\sum_m \psi_m |m\rangle\right) \\
\Leftrightarrow -h\sum_n\left(e^{-i\varphi}\psi_{\mathrm{mod}(n-1,\,N)} + e^{i\varphi}\psi_{\mathrm{mod}(n+1,\,N)}\right)|n\rangle &= \sum_n (E\psi_n)\,|n\rangle \\
\Longrightarrow\; -he^{-i\varphi}\psi_{\mathrm{mod}(n-1,N)} - he^{i\varphi}\psi_{\mathrm{mod}(n+1,N)} &= E\psi_n
\end{aligned}$$

where we took into account the fact that the system presents translational symmetry and the Dirac notation $c^{\dagger}_{n+1}c_n \equiv$

$|n+1\rangle\langle n|$. More explicitly,

$$
\begin{aligned}
E\psi_0 &= -he^{-i\varphi}\psi_{N-1} - he^{i\varphi}\psi_1 \\
&\vdots \\
E\psi_n &= -he^{-i\varphi}\psi_{n-1} - he^{i\varphi}\psi_{n+1}, 0 < n < N-1 \\
&\vdots \\
E\psi_{N-1} &= -he^{-i\varphi}\psi_{N-2} - he^{i\varphi}\psi_0
\end{aligned}
$$

Now, let us make the unitary transformation

$$\psi_n = \tilde{\psi}_n e^{-i\varphi n}$$

If we apply the above transformation and by manipulating accordingly, we obtain the following results:

$$
\begin{aligned}
E\tilde{\psi}_0 &= -h\tilde{\psi}_{N-1}e^{-i\varphi N} - h\tilde{\psi}_1 \\
E\tilde{\psi}_n &= -h\tilde{\psi}_{n-1} - h\tilde{\psi}_{n+1} \\
E\tilde{\psi}_{N-1} &= -h\tilde{\psi}_{N-2} - he^{i\varphi N}\tilde{\psi}_0
\end{aligned}
$$

from which we obtain the following matrix

$$
h(t) = \begin{bmatrix}
0 & -h & & & -he^{-i\varphi N} \\
-h & 0 & -h & & \\
 & \ddots & \ddots & \ddots & \\
 & & -h & 0 & -h \\
-he^{i\varphi N} & & & -h & 0
\end{bmatrix}
$$

Note that we can never completely get rid of the phases in the hoppings terms, due to the periodic boundary conditions. Therefore, we do not have gauge invariance.

C Single-Particle operators in the New Basis

Let us consider a general state $|\lambda\rangle$ as a consequence of applying a creation operator on the vacuum state,

$$c_\lambda^\dagger |0\rangle = |\lambda\rangle \tag{C.197}$$

If we apply the completeness relation in the previous equation, we determine

$$c_\lambda^\dagger |0\rangle = \sum_\beta \psi_\lambda(\beta) |\beta\rangle \tag{C.198}$$

where, as we can see, we made a change of basis, leading to a different Hilbert space via the projection term $\psi_\lambda(\beta) \equiv \langle\beta|\lambda\rangle$. Now, we can express the operator in the basis $|\beta\rangle$ in terms of the basis $|\lambda\rangle$ by doing the following procedure:

$$\begin{aligned}
c_\lambda^\dagger &= \sum_\beta \psi_\lambda(\beta) c_\beta^\dagger \\
\Leftrightarrow \left(\sum_{\lambda'} \psi_{\lambda'}^*(\beta)\right) c_\lambda^\dagger &= \left(\sum_{\lambda'} \psi_{\lambda'}^*(\beta)\right) \sum_\beta \psi_\lambda(\beta) c_\beta^\dagger \\
\Leftrightarrow \sum_{\lambda'} \psi_{\lambda'}^*(\beta) c_\lambda^\dagger &= \sum_{\lambda'} \left(\sum_\beta \psi_{\lambda'}^*(\beta) \psi_\lambda(\beta)\right) c_\beta^\dagger \\
\Leftrightarrow \sum_{\lambda'} \psi_{\lambda'}^*(\beta) c_\lambda^\dagger &= \sum_{\lambda'} \delta_{\lambda\lambda'} c_\beta^\dagger
\end{aligned} \tag{C.199}$$

assuming that the states corresponding to the indices $\{\lambda, \lambda'\}$ satisfy the orthogonality properties. From this manipulation, we determine the creation and annihilation operators in the new basis

$$c_\beta^\dagger = \sum_\lambda \psi_\lambda^*(\beta) c_\lambda^\dagger \tag{C.200}$$

$$c_\beta = \sum_\lambda c_\lambda \psi_\lambda(\beta) \tag{C.201}$$

D Hamiltonian of an Interacting system in Equilibrium

The chapter is based on the reference [92].

Let us consider a system of interacting fermionic particles whose equilibrium state is described by the equilibrium Hamiltonian, which in a given basis and in first quantization, can be written as

$$\begin{aligned}\mathcal{H} &= \langle \mathbf{r}| \mathcal{H}^{(1)} |\mathbf{r}\rangle + \langle \mathbf{r}, \mathbf{r}'| \mathcal{H}^{(2)} |\mathbf{r}', \mathbf{r}\rangle \\ &= \int d^3\mathbf{r}\Psi^\dagger(\mathbf{r}) \left[\frac{p^2}{2m} + U(\mathbf{r})\right] \Psi(\mathbf{r}) + \frac{1}{2}\int d^3\mathbf{r}d^3\mathbf{r}'\Psi^\dagger(\mathbf{r})\Psi(\mathbf{r}')V(\mathbf{r}-\mathbf{r}')\Psi(\mathbf{r}')\Psi(\mathbf{r})\end{aligned} \tag{D.202}$$

where we have two terms: a single- and two-particle Hamiltonians defined as $\mathcal{H}^{(1)}$ and $\mathcal{H}^{(2)}$, respectively. The first contains two energetic contributions: the kinetic term and the static potential term, in which the latter gives the contribution due to external influences[14]. Finally, we have the two-particle Hamiltonian $\mathcal{H}^{(2)}$ that represents the electron-electron interaction regulated by the term $V(\mathbf{r}-\mathbf{r}')$, usually dictated by a Coulomb interaction.

We want to write the Hamiltonian (D.202) in second quantization. With that goal in mind, let us expand the electronic wave function $\Psi(\mathbf{r})$ in an arbitrary localized basis $\{\phi_a\}$,

$$\begin{aligned}\Psi(\mathbf{r}) &= \sum_a \phi_a(\mathbf{r}) c_a \\ \Psi^\dagger(\mathbf{r}) &= \sum_a \phi_a^*(\mathbf{r}) c_a^\dagger\end{aligned}$$

where the operators $c_a\left(c_a^\dagger\right)$ corresponds to the annihilation(creation) fermionic operators within a general state a. The Hamiltonian (D.202) reads

$$\begin{aligned}\mathcal{H} &= \int d^3\mathbf{r}\Psi^\dagger(\mathbf{r}) \left[\frac{p^2}{2m} + U(\mathbf{r})\right] \Psi(\mathbf{r}) + \frac{1}{2}\int d^3\mathbf{r}d^3\mathbf{r}'\Psi^\dagger(\mathbf{r})\Psi(\mathbf{r}\prime)V(\mathbf{r}-\mathbf{r}')\Psi(\mathbf{r}')\Psi(\mathbf{r}) \\ &= \sum_{ab}\int d^3\mathbf{r}\left(\phi_a^*(\mathbf{r})c_a^\dagger\right)\left[\frac{p^2}{2m} + U(\mathbf{r})\right](\phi_b(\mathbf{r})c_b) \\ &+ \frac{1}{2}\sum_{abcd}\int d^3\mathbf{r}d^3\mathbf{r}'\left(\phi_a^*(\mathbf{r})c_a^\dagger\right)\left(\phi_b^*(\mathbf{r}')c_b^\dagger\right)V(\mathbf{r}-\mathbf{r}')\left(\phi_c(\mathbf{r}')c_c\right)\left(\phi_d(\mathbf{r})c_d\right) \\ &= \sum_{ab}\int d^3\mathbf{r}\phi_a^*(\mathbf{r})\left[\frac{p^2}{2m} + U(\mathbf{r})\right]\phi_b(\mathbf{r})c_a^\dagger c_b \\ &+ \frac{1}{2}\sum_{abcd}\int d^3\mathbf{r}d^3\mathbf{r}'\phi_a^*(\mathbf{r})\phi_b^*(\mathbf{r}')V(\mathbf{r}-\mathbf{r}')\phi_c(\mathbf{r}')\phi_d(\mathbf{r})c_a^\dagger c_b^\dagger c_c c_d \\ &= \sum_{ab} h_{ab}c_a^\dagger c_b + \frac{1}{2}\sum_{abcd} V_{cd}^{ab}c_a^\dagger c_b^\dagger c_c c_d\end{aligned} \tag{D.203}$$

This result can be written in terms of matrix elements, leading to a more compact form:

$$\mathcal{H} = \sum_{ab} h_{ab}c_a^\dagger c_b + \frac{1}{2}\sum_{abcd} V_{cd}^{ab}c_a^\dagger c_b^\dagger c_c c_d \tag{D.204}$$

[14] Such as for electrons moving in a periodic potential for a lattice of ions or for atoms in a lattice vibrating about their fixed equilibrium positions

where the quantities h_{ab} and V_{cd}^{ab} are defined as

$$h_{ab} = \int d^3\mathbf{r}\phi_a^*\left(\mathbf{r}\right)\left[\frac{p^2}{2m} + U\left(\mathbf{r}\right)\right]\phi_b\left(\mathbf{r}\right) \tag{D.205}$$

$$V_{cd}^{ab} = \int d^3\mathbf{r}d^3\mathbf{r}'\phi_a^*\left(\mathbf{r}\right)\phi_b^*\left(\mathbf{r}'\right)V\left(\mathbf{r}-\mathbf{r}'\right)\phi_c\left(\mathbf{r}'\right)\phi_d\left(\mathbf{r}\right) \tag{D.206}$$

In this new formulation, the free term, associated with the matrix h_{ab}, it tells us that we are annihilating a fermionic state b and creating another on the state a. The interaction term, associated with V_{cd}^{ab}, it corresponds to the fermionic interaction between two indistinguishable particles with an interaction range of $|\mathbf{r}-\mathbf{r}'|$.

E Symmetry Properties of the Electron-Electron Interaction Term

In this appendix, it is shown the details on how to arrive at the symmetry properties presented in equations (4.56) and (4.57), namely the Hamiltonian of the two-body interaction matrix elements. From the imposed symmetry $V(\mathbf{r}-\mathbf{r}') = V(\mathbf{r}'-\mathbf{r})$, which corresponds to the spatial inversion symmetry, we obtain

$$\begin{aligned} V_{cd}^{ab} &= \int d^3\mathbf{r}d^3\mathbf{r}'\phi_a^*(\mathbf{r})\,\phi_b^*(\mathbf{r}')\,V(\mathbf{r}-\mathbf{r}')\,\phi_c(\mathbf{r}')\,\phi_d(\mathbf{r}) \\ &= \int d^3\mathbf{r}d^3\mathbf{r}'\phi_a^*(\mathbf{r}')\,\phi_b^*(\mathbf{r})\,V(\mathbf{r}'-\mathbf{r})\,\phi_c(\mathbf{r})\,\phi_d(\mathbf{r}') \\ &= \int d^3\mathbf{r}d^3\mathbf{r}'\phi_a^*(\mathbf{r}')\,\phi_b^*(\mathbf{r})\,V(\mathbf{r}-\mathbf{r}')\,\phi_c(\mathbf{r})\,\phi_d(\mathbf{r}') \\ &= \int d^3\mathbf{r}d^3\mathbf{r}'\phi_b^*(\mathbf{r})\,\phi_a^*(\mathbf{r}')\,V(\mathbf{r}-\mathbf{r}')\,\phi_d(\mathbf{r}')\,\phi_c(\mathbf{r}) \\ &= V_{dc}^{ba} \end{aligned} \tag{E.207}$$

where from the first line to the second we interchanged the positions, i.e., $\mathbf{r} \leftrightarrow \mathbf{r}'$. It is also possible to the see what is the implication of this symmetry in the complex conjugate,

$$\begin{aligned} \left(V_{cd}^{ab}\right)^* &= \int d^3\mathbf{r}d^3\mathbf{r}'\phi_a(\mathbf{r})\,\phi_b(\mathbf{r}')\,V(\mathbf{r}-\mathbf{r}')\,\phi_c^*(\mathbf{r}')\,\phi_d^*(\mathbf{r}) \\ &= \int d^3\mathbf{r}d^3\mathbf{r}'\phi_d^*(\mathbf{r})\,\phi_c^*(\mathbf{r}')\,V(\mathbf{r}-\mathbf{r}')\,\phi_b(\mathbf{r}')\,\phi_a(\mathbf{r}) \\ &= V_{ba}^{dc} = V_{ab}^{cd} \end{aligned} \tag{E.208}$$

F Symmetry Properties of the Bethe-Salpeter Hamiltonian's Matrix Elements

In this appendix, we want to determine the symmetry properties of the effective two-particle Hamiltonian's blocks, namely the resonant and coupling blocks defined in (5.90). Let us start this by recalling the symmetry properties of the matrix elements of a generic interaction two-particle Hamiltonian defined above in equations (E.207) and (E.208):

$$V_{cd}^{ab} = V_{dc}^{ba} \tag{F.209}$$

$$\left(V_{cd}^{ab}\right)^* = V_{ba}^{dc} \tag{F.210}$$

Let us begin with the diagonal blocks. By taking into account the fermionic properties of being indistinguishable and interchangeable, we determine that

$$\begin{aligned}
\mathcal{H}_{o_2e_1}^{o_4e_3} &= \left(\epsilon_{o_2} - \epsilon_{e_1}\right)\delta_{o_2o_4}\delta_{e_3e_1} + \left(f_{e_1} - f_{o_2}\right)\left(V_{o_4e_1}^{o_2e_3} - W_{e_1o_4}^{o_2e_3}\right) \\
&= \left(\epsilon_{o_2} - \epsilon_{e_1}\right)\delta_{o_2o_4}\delta_{e_3e_1} - \left(\left(V_{e_3o_2}^{e_1o_4}\right)^* - \left(W_{o_2e_3}^{e_1o_4}\right)^*\right) \\
&= -\left[\left(\epsilon_{e_1} - \epsilon_{o_2}\right)\delta_{o_2o_4}\delta_{e_3e_1} + \left(V_{e_3o_2}^{e_1o_4} - W_{o_2e_3}^{e_1o_4}\right)\right]^* \\
&= -\left(\mathcal{H}_{e_1o_2}^{e_3o_4}\right)^* \\
\text{with } \mathcal{H}_{e_1o_2}^{e_3o_4} &= \left(\epsilon_{e_1} - \epsilon_{o_2}\right)\delta_{e_1e_3}\delta_{o_2o_4} + \left(V_{e_3o_2}^{e_1o_4} - W_{o_2e_3}^{e_1o_4}\right)
\end{aligned} \tag{F.211}$$

Futhermore,

$$\begin{aligned}
\mathcal{H}_{e_1o_2}^{e_3o_4} &= \left(\epsilon_{e_1} - \epsilon_{o_2}\right)\delta_{e_1e_3}\delta_{o_2o_4} + \left(V_{e_3o_2}^{e_1o_4} - W_{o_2e_3}^{e_1o_4}\right) \\
&= \left(\epsilon_{e_3} - \epsilon_{o_4}\right)\delta_{e_1e_3}\delta_{o_2o_4} + \left(\left(V_{e_1o_4}^{e_3o_2}\right)^* - \left(W_{o_4e_1}^{e_3o_2}\right)^*\right) \\
&= \left(\mathcal{H}_{e_3o_4}^{e_1o_2}\right)^*
\end{aligned} \tag{F.212}$$

meaning the diagonal blocks are hermitian.

Next, let us turn our attention to the off-diagonal blocks. Employing the same strategy as before, it yields

$$\begin{aligned}
\mathcal{H}_{o_2e_1}^{e_4o_3} &= \left(\epsilon_{o_2} - \epsilon_{e_1}\right)\delta_{o_2e_4}\delta_{o_3e_1} + \left(f_{e_1} - f_{o_2}\right)\left(V_{e_4e_1}^{o_2o_3} - W_{e_1e_4}^{o_2o_3}\right) \\
&= -\left[\left(V_{o_3o_2}^{e_1e_4} - W_{o_3o_2}^{e_4e_1}\right)\right]^* \\
&= -\left(\mathcal{H}_{e_1o_2}^{o_3e_4}\right)^* \\
\text{with } \mathcal{H}_{e_1o_2}^{o_3e_4} &= \left(V_{o_3o_2}^{e_1e_4} - W_{o_2o_3}^{e_1e_4}\right)
\end{aligned} \tag{F.213}$$

Additionaly, we observe that

$$\begin{aligned}
\mathcal{H}_{e_1o_2}^{o_3e_4} &= \left(V_{o_2o_3}^{e_4e_1} - W_{o_2o_3}^{e_1e_4}\right) \\
&= \left(V_{o_3o_2}^{e_1e_4} - W_{o_3o_2}^{e_4e_1}\right) \\
&= \mathcal{H}_{e_4o_4}^{o_2e_1}
\end{aligned} \tag{F.214}$$

meaning they are symmetric, i.e., $\mathcal{H}^{o_3e_4}_{e_1o_2} = \left(\mathcal{H}^{o_3e_4}_{e_1o_2}\right)^T$. Consequently, the off-diagonal possesses the following symmetry property:

$$\mathcal{H}^{e_4o_3}_{o_2e_1} = -\left(\mathcal{H}^{o_3e_4}_{e_1o_2}\right)^\dagger \tag{F.215}$$

In this way, the effective two-particle Hamiltonian is defined as

$$\mathcal{H}_{e-h} = \begin{bmatrix} \mathcal{H}^{o_4e_3}_{o_2e_1} & \mathcal{H}^{e_4o_3}_{o_2e_1} \\ -\left(\mathcal{H}^{e_4o_3}_{o_2e_1}\right)^\dagger & -\left(\mathcal{H}^{o_4e_3}_{o_2e_1}\right)^* \end{bmatrix} \tag{F.216}$$

G Wannier equation for 1D Systems

The Wannier equation for 1D system is defined as

$$\left(-\frac{\hbar^2}{2\mu}\nabla_x^2 - V\left(x\right) + E_{gap}\right)\psi\left(x\right) = E\psi\left(x\right) \tag{G.217}$$

where μ corresponds to the electron-hole pair's reduced mass. This equation represents nothing more than the Schrödinger equation for a hidrogenoid atom and constitutes an eigenvalue problem that needs to be solved. We can use *Finite Difference Method* to approximate the Laplace operator acting in the wavefunction as

$$\nabla_x^2\psi(x) = \frac{\psi\left(x_{n-1}\right) + \psi\left(x_{n+1}\right) - 2\psi\left(x_n\right)}{\left(\Delta x\right)^2} \tag{G.218}$$

in which $\Delta x \equiv \Delta x_n = x_{n+1} - x_n$ corresponds to the distance between consecutive nodes. Applying this in equation (G.217), it reads

$$\begin{aligned}&\left[-\frac{\hbar^2}{2\mu}\left(-\frac{2}{\left(\Delta x\right)^2}\right) - V\left(x\right) + E_{gap}\right]\psi\left(x_n\right) - \frac{\hbar^2}{2\mu}\left(\frac{1}{\left(\Delta x\right)^2}\right)\psi\left(x_{n-1}\right)\\ &- \frac{\hbar^2}{2\mu}\left(\frac{1}{\left(\Delta x\right)^2}\right)\psi\left(x_{n+1}\right) = E\psi\left(x\right)\end{aligned} \tag{G.219}$$

with the eigenvector being defined as

$$\boldsymbol{\psi} = \left[\psi\left(x_1\right), \psi\left(x_2\right), \ldots, \psi\left(x_{n-1}\right), \psi\left(x_n\right), \psi\left(x_{n+1}\right), \psi\left(x_{N-1}\right), \psi\left(x_N\right)\right]^T$$

for a system with a finite size. We can write a squared general matrix **A** with dimensions $N \times N$ with three nonzero diagonals:

$$\begin{aligned}a_{n,n-1} &= -\frac{\hbar^2}{2\mu}\left(\frac{1}{\left(\Delta x\right)^2}\right)\\ a_{n,n} &= E_{gap} - \frac{\hbar^2}{2\mu}\left(-\frac{2}{\left(\Delta x\right)^2}\right) - V\left(x_n\right)\\ a_{n,n+1} &= -\frac{\hbar^2}{2\mu}\left(\frac{1}{\left(\Delta x\right)^2}\right)\end{aligned}$$